AN ABSTRACT OF THE THESIS OF

Ae-young S. Lee for the degree of Master of Science in Civil Engineering presented on June 15, 2006.

Title: High-Cycle Fatigue Response of Diagonally-Cracked Conventionally Reinforced Concrete Bridge Girders.

Abstract approved:

Redacted for privacy

Christopher C. Higgins

The behavior of stirrups engaged by diagonal cracks and under service loads is largely unknown. Full-size laboratory specimens were loaded to induce diagonal cracks and subjected to high-cycle fatigue loading to represent a service life of 50 years. Tests indicated little change in the average stirrup stress range and mean while diagonal crack width and motion increased. Observed changes in stirrup strain range and crack motion were larger when stirrup spacing was wide or anchorage of longitudinal reinforcement was poor. Disregarding aggregate interlock and dowel forces, service level shear was attributed to the compression zone and transverse steel. These were reasonably calculated by Response 2000™, a sectional analysis program, by setting the concrete tensile strength very low.

High-Cycle Fatigue Response of Diagonally-Cracked Conventionally Reinforced Concrete Bridge Girders

by

Ae-young S. Lee

A THESIS

submitted to

Oregon State University

in partial fulfillment of
the requirements for the
degree of

Master of Science

Presented June 15, 2006
Commencement June 2007

Master of Science thesis of Ae-young S. Lee presented on June 15, 2006.

APPROVED:

Redacted for privacy

Major Professor, representing Civil Engineering

Redacted for privacy

Head of the Department of Civil, Construction, and Environmental Engineering

Redacted for privacy

Dean of the Graduate School

I understand that my thesis will become part of the permanent collection of Oregon State University libraries. My signature below authorizes release of my thesis to any reader upon request.

Redacted for privacy

Ae-young S. Lee, Author

ACKNOWLEDGEMENTS

Many thanks to:

- Dr. Higgins for extreme patience.
- the parents for support in all ways and especially for the food.
- grad students long gone—Melissa, Theresa, Tanarat, Brian—for laughter, friendship, explanations, guidance, and tons of lab work.
- the current crop of grad students—for goading/encouraging.
- the veggie house. Good people, good times. Hail to the king, baby.

TABLE OF CONTENTS

LIST OF FIGURES

LIST OF FIGURES (Continued)

Figure | Page

LIST OF TABLES

LIST OF APPENDIX FIGURES

LIST OF APPENDIX FIGURES (Continued)

LIST OF APPENDIX FIGURES (Continued)

LIST OF APPENDIX FIGURES (Continued)

HIGH-CYCLE FATIGUE RESPONSE OF DIAGONALLY-CRACKED CONVENTIONALLY REINFORCED CONCRETE BRIDGE GIRDERS

INTRODUCTION

Routine inspections in 2001 noted growing diagonal cracks on a number of state-owned bridges in Oregon (OTIA, 2005). This led to load restrictions and detours of major shipping routes, unplanned repairs and replacements, and political interest in the condition of these bridges. The subsequent survey of the state inventory identified these types of cracks in about 500 concrete bridges, the great majority of which were constructed from 1946 to 1962 and were of the reinforced concrete deck-girder (RCDG) structural category (Higgins, 2004b, p. 5). A research study was commissioned to examine diagonal cracks, which are associated with shear loads, in RCDG bridges. In the laboratory portion of the investigation, 44 full-size bridge girders were cast using the typical dimensions, detailing, and properties of the actual cracked bridges. Nine of these girders were subjected to cyclic loading to simulate high-cycle fatigue (HCF) from the millions of vehicles which have driven over in-service bridges since the 1950's. This paper presents the gathered data and specifically examines the role of the transverse steel, or stirrups, in the high-cycle fatigue performance of these members.

BACKGROUND

The HCF protocol is generally distinguished from low-cycle fatigue (LCF) as requiring a million or more cycles before causing failure while LCF may be in the thousands of cycles or less. In addition, LCF is characterized by plastic deformations while HCF behavior is typically elastic with linear stress-strain relationships (Constantinescu, Dang Van, & Maitournam, 2003, p. 562). HCF behavior of conventionally reinforced concrete (CRC) beams is influenced by the concrete behavior, reinforcing steel behavior, and the interaction between the concrete and reinforcing steel. Previous research on HCF of concrete structures has focused on plain concrete, fatigue of beams, and reinforcing steel (ACI SP-41, 1974; ACI SP-75, 1982; ACI Committee 215, 1992). The RILEM Committee (1984) mentioned the need to examine stirrups, which can vary in behavior under constant load and can experience bending and dowelling from the diagonal cracks.

High-Cycle Fatigue of CRC Beams

Early studies on the fatigue behavior of concrete beams without shear reinforcing were conducted by Chang and Kesler (1958). This research focused on small-sized specimens 4 x 6 in. containing only flexural reinforcing steel. Results indicated that the fatigue strength was less than the static strength when diagonal-cracking occurred in the specimens. The data also indicated that diagonal cracking from repeated loading did not damage the shear-moment carrying capacity of the beam. Based on statistical analysis of all test results, the fatigue reduction factor to achieve 10,000,000 cycles with 50% probability with respect to cracking was 0.57 and with respect to failure was 0.63.

Kaar and Mattock (1963) tested 24 ft long half-scale highway bridge girders having #2 bar stirrups sufficient to resist two-thirds the shear at the ultimate load. The girders were cycled at a range of 25 to 50% the load required to produce the maximum bending moment before being loaded statically to failure. During cycling the maximum recorded stresses increased greatly while the average stresses had only a small increase. Crack widths increased rapidly in the first ten thousand cycles and more slowly after that. Some cracks were observed to decrease in width due to new cracks forming adjacently. The cracks were restrained at the flexural steel and also tapered towards the compression zone.

Hawkins (1974) tested 30 small-sized beams 7 x 14 in. containing #3 stirrups. Specimens exhibited several failure modes including flexure, bond, splitting, and stirrup fractures. Results indicated that the fatigue stresses caused fracture at stirrup bends and the allowable stress should be reduced for these locations.

Okamura, Farghaly, and Ueda (1981) studied shear fatigue failure of stirrups in 17 squat rectangular beams, 9.8 in. high and 11.8 in. wide. The applied maximum shears were between 44 and 62% of the static strengths. When a stirrup leg fractured the strain in the opposite leg abruptly increased and adjacent stirrups were not affected. Crack extensions were accompanied by strain increases but at least one other stirrup stopped increasing in strain due to a redistribution of stresses. While individual stirrups deviated from each other greatly the average strain steadily increased

Behavior and analysis of CRC beams under high-cycle shear fatigue was reported by Ueda and Okamura (1981, 1983). Specimens consisted of eleven T-beams with stirrups, four rectangular beams with bent-up flexural reinforcing, and sixteen rectangular beams without stirrups. Rectangular beams were 11.8 x 11.8 in., T-beams were 19.7 in. high, 7.9 in. web width, 19.7 in. flange width, and 5.9 in. flange thickness. Two sizes of beams without stirrups were studied: 7.9 x 19.7 in. and 9.8 x 15.7 in. Span to depth ratios were 2.0 and 4.0. Fatigue loading histories were varied for different specimens and the maximum applied shear was 0.62 of the calculated static strength. The average measured stress range in the specimens was approximately 14.5 ksi and an empirical relationship was developed to predict the stirrup stress range. Nine of the eleven T-beams exhibited stirrup fractures and were isolated in the short shear-span length of the specimens.

The shear-fatigue behavior of concrete beams with both normal and high-strength concrete was investigated by Kwak and Park (2001). Beam specimens were 5.9 x 11.8 in. and contained 4-#6 flexural reinforcing bars. Specimens with and without shear reinforcing were investigated. Stirrups consisted of #3 bars and spacing varied from 3.9 to 7.8 in. Stirrup fractures were observed for the wider stirrup spacing (stress ranges in stirrups were not reported). Fatigued specimens failed at loads of approximately 60% of the static strength around 2 million cycles and high-strength concrete exhibited reduced fatigue capacity compared with normal-strength concrete.

Fatigue tests of deep beams were performed by Teng *et al.* (1998). Seven specimens were subjected to high-cycle fatigue. Specimen size was 23.6x49.2 in. and the test span to specimen height ratio was 1.0. Three different web reinforcing schemes were included in the test program; no transverse or skin steel, stirrups only, and stirrups with skin steel. The load range applied during fatigue tests varied from 0.2 to 0.8, 0.4 to 0.8, and 0.2 to 0.6 of the static strength for the different specimens. Results suggested that deep beams failing in shear under static loads may fail in flexure under fatigue loads.

Shear fatigue of prestressed concrete girders has been investigated by Hanson *et al.* (1970), Price and Edwards (1971), and Kreger et al. (1989). Kwak *et al.* (1991) studied the shear-fatigue behavior of small-scale beams containing both flexural and transverse steel combined with steel fiber reinforcement. Results of these studies are not directly comparable with conventional CRC beams.

High-Cycle Fatigue of Bond

Rehm and Eligehausen (1979) performed pull-out tests using constant amplitude loading to develop a relationship between slip and the number of cycles, if bond failure in fatigue was not reached. Repeated loading produced bond deterioration due to micro-cracking and micro-crushing of concrete around the reinforcing bar. Bond fatigue of pull-out specimens was also investigated by Balazs (1998). Repeated loading histories included constant, variable, and random amplitudes. Results indicated that constant amplitude load histories provided an upper-bound compared with variable amplitude tests. Specimens avoided fatigue failure until the slip magnitude reached that of the monotonic bond strength. Bresler and Bertero (1966) cast reinforcing bars having strain gages along the bonded length into concrete prisms to test in tension. The formation of the crack, debonding, and strain under changing loads were tracked as the bars were loaded cyclically. Bond effectiveness depended on the magnitude of the previous maximum load.

High-Cycle Fatigue of Reinforcing Steel

HCF of reinforcing steel has been studied by Hanson *et al.* (1968), Hanson *et al.* (1974), Helgason and Hanson (1974), Jhamb and MacGregor (1974), Corley *et al.* (1978), and Kreger *et al.* (1989). Fatigue tests have been conducted on reinforcing bars in air and bars embedded in flexural beams. Fatigue life of embedded reinforcing is typically longer than that of an equivalent bar in air due to bond that reduces the reinforcing bar stress away from locally high stresses across a crack. Fatigue cracks typically initiate at the transverse rib along the surface of the bar and the fatigue behavior depends on the stress conditions, reinforcing bar geometry including deformation height, base radius, width and bar diameter, as well as material properties (Hanson *et al.*, 1974; ACI-215, 1992). Fatigue life has generally expressed in terms of the stress range (Hanson *et al.*, 1974). The current ACI specification (ACI-318, 2002) does not address fatigue of reinforcing steel although ACI Committee 215 (1992) recommends a maximum service-level stress range, σ_r (ksi), for straight deformed reinforcing bars of:

$$\sigma_r = 23.4 - 0.33\sigma_{\min} \tag{1}$$

where σ_{min} (ksi) is the minimum stress with tension taken as positive and compression taken as negative. The σ_r need not be taken as less than 20 ksi. The current AASHTO provisions (2002) specify a maximum stress range for flexural reinforcement at service loads with impact be calculated as:

$$\sigma_r = 21 - 0.33\sigma_{min} + 8\frac{r}{h} \tag{2}$$

where σ_{min} (ksi) is the minimum stress as defined previously, and r/h is the ratio of the base radius to transverse deformation height. When the r/h ratio is not known, a value of 0.3 is recommended.

The fatigue behavior of full-sized RC bridge girders in shear dominated response under realistic service-level stress ranges has not previously been investigated. Small laboratory specimens often introduce failure mechanisms unlikely to occur in real bridge girders. Additionally, flexural details that may impact shear fatigue behavior have not been studied.

LABORATORY TESTING

Nine full-size girders were subjected to high-cycle fatigue to examine response during loading and assess changes that occur due to the fatigue load cycling. After imposing significant diagonal cracks the specimens underwent cyclic loading before being tested to failure. These three stages are referred to as Precracking, Fatigue, and Failure. The beam naming convention was as follows: The first number referred to the casting order since the 44 beams of the full study were made in groups of four, the T and IT referred to beam configuration, and the last number gave the stirrup spacing in inches. Some specimens had an additional number to differentiate beams with identical detailing in the same cast group.

The specimens, loading, instrumentation, and cracks are shown in elevation view and cross-section in Appendix A. All specimens were 26 ft long and had the same T-beam cross-section, with a 6 in. x 36 in. deck and 42 in. x 14 in. stem. Specimen variables included beam configuration, stirrup spacing, and flexural reinforcement anchorage details. Three of the specimens were tested in the T configuration to represent positive moment with the deck in flexural compression and six were rolled to test in an inverted-T position to represent negative moment with the deck in flexural tension. Stirrup spacings were 10 in., 12 in., and 18 in. The typical flexural reinforcement extended the full length of the beam and were hooked in the

T beams, except 8IT10 and 9IT12-1 which each had two flexural cut-offs and 9T12-4 which had flexural cut-offs and no hooks at the beam ends.

Concrete mixes and steel were chosen to reflect 1950's vintage material properties and are summarized in Table 1. The average concrete strength, f'_c, was 4402 psi in the stem and 4158 psi in the deck. The stirrups in all specimens were from a single heat of ASTM A615 Grade 40 reinforcing steel with a yield stress of 50.7 ksi.

Instrumentation included load cells, strain gages, and displacement transducers. General strain gage and transducer placement can be seen in Figure 1. The load cells measured applied loads and for some of the initial beams a load cell was placed at the south support reaction during fatigue loading to verify that force distribution may be calculated by static analysis. Stirrups instrumented with a strain gage in the laboratory were cast into most of the specimens; these were placed such that the gages would be at 22 in. from the base of the stem on the east leg according to beam orientation during testing. Various displacements were measured by the transducers including midspan deflection and diagonal crack movements. Before any loading, the east face of each specimen was whitewashed and marked with a 1 ft grid to facilitate the monitoring of crack propagation. The locations of the stirrups were also marked on the east face using a rebar locator. As testing was carried out, individual displacement transducers were mounted at selected diagonal cracks on the west face to monitor diagonal crack growth and activity. Additional strain gages were applied to the west legs of stirrups after initial cracking to monitor the reinforcement strains at the locations crossing diagonal cracks.

Precracking Stage

In order to represent the field observed conditions and engage the stirrups, all specimens were initially loaded in the four-point setup shown in Figure 2 to produce diagonal cracks before fatiguing. A spreader beam with load points spaced 24 in. apart applied a force at midspan which was measured with a 500 kip capacity load cell mounted to the hydraulic actuator. The support spacing was 24 ft for the T beams but 21.7 ft for all the IT beams except for the first fatigue specimen, 3IT12, since anchorage failures were noted in the IT control tests of the full study; the IT beams lacked the hooks of the T specimens but the shorter span length ensured sufficient straight-bar development length of the flexural steel.

In general, precracking was performed by placing and then removing the applied force, increasing the load by a constant increment at each step. As diagonal cracks formed, individual crack displacement transducers were attached to cracks of interest and these were also monitored with an Oregon Department of Transportation (ODOT) crack comparator at load and after unloading. This was done until crack widths, shown in Table 2, measured without load by the crack comparator were reflective of the range of widths observed in the field. The imposed diagonal cracks were at least 0.025 in. The crack widths at maximum precrack load are also shown. It was observed that a number of strain gages near a crack reach yield in precracking. The greatest diagonal displacement activity occurred in the portion of the shear span closest to the load.

Upon completion of precracking, locations were identified on the north and south sides of the beams where diagonal cracks crossed stirrups. After the stirrup locations were reconfirmed, concrete was removed from around the stirrups at the diagonal crack locations from the west face. The embedded stirrup leg was exposed for a length of approximately 2 in. and strain gages were attached to the prepared stirrup surfaces within the deformation pattern of the bar.

Fatigue Stage

Upon achieving the desired diagonal crack widths, the specimens were moved to the test frame illustrated in Figure 3. The high-cycle fatigue loading was performed in load control by a 110 kip capacity fatigue-rated actuator, mounted to the steel reaction frame, in series with a load cell and spreader beam identical to the precracking arrangement. The cyclic loading was sufficiently low such that flexural anchorage was not of concern so all beams were tested at a support spacing of 24 ft. Simulated dead load—representing the weight associated with a bridge girder such as deck, diaphragms, railing, wearing surface, etc.—not including self-weight, was applied concurrently by a hydraulic cylinder at 4 ft north of the beam centerline. An attached hydraulic accumulator was used to compensate for the pressure drop in the cylinder due to specimen deformation under fatigue load cycling. The resulting dead load typically averaged 80 to 100 kips and remained fairly steady during fatigue load cycling with small ranges in the later beams. Adjustments were made to the hydraulic accumulator as necessary due to hydraulic oil temperature changes and seal leakage that occasionally caused a loss of applied dead load. The applied load ranges and means as measured by the load cells can be compared in Figs. 4 and 5, and the plots are also shown in Appendix B. The offset application of dead load and diagonal cracks produced a complicated stress field in the north shear span. Therefore, only the south span will be examined here.

Fatigue load was based on field measurements from four in-service bridges as reported by Higgins (in pub. queue). During the period of observation of 85 instrumented stirrups in the four different bridges, the highest single stirrup stress range recorded at any location was 11.5 ksi. The collected data was evaluated to compute the equivalent constant amplitude stress range for each stirrup, extended out to approximate 50 years of service, and finally used to calculate the laboratory stress range required to produce equivalent damage over 2,000,000 cycles, a common length of testing in fatigue studies. This was accomplished by applying Miner's Rule for fatigue damage accumulation, recognizing that the bridges are assumed to be reaching the end of a 50 year design life, in the form of the equation:

$$SR_{eqv} = \sqrt[3]{\sum \frac{n_i}{N_{tot}} SR_i^3} \tag{3}$$

where SR_i is the i^{th} stress range, n_i is the number of cycles observed for the i^{th} stress range, and N_{tot} is the total number of cycles at all stress ranges. All calculated equivalent laboratory stress range values were under 8.7 ksi except one that was 13.8 ksi. The magnitude of fatigue load during testing, chosen to vary from 4 to 84 kips, produced in each beam at least one measured stirrup stress range of about 13.8 ksi (476 $\mu\varepsilon$). The shear loading in the south span is summarized in Table 3, with estimated values based on the other specimens where no measurements were available. The average load placed on the stirrups during fatigue cycling was 30% and ranged from 19% to 40% of the nominal shear capacity based on modified compression field theory (MCFT) as presented in the American Association of State Highway and Transportation Officials (AASHTO) Load and Resistance Factor Design (LRFD) Bridge Design Specifications (AASHTO, 2002).

Fatigue load cycling was performed at 2.4 Hz which enabled 2,000,000 cycles to be completed in about 10 full days, barring equipment fatigue and ruptures or pauses for other tests that used the same hydraulic system. During this time, only the load cells, strain gages, and individual crack sensors recorded data. Where available, plots of load ranges and means, south individual crack displacement ranges and means, and south strain ranges and means are organized by specimen and shown in Appendix B. Note that the crack means had been adjusted to begin at about zero but most of the strain means were not.

At intervals of approximately 100,000 cycles up to 500,000 cumulative cycles and then every 250,000 cycles until 2 million cumulative cycles, the fatigue loading was suspended to conduct controlled tests to confirm fatigue load cycling behavior and to capture data from the sensors that are detached during cycling. With the fatigue load at 2 kips to maintain contact and the dead load held at 80-100 kips, crack widths were measured using the ODOT crack comparator. Midspan and diagonal displacement sensors were then reattached and a typical loading sequence was performed: 10 cycles, fatigue load ranging from 4 to 84 kips, 0.5 Hz; 5 cycles, 4 to 104 kips, 0.1 Hz; and 10 cycles, 4 to 84 kips, 0.5 Hz. The first 15 cycles ensured seating of the reapplied sensors and data were taken from the final 10 cycles of this sequence where possible. These check tests are discussed in further detail subsequently.

All specimens underwent 2,000,000 cycles but variations in data collection occurred. Test descriptions of each beam are summarized below. Some of the instrumentation information is also provided with the specimen plans in Appendix A.

Specimen 3IT12

This first IT specimen had been precracked at a 24 ft span to a diagonal crack width of 0.025 in. after an applied load of 260 kips; it was then accidentally loaded up to 300 kips that corresponds to 81% of nominal shear capacity but no further cracking was noted. Three of the four crack gages were then moved and four additional strain gages were added—two to the north side and two to the south side, each on a different crack—before fatiguing. The combined applied cyclic and dead loads caused a shear ranging from a minimum of 25% to a maximum of 39% nominal shear capacity. Check tests were performed at approximately 1,000, 750,000, 1,000,000, 1,250,000, 1,500,000, and 1,750,000 cycles. Those performed at 2,300 and 5,600 were not considered since no significant difference was noticed from the 1,000 check test.

On the south side of the beam, the individual crack transducer locations and a couple other spots were monitored with the ODOT crack comparator at various times, not necessarily along with a check test. The measurements showed a small initial increase followed by no discernable change or a very subtle increase, difficult to ascertain by eye. About four diagonal crack extensions were noted along with a number of vertical cracks extending down from the stem end that may be the result of shrinkage or misapplied whitewash, see Figure A1a.

The data recorded during fatigue load cycling is shown in Figures B1a-c. The very steady load ranges in Figure B1a likely indicate a steady load mean as the equipment was relatively unused at this point. The range of the dead load is high, and it can be seen in the figure and Table 3 that the resulting applied load range is smaller than that of later beams. Under this load, the crack ranges showed a constant increase while the strain ranges remained nearly level.

Specimen 3T12

This specimen had been precracked to a diagonal crack width of 0.025 in. after an applied load of 260 kips that corresponds to 78% of nominal shear capacity. Internal strain gage GS6 was noted as broken before precracking. Then one crack gage was moved and another was added along with four additional strain gages—two to the north side and two to the south side, each on a different crack. The combined applied cyclic and dead loads caused a shear ranging from a minimum of 25% to a maximum of 40% nominal shear capacity. Being the first beam tested, a variety of load combinations were applied during the initial cycles and for check tests. Check tests were performed at approximately 4,000, 1,250,000, 1,610,000, and 2,000,000 cycles.

The same crack behavior of an initial increase followed by nearly no change was recorded as measured by the ODOT crack comparator. Six new cracks and extensions were marked after fatigue loading, see Figure A2a.

The data recorded during fatigue load cycling is shown in Figures B2a-c. The last half of the fatigue load cycling data was captured, again showing steady load ranges that imply steady load means and a high dead load range that gives a smaller applied load range. The crack ranges show a constant decrease and a number of the strain gages also show a slight decrease. GS3 appears to break after 1,600,000 cycles but functions in the failure stage.

Specimen 3IT18

This specimen had the widest stirrup spacing at 18 in. and had been precracked to a diagonal width of 0.07 in. after an applied load of 225 kips that corresponds to 71% of nominal shear capacity. The individual crack displacement sensors were left in place from precracking and six additional strain gages were applied—three to the north along the same crack and three to the south along the same crack. The combined applied cyclic and dead loads caused a shear ranging from a minimum of 22% to a maximum of 48% nominal shear capacity. Check tests were done at approximately 0, 100,000, 200,000, 300,000, 400,000, 500,000, 750,000, 1,000,000, 1,250,000, 1,500,000, 1,710,000, and 2,000,000 cycles. Problems with the dead load cylinder caused abrupt changes at before 700,000 cycles and just after 1,800,000 cycles.

During fatigue loading, an abrupt change was registered just after 1,765,000 cycles that was nearly obscured by the loss of dead load just after 1,800,000 cycles. It can be seen that the values suddenly increase or decrease in Figure 6, which focuses on the relevant sections of Figures B3e and B3f with the dead load discrepancy and scatter ignored with solid lines. Examination of the stirrups after the failure stage revealed that two legs had undergone brittle fracture unlike other stirrup legs that exhibited a more ductile necking, pictured in Figure 7. The approximate locations of the brittle fractures are given in Figure 8. Looking at this drawing in conjunction with Figure A3a, GS7 is at a diagonal crack and the fracture was 2 in. above on the stirrup's west leg; the other fracture is on the east leg of the stirrup about 9 in. below GS2 at a short crack that merges with the longer crack below it on the west face. From the behavior of GS3 and GS7 the brittle fracture of the stirrup on which they were located likely occurred during fatigue at the time of the abrupt changes. The other brittle fracture did not have a strain gage conveniently placed close by on the same stirrup leg so the timing is unsure; the gage GS3, opposite the first fracture, increased until the gage failed but at 1,765,000 cycles the gage GS6, opposite the second fracture, appeared to increase and then hold steady. While the two fractures may have occurred at the same time and the stirrup leg with GS6 merely did not behave identically to GS3, the second fracture may have come at failure.

Using the ODOT crack comparator, the south side behaved in the same manner as the previous beams of showing an initial increase followed by little change, until fracture occurred. Then a noticeable jump was found only on the south side, with the gages on the main diagonal crack showing increases and the one location on another crack decreasing slightly. New cracks and extensions were noted along the main diagonal crack on the south side where fracture was later discovered to have happened, see Figure A3a.

The data recorded during fatigue load cycling is shown in Figures B3a-f. Where the loading is constant the trends in the cracks and strains can be noted. The cracks showed a steady rise in both range and mean until fracture, and at a higher rate when the dead load was adjusted. The strains overall remained fairly level until the fractures occurred, although individual strains showed slight increases or decreases.

Specimen 5IT12-1

This specimen had been precracked to a diagonal crack width of 0.05 in. after an applied load of 330 kips that corresponds to 93% of nominal shear capacity. Then five additional strain gages were added—two on the south side along the same crack and three on the north side. The combined applied cyclic and dead loads caused a shear ranging from a minimum of 18% to a maximum of 40% nominal shear capacity. Check tests were performed at approximately 144,000, 315,000, 526,000, 750,000, 1,000,000, 1,250,000, 1,500,000, 1,750,000, and 2,000,000 cycles. No strain data was collected from 1,171,500 to 1,531,400 cycles due to equipment failure; no strain data is available for the two check tests performed in that interval.

The same crack behavior of an initial increase followed by nearly no change was recorded as measured by the ODOT crack comparator. No new cracks or extensions were found after fatigue loading, see Figure A4a.

The data recorded during fatigue load cycling is shown in Figures B4a-e. The crack mean appeared to have a steady increase while the range remained nearly level after an initial increase. The strain ranges were steady although individual gages registered slight increases or decreases.

Specimen 6IT10

This beam was cast without strain gages. Precracking had been applied to cause a diagonal crack width of 0.04 in. after a load of 375 kips that corresponds to 89% nominal shear capacity. After this stage some changes were made to the north side individual crack sensors and one was added to the south side. Six strain gages were applied to each side; on the south there were four along the same crack and two on the eventual failure crack. The combined applied cyclic and dead loads caused a shear ranging from a minimum of 15% to a maximum of 35% nominal shear capacity. Check tests were performed at approximately 0, 100,000, 200,000, 301,000, 400,000, 500,000, 750,000, 1,000,000, 1,250,000, 1,500,000, and 1,750,000 cycles. The loading equipment began showing signs of fatigue itself during the fatigue load cycling of this beam, causing abrupt changes before 300,000 cycles, about 600,000 cycles, after 1,100,000 cycles, and at 1,400,000 cycles.

In general, the same crack behavior of an initial increase followed by nearly no change was recorded as measured by the ODOT crack comparator although the inconstant loading likely affected measurements of this small scale and such trends were not immediately obvious. No new cracks or extensions were found after fatigue loading, see Figure A5a.

The data recorded during fatigue load cycling is shown in Figures B5a-f. The dead load cylinder problems caused the data to appear quite choppy but trends can be observed where the load was constant for a time. The crack means and ranges show a steady increase. The strain means do not change but the ranges appear to increase slightly overall. The gage GS3 is spotty but functions correctly in the failure stage.

Specimen 6T10

This was the second beam cast without strain gages. Precracking had been applied to cause a diagonal crack width of 0.07 in. after a load of 400 kips that corresponds to 108% nominal shear capacity. The individual crack displacement gages were left in place and eight strain gages were added to each side. On the south side there were two strain gages on the same crack and two other cracks had three strain gages each. The combined applied cyclic and dead loads caused a shear ranging from a minimum of 16% to a maximum of 38% nominal shear capacity. Check tests were performed at 0, 100,000, 200,000, 300,000, 400,000, 494,000, 750,000, 1,000,000, 1,250,000, 1,500,000, 1,750,000, and 2,000,000 cycles. Problems were encountered with the dead load cylinder that caused some abrupt changes after 473,000 cycles, near 710,000 cycles, around 1,250,000 cycles, and after 1,600,000 cycles.

In general, the same crack behavior of an initial increase followed by nearly no change was recorded as measured by the ODOT crack comparator although the inconstant loading likely affected measurements of this small scale and such trends were not immediately obvious. About seven new cracks or extensions were found after fatigue loading, see Figure A6a.

The data recorded during fatigue load cycling is shown in Figures B6a-f. The crack ranges all showed an increase while the means slightly increased or decreased. The strains were all nearly constant in range and mean, although the range of GS8 seemed to increase. The gage GS3 appears to break early on but functions in the failure stage.

Specimen 8IT10

This beam was detailed such that the two outer flexural reinforcement bars extended only 7 ft from centerline instead of the whole length. An attempt had been made to predict the precracking load with this specimen: The ultimate strength of a similarly detailed beam was identified, factors for strength reduction were calculated based on stem concrete strength and the cut bars using information from previously tested beams, and 85% of this reduced strength was taken to be the precracking load. This specimen had been precracked to a diagonal crack width of 0.03 in. after an applied load of 350 kips that corresponds to 89% the nominal shear capacity based on AASHTO LRFD MCFT. It was then discovered that the beam had been flipped such that the embedded strain gages were on the west stirrup legs. Three strain gages were applied to three different diagonal cracks on the east legs of selected stirrups and associated individual crack displacement transducers were mounted on the east face of the beam. The combined applied cyclic and dead loads caused a shear ranging from a minimum of 15% to a maximum of 35% nominal shear capacity. Check tests were performed at 200,000, 300,000, 400,000, 500,000, 750,000, 1,000,000, 1,750,000, and 2,000,000 cycles. Dead load cylinder problems caused a small jump at about 1,350,000 cycles and a loss of load after 1,800,000 cycles.

In general, the same crack behavior of an initial increase followed by nearly no change was recorded as measured by the ODOT crack comparator. Most of the main diagonal cracks on the south side exhibited new extensions after fatigue loading, see Figure A7a.

The data recorded during fatigue load cycling is shown in Figures B7a-f. The crack means appear to remain level while the ranges all increased. A couple of the strain means show a slight increase but nearly all remain level. The GS3 strain behaved strangely during the first half of fatigue load cycling. The sensor was engaged in precracking and showed a very large strain which may have caused the odd initial readings. For the last half of fatigue load cycling GS3 showed a level range and mean.

Specimen 9IT12-1

This beam was detailed in the same way as 8IT10, so that the two outer flexural reinforcement bars extended only 7 ft from centerline instead of the whole length. The specimen had been precracked to a diagonal crack width of 0.025 in. at an applied load of 300 kips that corresponds to 84% nominal shear capacity. Then two strain gages were added to the north side and four were applied to the south along the same diagonal crack although it branched near mid-height. The combined applied cyclic and dead loads caused a shear ranging from a minimum of 17% to a maximum of 39% nominal shear capacity. Check tests were performed at 0, 100,000, 200,000, 300,000, 400,000, 500,000, 750,000, 1,000,000, 1,250,000, 1,500,000, 1,750,000, and 2,000,000 cycles. Due to equipment problems no south diagonal displacement or south individual crack sensor data were recorded during the first check test. Dead load problems caused little jumps in data at after 600,000 cycles, before 1,000,000 cycles, at 1,250,000 cycles, and around 1,700,000 cycles.

In general, the same crack behavior of an initial increase followed by nearly no change was recorded as measured by the ODOT crack comparator. A few new crack extensions were noted on the south side after fatigue loading, including at a flexural crack at the longitudinal reinforcement cut-off, see Figure A8a.

The data recorded during fatigue load cycling is shown in Figures B8a-f. The crack means and ranges show a subtle increase. The strain gages register nearly no change. The gage GS5 recorded very high numbers during the first half of fatigue load cycling but then seemed to steady into values in the same range as the other strain gages. Since GS5 behaved normally in the precrack and failure stages and no other instrument seemed to react in the same manner, the first half of fatigue load cycling is ignored for this gage.

Specimen 9T12-4

This T-specimen was detailed with two flexural reinforcement bars extending only 7 ft from the centerline and three flexural reinforcement bars extending the full length of the beam but terminating without anchorage hooks. The specimen had been precracked to a diagonal crack width of 0.06+ in. at an applied load of 250 kips that corresponds to 85% nominal shear capacity. One crack gage was moved to allow placement of a strain gage and two more were added; three additional strain gages were applied to the south side, two on the eventual failure crack. The combined applied cyclic and dead loads caused a shear ranging from a minimum of 20% to a maximum of 48% nominal shear capacity. Check tests were performed at

0, 100,000, 200,000, 300,000, 400,000, 500,000, 750,000, 1,250,000, 1,500,000, 1,750,000, and 2,000,000 cycles. Problems with the dead load cylinder, including a memorable oil leak, caused jumps in the data between 500,000 and 600,000 cycles, after 1,000,000 cycles, and after 1,600,000 to the end of fatigue load cycling.

In spite of load loss, slight increases in crack size were recorded as measured by the ODOT crack comparator. A few new crack extensions were noted after fatigue loading, see Figure A9a.

The data recorded during fatigue load cycling is shown in Figures B9a-f. Though the dead load decreases, both the means and ranges of the crack gages increase. A number of the strain gages also increase in range and mean.

<u>Failure Stage</u>

Upon completion of fatigue load cycling the specimens were moved back to the precrack setup and loaded until failure. Total applied load versus midspan displacements, individual crack displacements, strain gage data, and diagonal displacements recorded during precracking and failure were plotted. For these graphs and more information on fabrication methods, material tests, equipment, laboratory test procedures, and ultimate shear capacity of the fatigued beams see the full report (Higgins, 2004a).

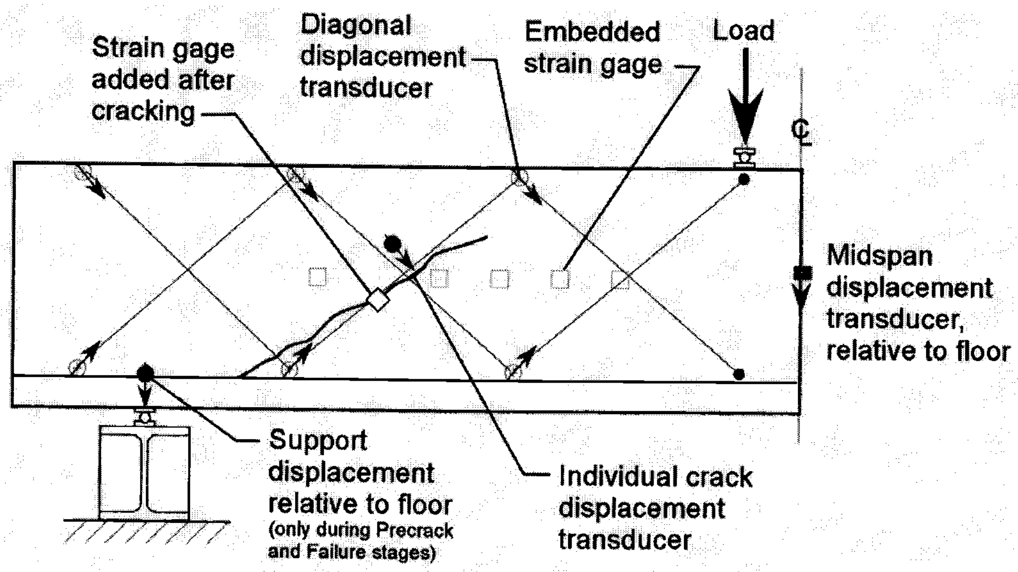

Figure 1–View of typical instrumentation, west face of the specimen.

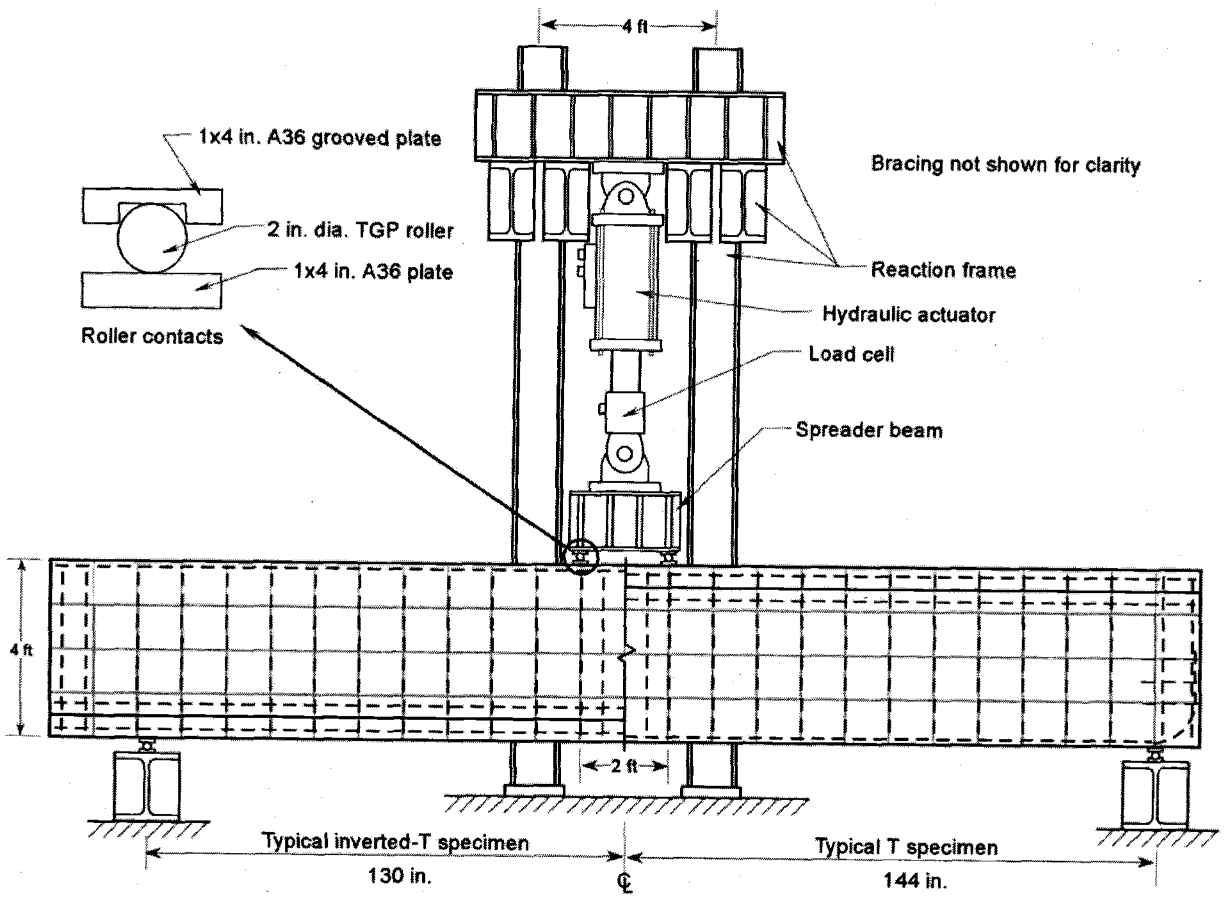

Figure 2–Laboratory setup for precracking and failure stages.

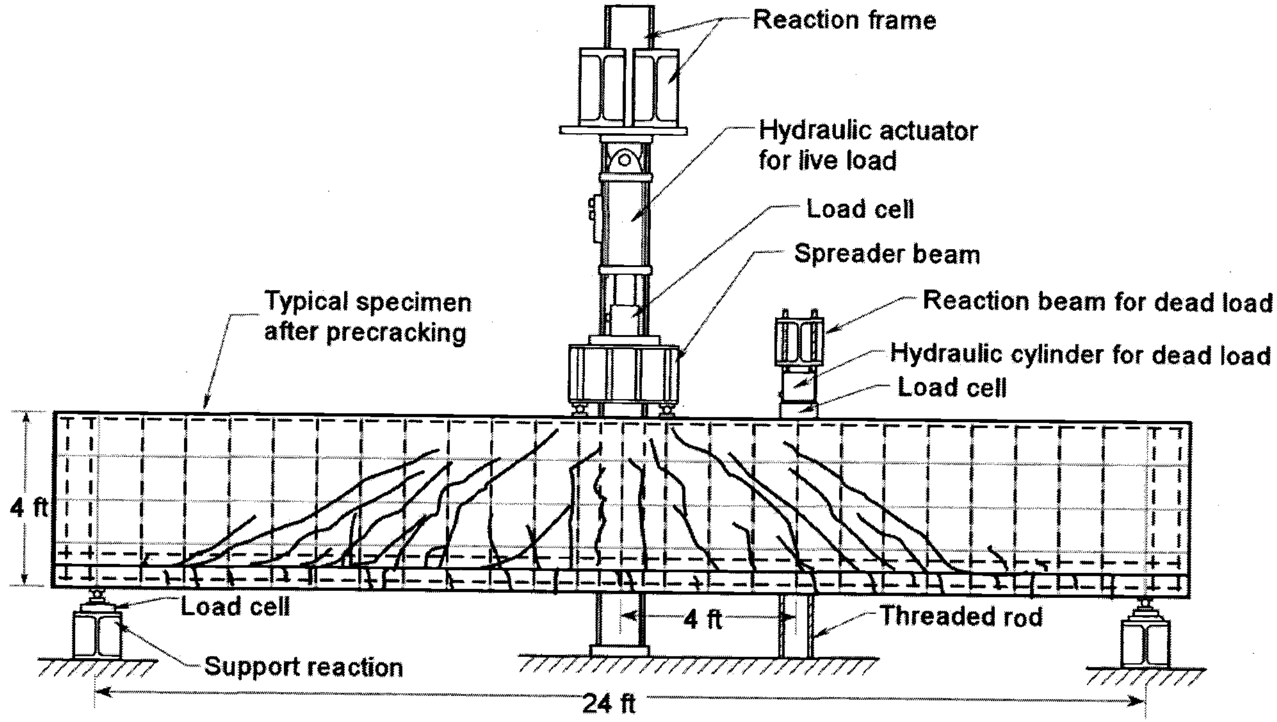

Figure 3–Laboratory setup for high-cycle fatigue.

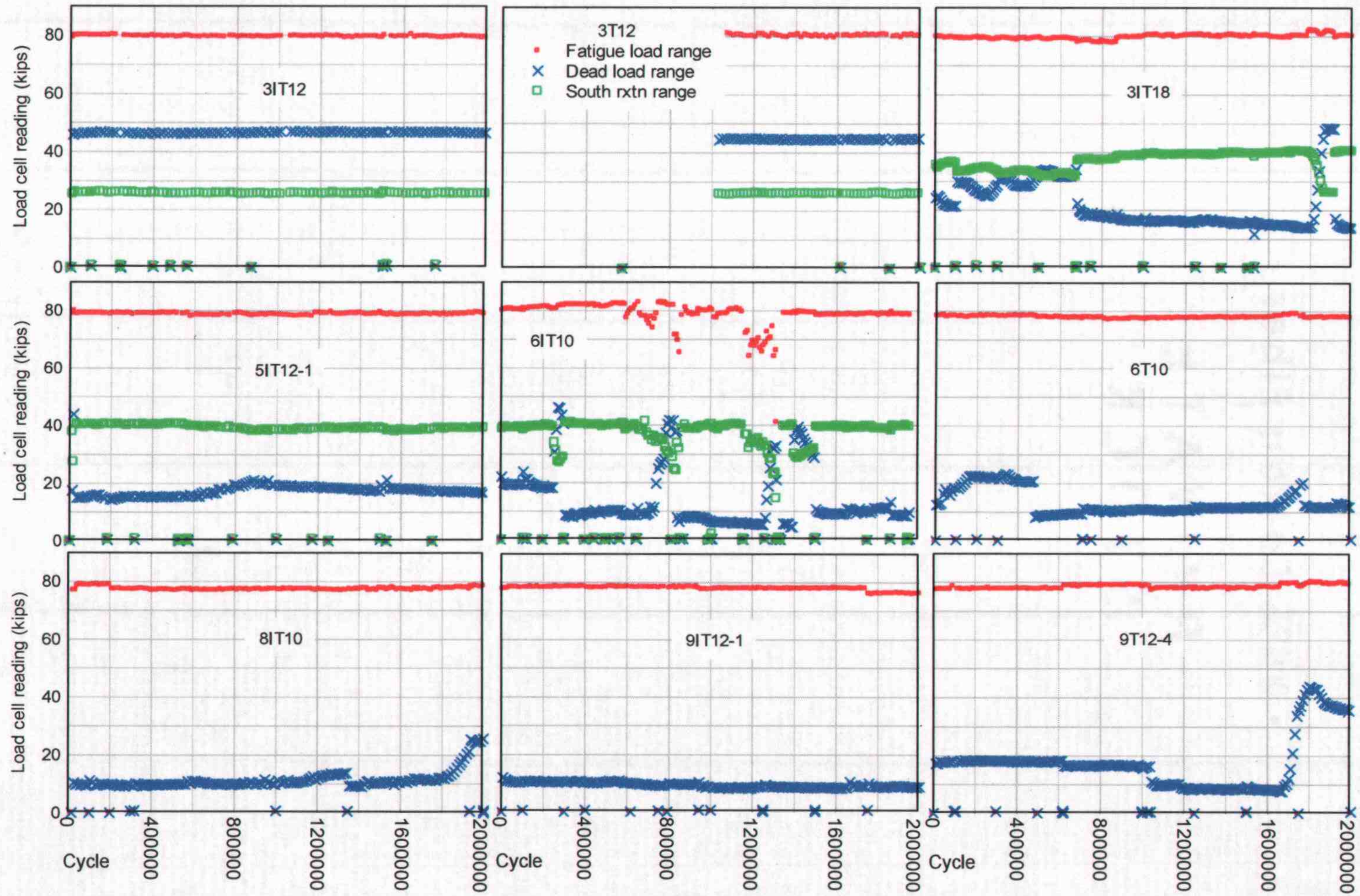

Figure 4–Load ranges during cycling.

Figure 5–Load means during cycling.

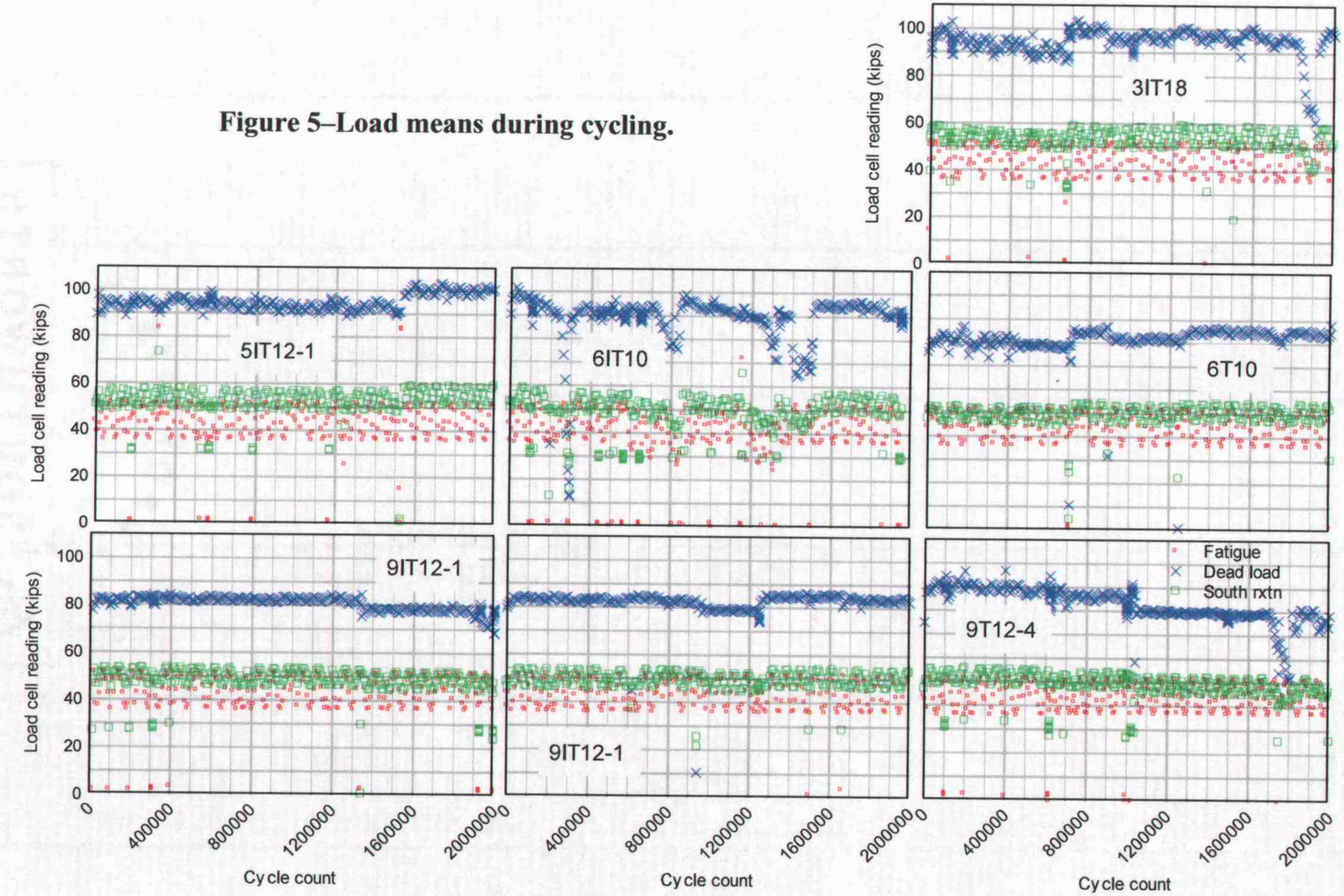

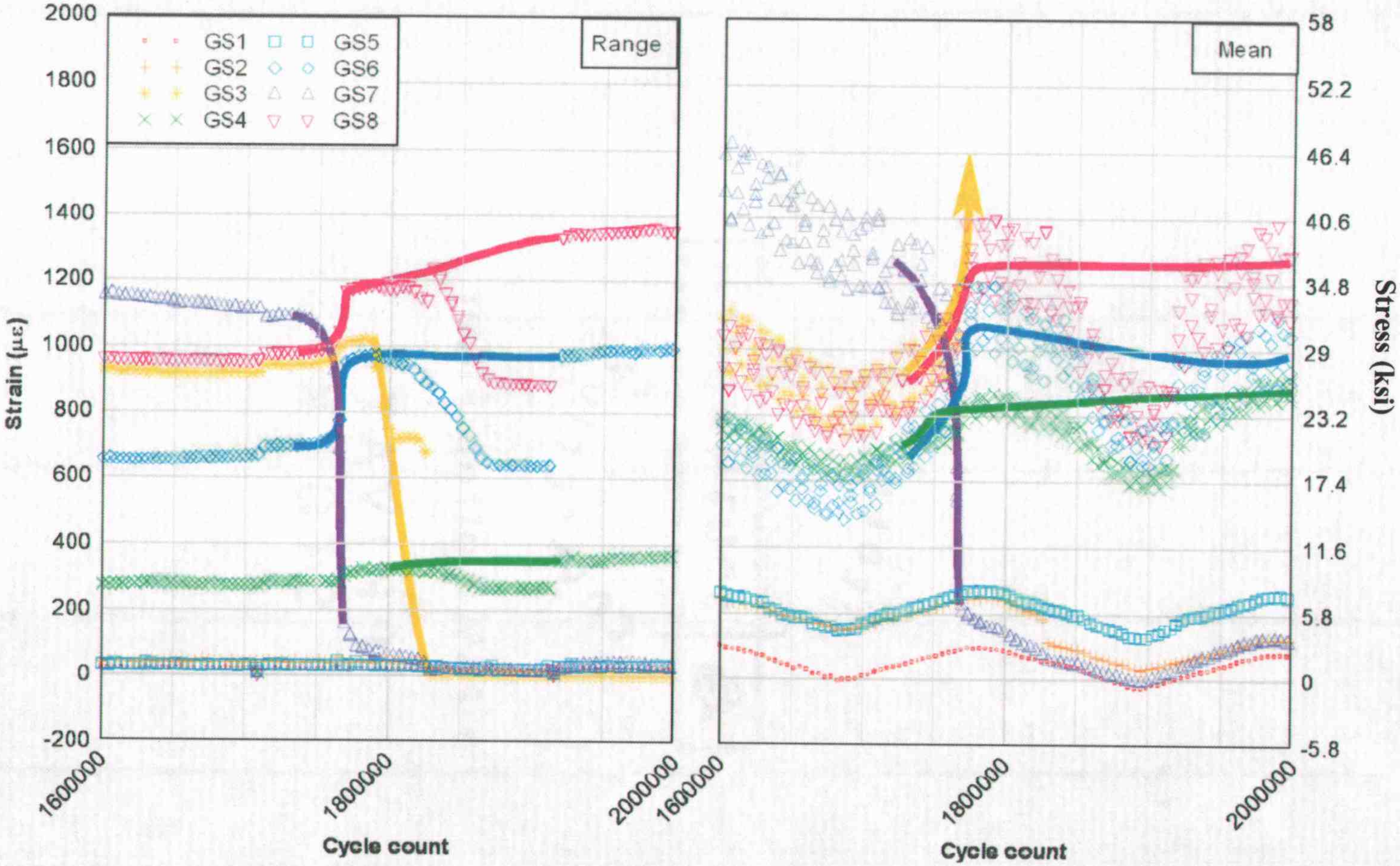

Figure 6–Detail of specimen 3IT18 south strain ranges and means showing an abrupt change at 1,765,000 cycles.

Figure 7–Examples of stirrup failure: a ductile necking from specimen 3IT12 and the brittle fracture below GS2 from specimen 3IT18.

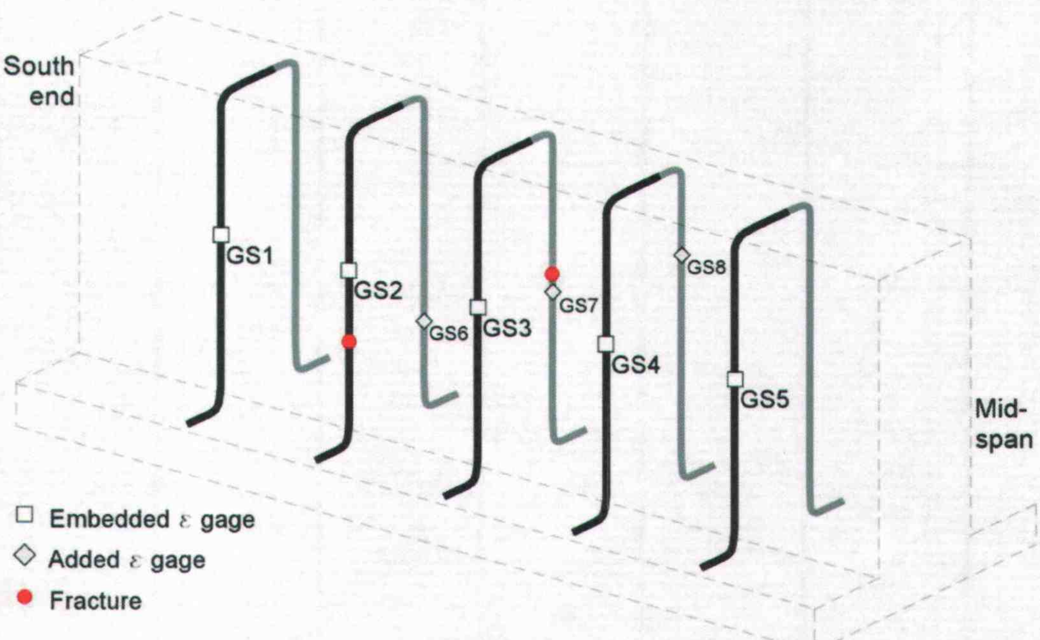

Figure 8–Showing brittle fracture locations in specimen 3IT18.

Table 1–Concrete and steel properties on the days of the tests.

Specimen	Concrete			Reinforcing Steel											
	Stem		Deck	#4 Grade 40			#11 Grade 60			#6 Grade 60			#4 Grade 60		
	f'_c (psi)	ε'_c	f'_c (psi)	σ_y (ksi)	σ_u (ksi)	σ_f (ksi)/ ε_f	σ_y (ksi)	σ_u (ksi)	σ_f (ksi)/ ε_f	σ_y (ksi)	σ_u (ksi)	σ_f (ksi)/ ε_f	σ_y (ksi)	σ_u (ksi)	σ_f (ksi)/ ε_f
3IT12	4180	NA	3455				69.7	103.7	82.0/ 0.220	60.7	88.1	70.8/ 0.325	67.3	107.1	NA
3T12	3990	0.0021	3660												
3IT18	3915	0.0018	3220												
5IT12-1	3700	0.0018	4610				69.2	103.3	81.3/ 0.215	59.5	83.8	69.5/ 0.220	59.8	100.3	77.7/ 0.262
6T10	4595	0.0024	4195	50.7	78.9	71.1/ 0.286	71.6	106.4	83.0/ 0.221	62.9	89.1	70.4/ 0.223	NA	NA	NA
6IT10	5495	0.0025	3875												
8IT10	4750	0.0020	4090				74.9	98.9	74.0/ 0.265	63.6	91.1	85.0/ 0.298	67.1	110.8	NA
9IT12-1	4285	0.0021	5405				70.8	96.1	68.5/ 0.271	62.6	90.0	89.0/ 0.287	NA	NA	NA
9T12-4	4705	0.0025	4910												
Avg.	4429	0.0021	4246				71.2	101.7	77.8/ 0.238	61.9	88.4	76.9/ 0.271	64.7	106.1	77.7/ 0.262
COV (%)	13.1	13.3	16.6				3.2	4.1	8.1/ 11.4	2.7	3.2	12.1/ 17.3	6.6	5.0	NA

Table 2–Precrack stage crack widths.

Specimen	Precrack Load (kips)	Maximum w_{cr} (in)	
		At no load	At precrack load
3IT12	300	0.025	0.040
3T12	260	0.025	0.050
3IT18	225	0.070	0.105
5IT12-1	330	0.050	0.060
6IT10	375	0.040	0.070
6T10	400	0.070	0.110
8IT10	350	0.030	0.060
9IT12-1	300	0.025	0.060
9T12-4	250	0.06+	0.095

Table 3–South span shear during fatigue load cycling.

Specimen	V_{AASHTO} (kips)	Mean, south V (kips)	Range, south V (kips)	Minimum south V (kips)	Maximum south V (kips)	Mean % V_{AASHTO}	Min % V_{AASHTO}	Max % V_{AASHTO}
3IT12	185	59	26	46	72	32	25	39
3T12	168	54	26	41	67	32	24	40
3IT18	156	55	40	35	75	35	22	48
5IT12-1	180	52	40	32	72	29	18	40
6IT10	210	53	40	33	73	25	15	35
6T10	185	50	40	30	70	27	16	38
8IT10	198	50	40	30	70	25	15	35
9IT12-1	180	50	40	30	70	28	17	39
9T12-4	147	50	40	30	70	34	20	48
					Average	30	19	40

LABORATORY RESULTS

Summary of Laboratory Testing

- Diagonal cracks were imposed on nine full-sized specimens that were then loaded for 2,000,000 cycles to simulate 50 years of use on the stirrups based on data gathered from in-service bridges. The stirrup stress range required to produce the estimated equivalent service life damage in this number of cycles was calculated to be 13.8 ksi.
- The average simulated loading range on the nine specimens was 19% to 40% of the AASHTO LRFD MCFT nominal shear capacity. Applying equation (3) to the recorded cycling strain ranges and multiplying by 29,000 ksi, an equivalent constant stress range was calculated for all the monitored locations on the south side of the specimens, shown in Table 4. All specimens had at least one location register a stress range of about 13.8 ksi or above, especially at gages located directly on a diagonal crack.
- Values collected during cycling are given in Tables 5 and 6 and show the ranges and means at the beginning and end of the fatigue phase. The changes due to cycling in these values are more easily viewed in Figure 9. Strain ranges and means either increase or decrease but generally change very little, although the average measured means increase very slightly

when equipment irregularities are accounted for. The crack ranges and means typically increase.

- In general, cracks exhibited an initial increase followed by either no apparent change or a very subtle increase that was detectable by the displacement transducers and sometimes by the ODOT crack comparator over many cycles.
- Crack widths were not reliable indicators of changes in strains. Crack extensions were not reliable indicators of changes in strains or crack widths. However, although actual diagonal crack width is determined by several variables including stirrup spacing and amount of longitudinal reinforcement, the change in diagonal crack width exhibited a linear relationship to strain range as plotted in Figure 10, shown with a best fit line. Strain gages applied at a diagonal crack and two embedded gages that were likely fully debonded were matched with associated crack displacement transducers. Higher cycling ranges caused cracks to become wider. The scatter of data may be the result of the placement of the diagonal crack displacement sensors, which were located at a distance from the strain gages.
- Brittle stirrup fracture occurred only in the specimen with the widest spacing, 3IT18. The first incident was accompanied by a decrease in strain of the gage on the same stirrup leg and a large increase of the opposite

stirrup leg. The crack magnitude also increased as recorded by hand measurement using the ODOT crack comparator and by the individual crack displacement sensors. Crack extensions associated with the fracture can be viewed on Figure A3a but are not a reliable visual indicator of the fracture since other beams displayed similar extensions without the same cause.

- During cycling, stirrup movement relative to the surrounding concrete due to debonding was observed at the locations of the applied strain gages where short lengths of reinforcement had been exposed. It may be assumed that the same movement occurs at any location where a diagonal crack crosses a stirrup.

The checktest data is summarized in Tables 7 and 8. The loads are also provided because fluctuations in the dead load cylinder impacted the recorded data. Since the checktests were to be conducted at the same loads specified for the cycling, they produced the same conclusions concerning changes in strain and crack range and mean. This is apparent when Figure 11 is compared to Figure 9. Thus the trends in the other data collected during checktests may be considered representative of behavior during cycling.

Since the checktest data was gathered continuously and more instruments were engaged, a more comprehensive description of behavior may be drawn from the checktests. Also, this collection of discrete points within the cycling facilitated the examination of other factors, namely gage location, crack angle, and distance of the strain gage from the crack.

The checktests may be summarized as follows:

- The midspan and diagonal displacement transducers were detached during cycling to avoid fatigue of the instruments, preventing accurate measurement of mean response values since residual displacements from each bout of cycling were unknown. The ranges are depicted in Figs. 12 and 13. Midspan displacement ranges show virtually no change. For the south diagonal displacement ranges, labeled Gr1-6 in Appendix A but named DDS1-6 in Fig. 13, the greatest activity is in the middle of the shear span and most have an increase. The specimens showing increases do not necessarily show crack extensions.
- It was stated above that strain range appeared to either remain fairly constant or increase and decrease a small amount while the crack ranges showed an overall increase. These changes do not distinguish themselves when graphed against horizontal position, vertical position, crack angle estimated from pictures (those near or on a crack for the strain gages), or

distance from the crack estimated from pictures (for strain gages only), Figures 14 and 15. No statement about these variables can be made regarding stirrup spacing, T or IT configuration, or anchorage details.

- Plotting the values themselves, position does not appear to impact strain or crack range magnitudes, Figure 16, showing ranges versus horizontal and vertical position of crack gages and only the added strain gages. Two specimens show higher strain ranges, the beam 3IT18 having the largest stirrup spacing and 9T12-4 having the cut and straight flexural anchorage. Two beams show higher crack ranges, the beams 9IT12-1 and 9T12-4 having the cut and straight flexural anchorage; the other specimen with cut flexural anchorage, 8IT10, did not have similar crack ranges, likely because of smaller stirrup spacing.
- Again plotting the values, crack range does not appear to be affected by crack angle but strain range from the added strain gages shows an increase with smaller crack angle, Figure 17. Specimen 9T12-4 displayed high strain ranges and had the steepest crack angles, closer to the 60-80° angles of the cracks observed in the field.
- Strain gages closer to a diagonal crack recorded a higher strain range, Figure 18.

Measurements on a Common Diagonal Crack or Stirrup

Some strain gages were applied to follow the path of a diagonal crack as it crossed multiple stirrups. Table 9 lists pairs of gages on a common crack and Figure 19 plots the equivalent constant strain range where more than two strain gages were placed on a common crack; the strain ranges within each checktest behaved similarly in relation to each other. The typical behavior appears to be larger strain ranges in the middle of the crack for stirrups crossed at the mid-height of the web, and tapering down toward the ends of the crack near the compression zone and at the flexural tensile steel. In the tabulated pairs, the larger strain range always corresponded to the gage located closer to the mid-height of the web. The crack on 6T10 monitored by strain gages GS6, 7, and 8 was only instrumented on the upper half of the crack and shows an incomplete curve. The length of the crack on 6IT10 monitored by GS1, 2, 3, and 4 was largely covered by the gages but appeared to experience interference from the eventual failure crack close-by. The crack on the specimen 3IT18 had higher magnitude strain ranges, as these occurred on the eventual failure crack and this specimen had the largest stirrup spacing.

Strain gages on the same stirrup are noted in Table 10. The majority of the pairs, not highlighted in the table, consisted of one embedded strain gage and one added strain gage, on opposite stirrup legs. Some of these added gages were sufficiently far away from the nearest diagonal crack such that they did not exhibit significant strain, but there is no clear demarcation to identify the distance required to register appreciable strain. The pairs on specimens 6IT10 and 6T10 were on the same stirrup leg but different diagonal cracks. In both cases the gage closer to the mid-height of the respective diagonal crack had a higher strain range. The remaining highlighted pairs were on different stirrup legs but nearly opposite each other, on the same diagonal crack. It can be seen that small distances from the crack can result in a reduction of measured strain magnitude. It was observed during the experiments that the diagonal cracks did not cross the stirrup leg at the same elevation, likely the cause of the unequal measurements in gage values.

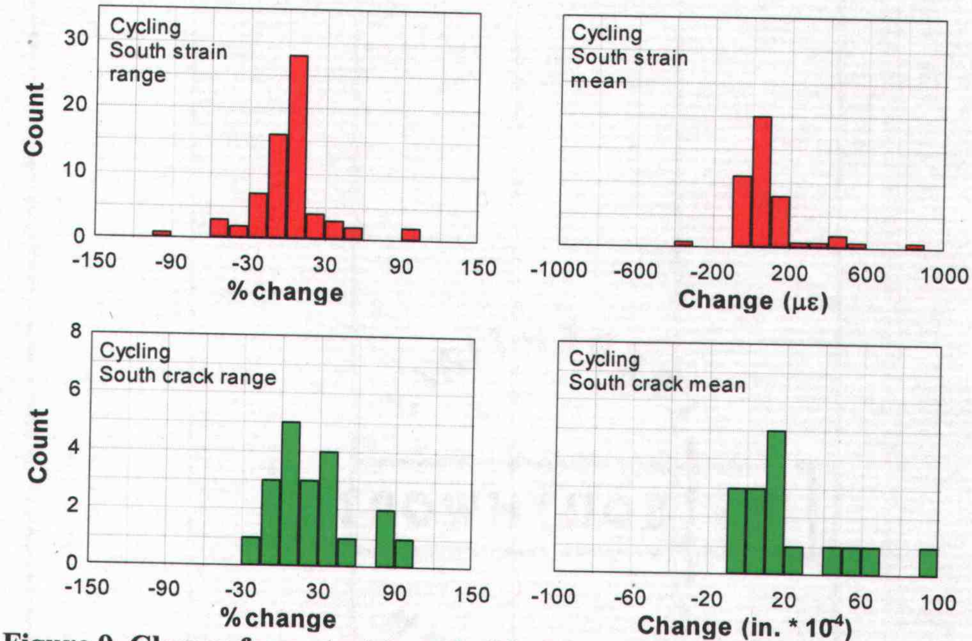

Figure 9–Change from start to end of fatigue testing in stirrup strain and diagonal crack ranges and means due to cycling.

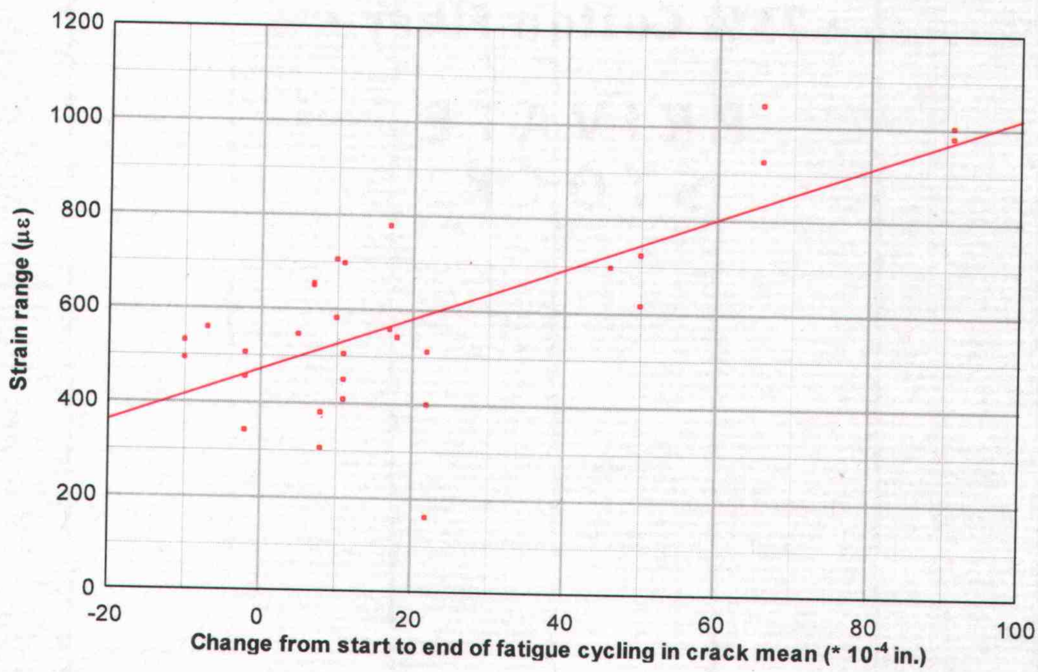

Figure 10—Fatigue cycling strain range vs. change in crack size.

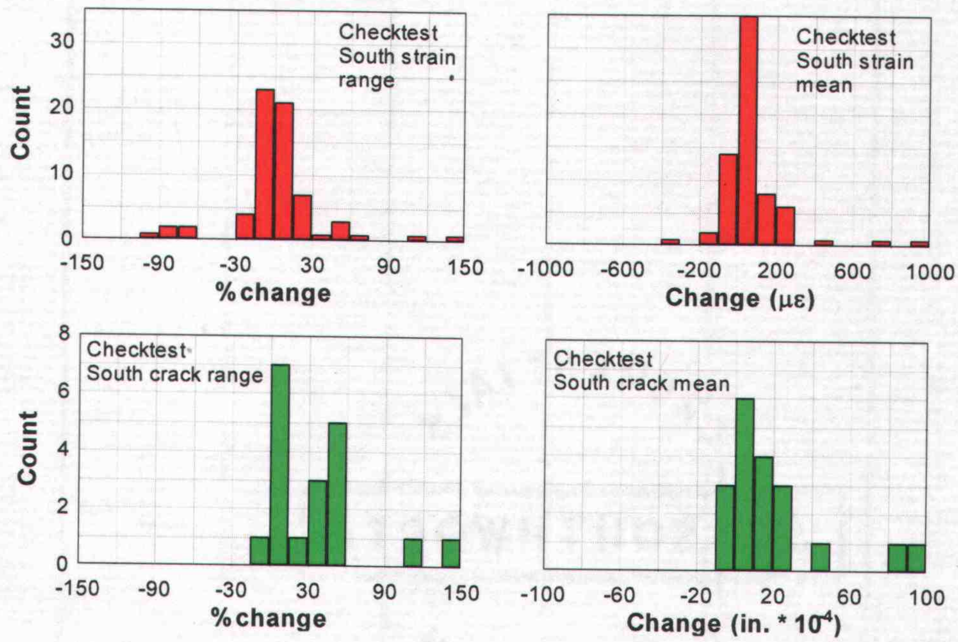

Figure 11–Change from start to end of fatigue testing in stirrup strain and diagonal crack ranges and means during checktests.

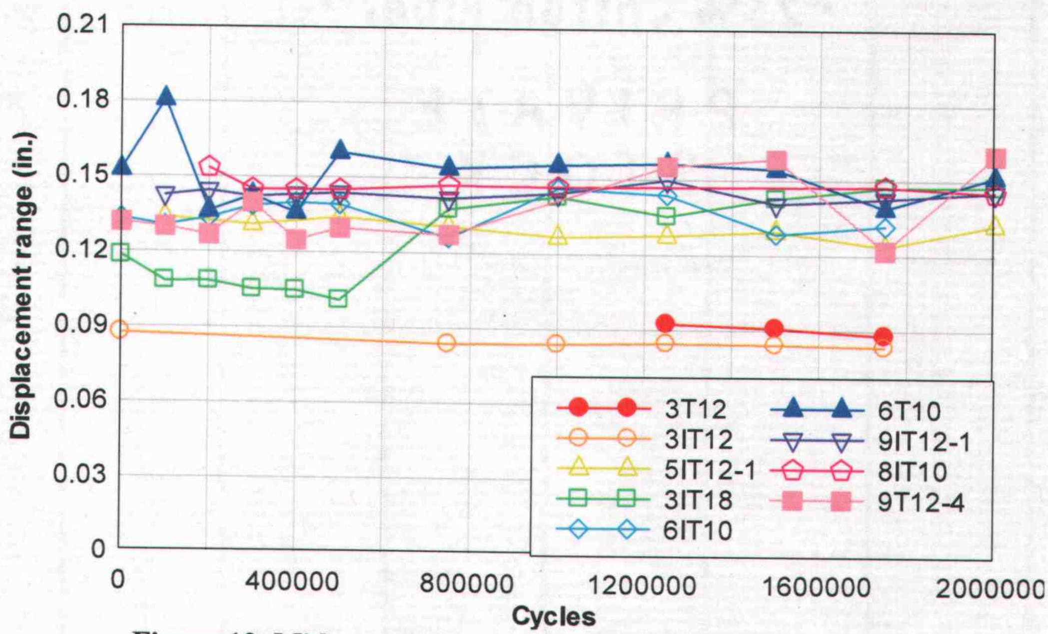

Figure 12–Midspan displacement ranges during checktests.

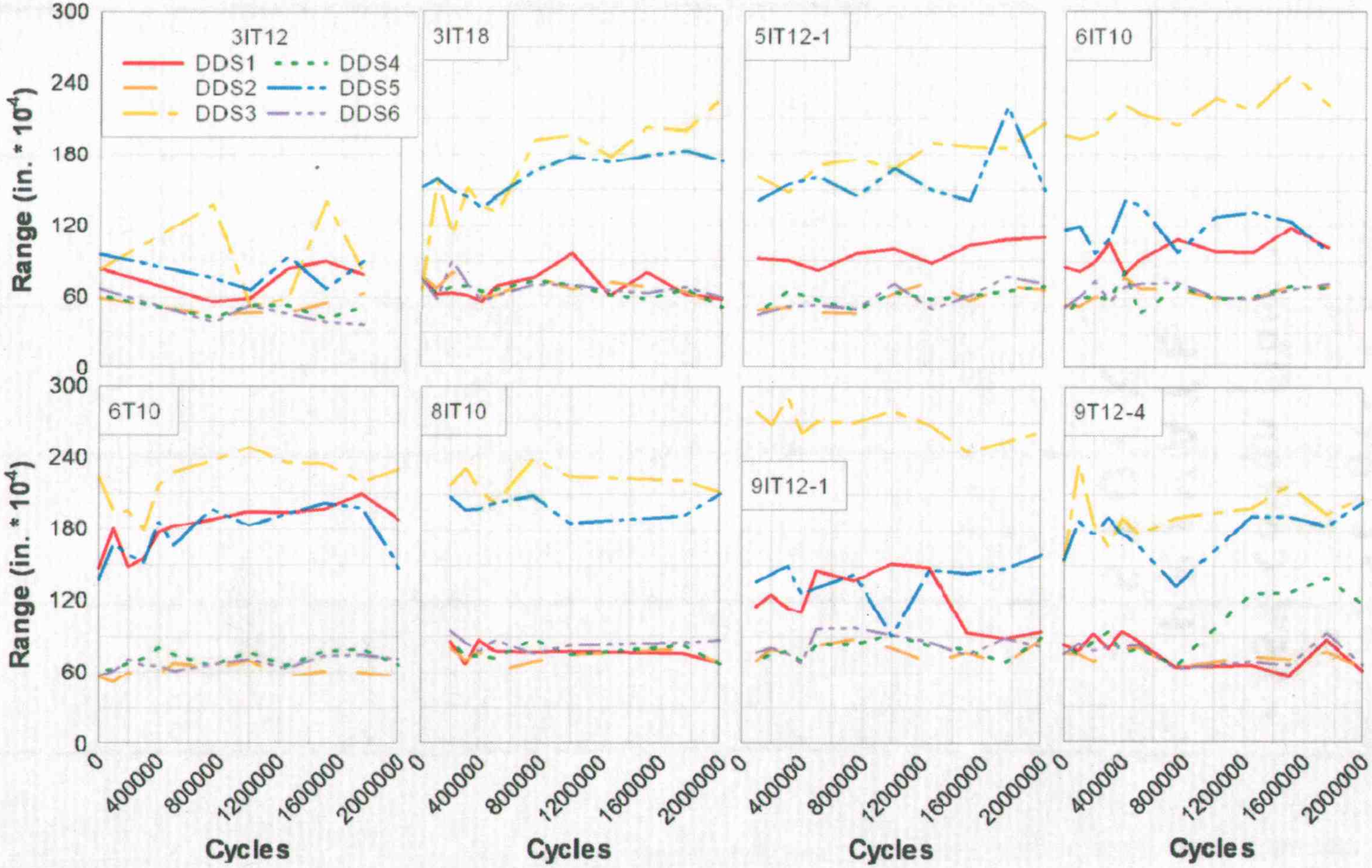

Figure 13—South diagonal displacement ranges during checktests.

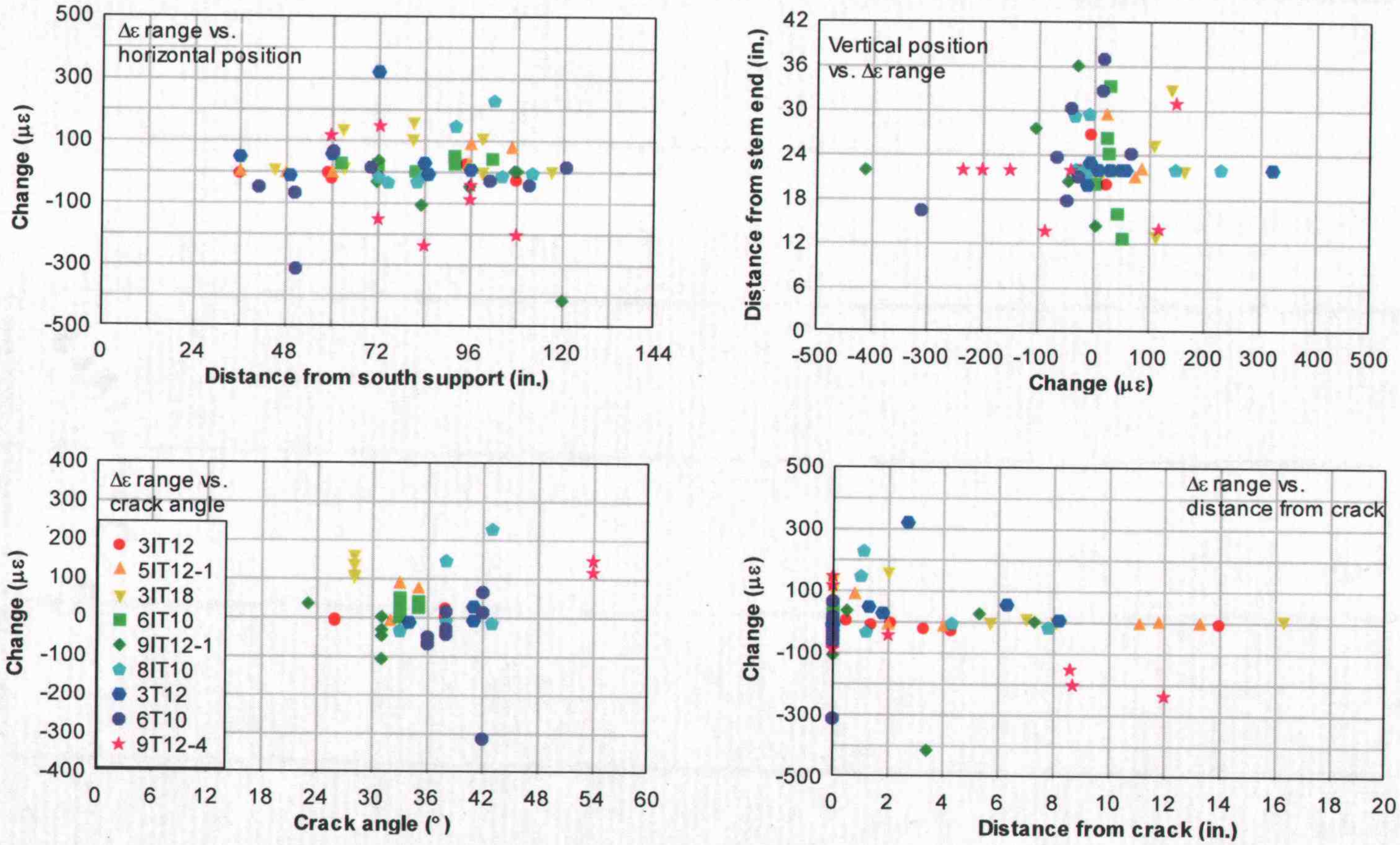

Figure 14–Change from start to end of testing in strain range due to fatigue cycling, compared to various factors.

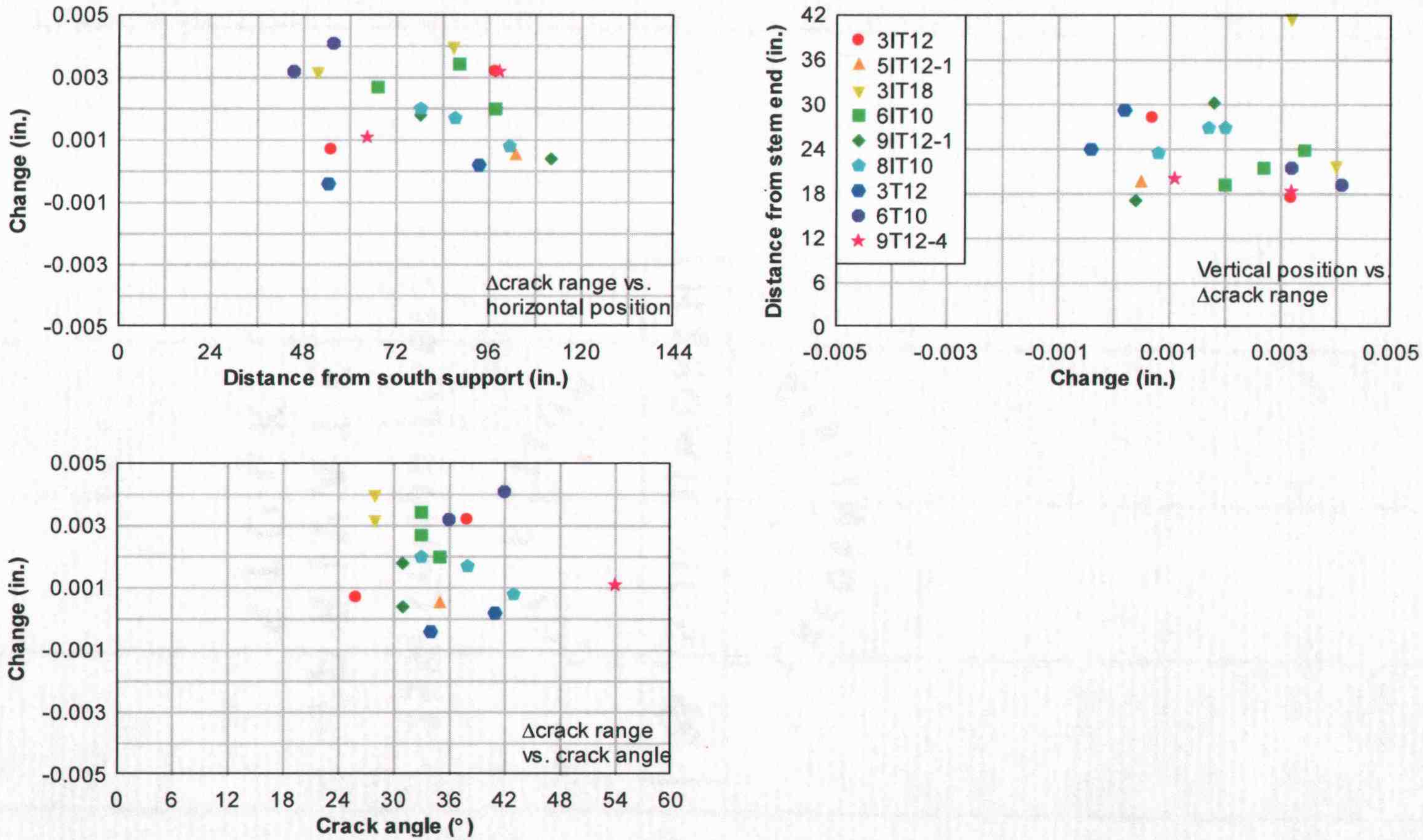

Figure 15–Change from start to end of testing in crack range due to fatigue cycling, compared to various factors.

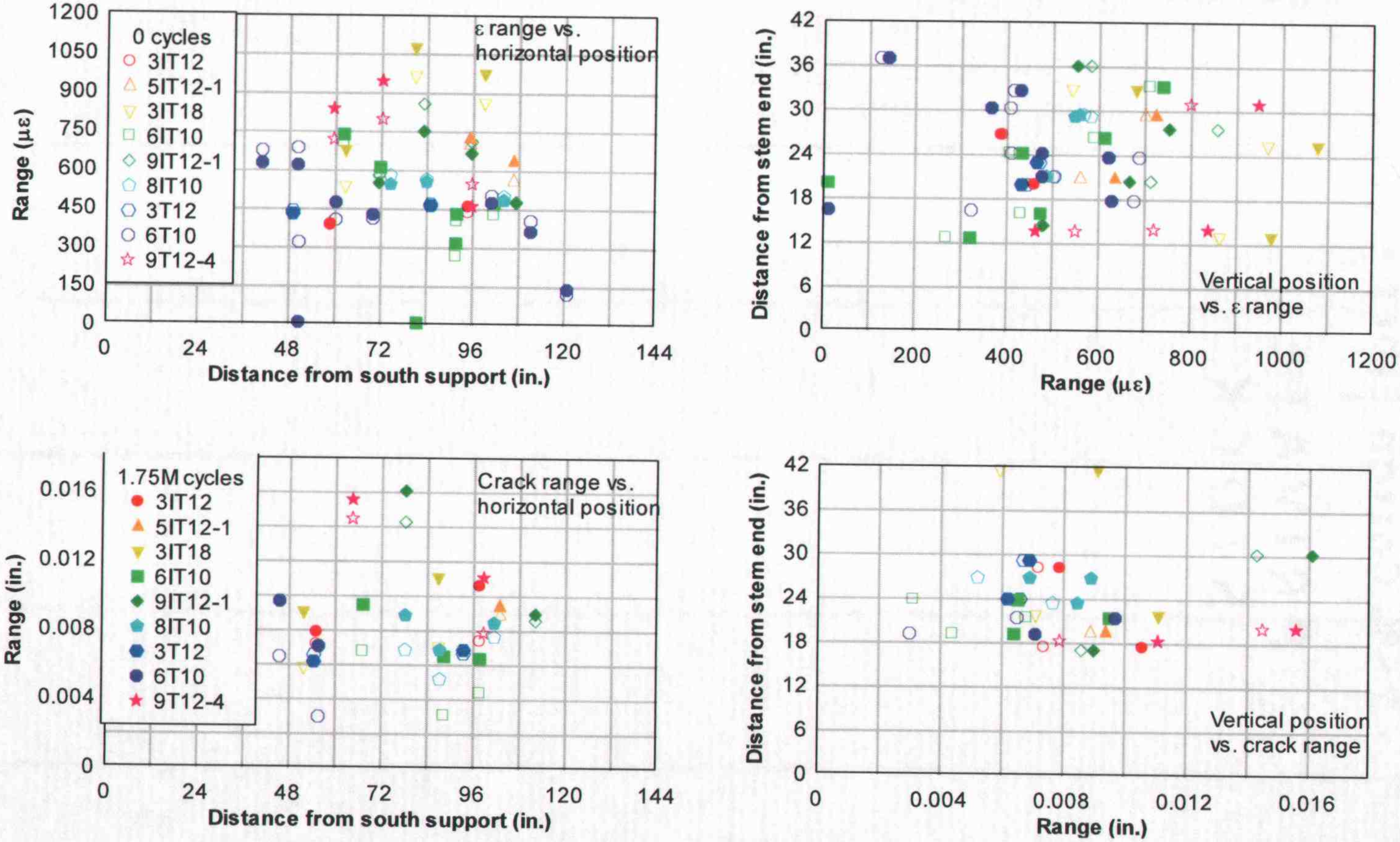

Figure 16–Crack and added strain ranges at the beginning and end of fatigue cycling, compared to position.

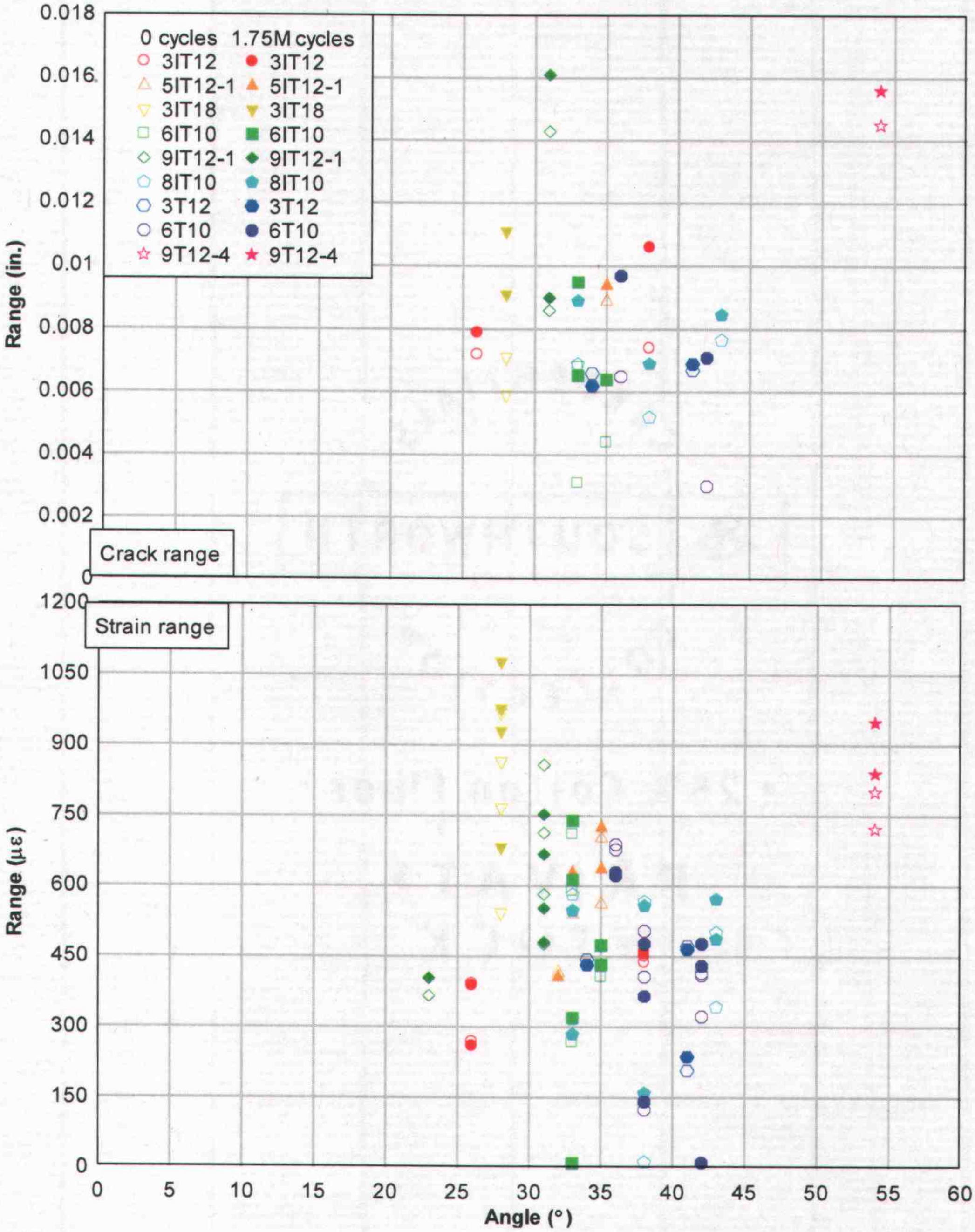

Figure 17–Crack and strain range at the beginning and end of cycling, compared to crack angle.

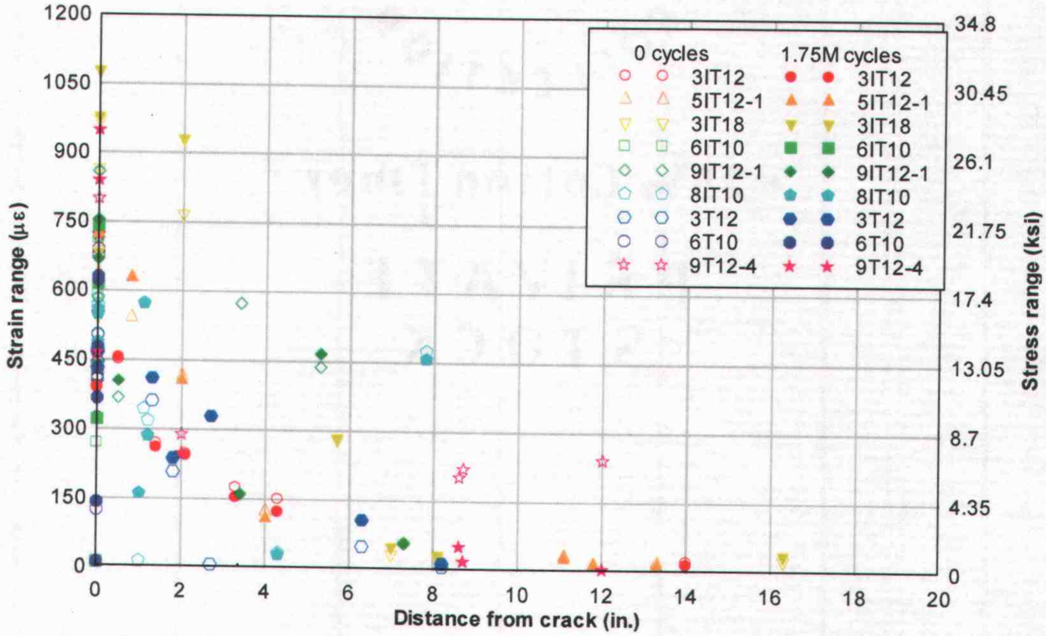

Figure 18–Strain range at the beginning and end of cycling, all strain gages compared to distance from the nearest diagonal crack.

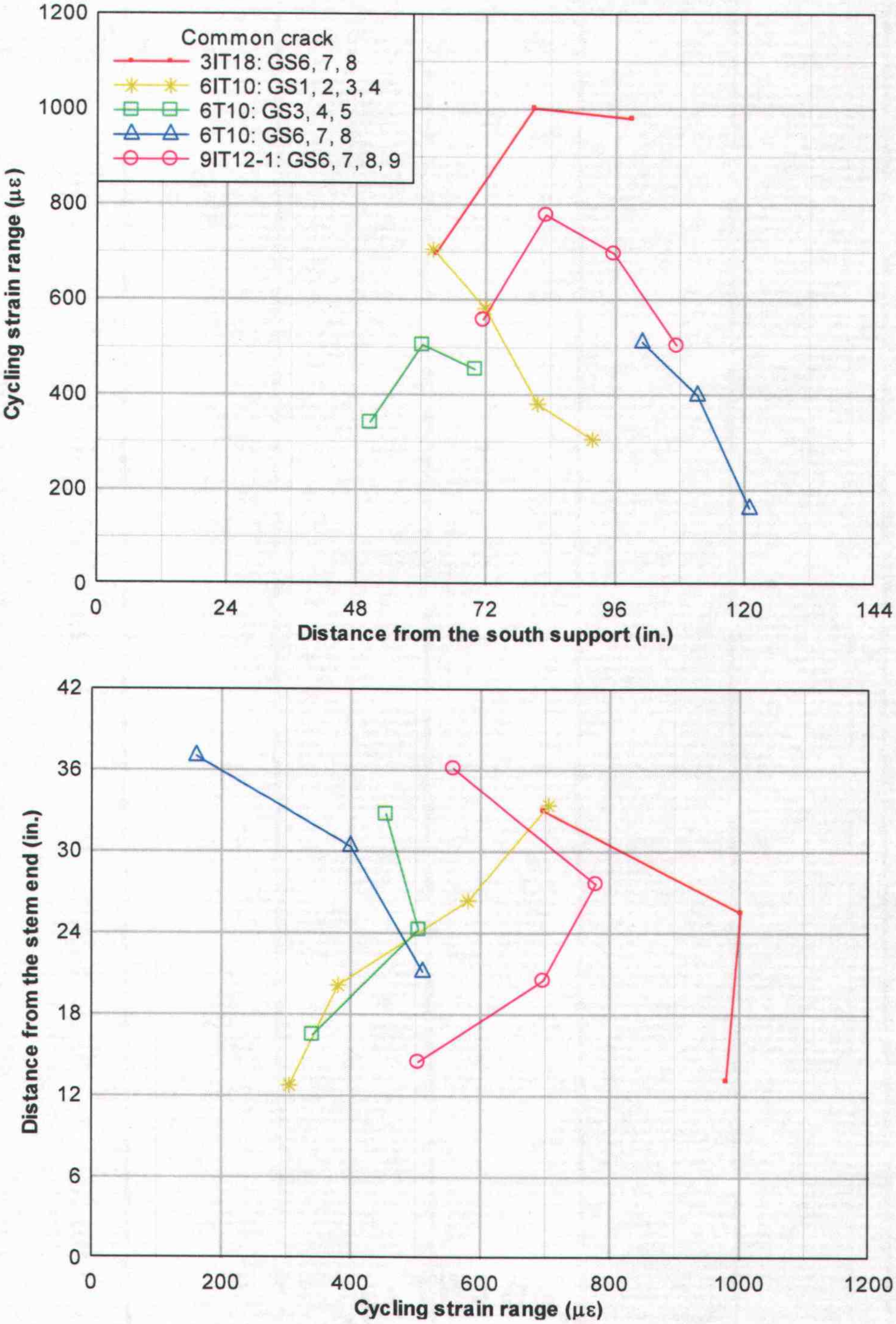

Figure 19—Equivalent constant amplitude strain ranges along a common crack vs. position.

Table 4–Equivalent constant stress ranges during cycling.

Specimen	Stress range (ksi)								
	GS1	GS2	GS3	GS4	GS5	GS6	GS7	GS8	GS9
3IT12	0	5	8	7	13	4	11	13	---
3T12	10	1	9*	7	1	broken	14	15	---
3IT18	1	1	23*	8	1	20	29	28	---
5IT12-1	0	0	1	3	12	17	18	21	---
6IT10	20	17	11*	9	12	13	---	---	---
6T10	19	19	10*	15	13	15	12	5	---
8IT10	13	10	4	15	1	16	16	14	---
9IT12-1	11	12	broken	2	11*	16	23	20	15
9T12-4	broken	1	1	6	1	27	30	16	---

*adjusted for equipment problems

Table 5–Strain and crack ranges at the start and end of cycling.

Specimen	Strain Gage	e Range (ue) After precrack	e Range (ue) After 2million cycles	Change (ue)
3IT12	GS1	10	5	-5
	GS2	170	150	-20
	GS3	250	255	5
	GS4	230	240	10
	GS5	430	450	20
	GS6	130	120	-10
	GS7	390	390	0
	GS8	420	460	40
3T12	GS1	360	350	-10
	GS2	50	40	-10
	GS3	320	310*	-10
	GS4	230	190	-40
	GS5	5	5	0
	GS6	**	**	**
	GS7	500	460	-40
	GS8	460	420	-40
3IT18 before fracture	GS1	15	20	5
	GS2	30	40	10
	GS3	800	920	120
	GS4	230	280	50
	GS5	20	30	10
	GS6	850	960	110
	GS7	990	1130	140
	GS8	550	660	110
5IT12-1	GS1	5	10	5
	GS2	5	10	5
	GS3	30	20	-10
	GS4	120	110	-10
	GS5	420	400	-20
	GS6	570	630	60
	GS7	600	650	50
	GS8	730	740	10
6IT10	GS1	720	750	30
	GS2	600	620	20
	GS3	410***	440*	30
	GS4	290	330	40
	GS5	410	440	30
	GS6	460	480	20

Specimen	Strain Gage	e Range (ue) After precrack	e Range (ue) After 2million cycles	Change (ue)
6T10	GS1	650	650	0
	GS2	650	650	0
	GS3	350***	10*	-340
	GS4	440	520	80
	GS5	410	470	60
	GS6	470	530	60
	GS7	360	410	50
	GS8	110	170	60
8IT10	GS1	440	420	-20
	GS2	350	300	-50
	GS3	10*	170	160
	GS4	410	470	60
	GS5	30	20	-10
	GS6	570	480	-90
	GS7	590	500	-90
	GS8	550	440	-110
9IT12-1	GS1	400	400	0
	GS2	440	430	-10
	GS3	**	**	**
	GS4	50	50	0
	GS5	530*	220	-310
	GS6	570	550	-20
	GS7	800	760	-40
	GS8	700	690	-10
	GS9	500	480	-20
9T12-4	GS1	460	600***	140
	GS2	40	30	-10
	GS3	5	2	-3
	GS4	180	190	10
	GS5	5	4	-1
	GS6	840	890	50
	GS7	960	980	20
	GS8	530	460	-70

*gage appears to be broken but works in precracking and failure, ranges were estimated
**indicates a broken gage
***data is spotty, ranges were estimated

Specimen	Crack Gage	Crack Range (in.)* After precrack	Crack Range (in.)* After 2million cycles	% change
3IT12	#4	0.0068	0.0091	34
	#5	0.0060	0.0072	20
3T12	#4	0.0066	0.0056	-15
	#6	0.0066	0.0059	-11
3IT18**	#4	0.0085	0.0106	25
	#5	0.0068	0.0094	38
5IT12-B1	#5	0.0090	0.0093	3
6IT10	#4	0.0075	0.0095	27
	#5	0.0046	0.0062	35
	#6	0.0033	0.0063	91
6T10	#4	0.0062	0.0098	58
	#5	0.0038	0.0070	84
	#6	0.0076	0.0134	76
8IT10	#4	0.0063	0.0072	14
	#5	0.0044	0.0062	41
	#6	0.0074	0.0075	1
9IT12-B1	#4	0.0132	0.0143	8
	#5	0.0082	0.0088	7
9T12-B4	#4	0.0132	0.0124	-6
	#5	0.0081	0.0080	-1

*where data is spotty the ranges were taken at earliest and latest possible times
**before fracture

Table 6–Strain and crack means at the start and end of cycling.

Specimen	Strain Gage	e Mean (ue) After precrack	e Mean (ue) After 2million cycles	Change (ue)
3IT12	GS1			
	GS2			
	GS3			
	GS4			
	GS5			
	GS6			
	GS7			
	GS8			
3T12	GS1			
	GS2			
	GS3			
	GS4			
	GS5			
	GS6			
	GS7			
	GS8			
3IT18 before fracture	GS1	-20	50	70
	GS2	30	210	180
	GS3	570	730	160
	GS4	440	960	520
	GS5	80	210	130
	GS6	370	700	330
	GS7	1020	1440	420
	GS8	790	930	140
5IT12-1	GS1			
	GS2			
	GS3			
	GS4			
	GS5			
	GS6			
	GS7			
	GS8			
6IT10	GS1	1150	1200	50
	GS2	880	930	50
	GS3	570***	530*	-40
	GS4	370	330	-40
	GS5	570	580	10
	GS6	610	630	20

Specimen	Strain Gage	e Mean (ue) After precrack	e Mean (ue) After 2million cycles	Change (ue)
6T10	GS1	80	130	50
	GS2	50	50	0
	GS3	80***	0*	-80
	GS4	90	50	-40
	GS5	50	10	-40
	GS6	80	110	30
	GS7	50	50	0
	GS8	90	120	30
8IT10	GS1	490	550	60
	GS2	30	200	170
	GS3	0*	-360	-360
	GS4	70	240	170
	GS5	130	180	50
	GS6	470	450	-20
	GS7	490	460	-30
	GS8	430	390	-40
9IT12-1	GS1	370	360	-10
	GS2	550	590	40
	GS3	**	**	**
	GS4	100	140	40
	GS5	600*	510	-90
	GS6	930	930	0
	GS7	730	770	40
	GS8	690	710	20
	GS9	460	470	10
9T12-4	GS1	350	520***	170
	GS2	0	50	50
	GS3	0	0	0
	GS4	160	360	200
	GS5	10	-20	-30
	GS6	450	860	410
	GS7	700	1550	850
	GS8	300	480	180

*gage appears to be broken but works in precracking and failure, means were estimated
**indicates a broken gage
***data is spotty, means were estimated

Specimen	Crack Gage	Crack Mean (in.)* After precrack	Crack Mean (in.)* After 2million cycles	Change (in.)
3IT12	#4			
	#5			
3T12	#4			
	#6			
3IT18*	#4	-0.0004	0.0087	0.0091
	#5	-0.0002	0.0044	0.0046
5IT12-B1	#5	0	0.0050	0.0050
6IT10	#4	0	0.0010	0.0010
	#5	-0.0001	0.0010	0.0011
	#6	0	0.0008	0.0008
6T10	#4	0.0006	0.0013	0.0007
	#5	-0.0001	-0.0003	-0.0002
	#6	-0.0005	0.0017	0.0022
8IT10	#4	0	0.0005	0.0005
	#5	0	-0.0007	-0.0007
	#6	0	-0.0010	-0.0010
9IT12-B1	#4	0.0001	0.0018	0.0017
	#5	0.0002	0.0013	0.0011
9T12-B4	#4	-0.0015	0.0051	0.0066
	#5	-0.0010	0.0008	0.0018

*where data is spotty the means were taken at earliest and latest possible times
**before fracture

Table 7--Checktest load (kips), strain (me), and crack (in.) ranges.

Beam	Gage	Checktest 0	100k	200k	300k	400k	500k	750k	1M	1.25M	1.5M	1.75M	2M
3IT12	mts	79.939						80.008	80.09	80.058	80.141	80.017	
	DL	46.688						46.726	47.083	47.325	46.968	47.153	
	rxtn	25.991						25.691	25.98	25.96	25.97	25.836	
	GS1	22						21	16	20	17	15	
	GS2	175						170	161	158	157	153	
	GS3	269						270	268	265	269	260	
	GS4	247						252	248	247	253	244	
	GS5	451						456	446	459	441	455	
	GS6	150						137	125	130	123	122	
	GS7	392						389	384	390	385	388	
	GS8	438						449	436	455	439	462	
	#4	0.0074						0.0086	0.0084	0.0090	0.0091	0.0106	
	#5	0.0072						0.0069	0.0076	0.0071	0.0071	0.0079	
3T12	mts	81.052								80.557	80.406		80.315
	DL	44.169								45.023	45.31		44.226
	rxtn	25.826								26.156	25.629		25.97
	GS1	361								363	368		411
	GS2	49								63	69		106
	GS3	6								328	b		b
	GS4	208								210	194		237
	GS5	6								6	9		14
	GS6	b								b	b		b
	GS7	444								460	435		433
	GS8	472								492	471		466
	#4	0.0067								0.0070	0.0069		0.0069
	#6	0.0066								0.0068	0.0061		0.0062
3IT18	mts	80.058	80.054	79.948	80.026	80.026	80.026	81.752	82.951	82.608	82.663	82.7	82.553
	DL	17.754	27.186	26.274	29.233	27.448	31.682	12.499	10.427	11.364	9.0875	8.1947	7.8632
	rxtn	36.094	32.85	33.181	32.127	32.809	31.393	37.953	39.244	39.151	39.689	40.102	40.308
	GS1	25	23	30	20	24	22	19	23	37	25	36	32
	GS2	33	36	35	36	34	35	37	42	43	42	49	19
	GS3	766	698	14	200	731	337	37	15	903	921	929	b
	GS4	281	223	229	225	237	218	250	257	305	281	283	395
	GS5	27	27	27	22	27	24	33	34	43	34	32	40
	GS6	542	514	521	510	511	496	623	667	661	660	681	970
	GS7	969	890	921	900	917	879	1080	1125	1113	1103	1077	34
	GS8	865	774	795	778	792	760	911	944	956	953	977	1325
	#4	0.0071	0.0083	0.0086	0.0085	0.0085	0.0082	0.0097	0.0100	0.0099	0.0104	0.0111	0.0132
	#5	0.0059	0.0064	0.0071	0.0067	0.0072	0.0072	0.0076	0.0078	0.0084	0.0086	0.0091	0.0096
5IT12-1	mts		79.866		79.99		80.127	80.072	80.086	80.072	79.935	80.113	80.15
	DL		9.2342		9.5467		9.1003	10.012	14.094	14.578	12.117	12.805	11.326
	rxtn		39.42		39.658		39.833	39.162	37.953	38.201	38.883	38.377	39.151
	GS1		16		13		11	12	15	e	e	15	18
	GS2		20		17		14	9	17	e	e	15	17
	GS3		33		35		32	32	27	e	e	27	26
	GS4		123		125		121	117	112	e	e	108	117
	GS5		416		411		419	419	408	e	e	406	403
	GS6		541		546		570	576	587	e	e	628	596
	GS7		561		587		602	595	596	e	e	636	593
	GS8		702		713		723	711	713	e	e	725	691
	#5		0.0089		0.0093		0.0096	0.0094	0.0097	0.0097	0.0092	0.0094	0.0090
6IT10	mts	82.718	83.025	82.141	83.267	83.034	82.457	83.377	83.432	83.794	82.132	81.972	
	DL	11.855	12.869	11.345	7.8376	9.7444	10.153	23.672	6.6004	8.1501	17.977	9.5914	
	rxtn	40.174	39.42	39.255	40.753	40.246	39.844	35.67	41.414	41.218	36.652	39.709	
	GS1	711	720	722	762	768	755	679	794	777	671	739	
	GS2	590	601	602	629	633	621	557	651	642	556	613	
	GS3	8	11	233	426	433	435	346	12	442	390	11	
	GS4	268	292	300	333	338	336	299	349	339	289	321	
	GS5	407	402	401	443	445	441	385	458	437	371	434	
	GS6	431	452	457	490	493	490	432	509	485	419	474	
	#4	0.0068	0.0085	0.0084	0.0083	0.0088	0.0087	0.0090	0.0088	0.0093	0.0085	0.0095	
	#5	0.0044	0.0051	0.0053	0.0050	0.0053	0.0059	0.0050	0.0058	0.0059	0.0056	0.0064	
	#6	0.0031	0.0042	0.0062	0.0047	0.0049	0.0051	0.0048	0.0057	0.0058	0.0056	0.0065	

Table 7--Checktest load (kips), strain (me), and crack (in.) ranges (cont.).

		Checktest											
Beam	Gage	0	100k	200k	300k	400k	500k	750k	1M	1.25M	1.5M	1.75M	2M
6T10	mts	82.059	82.576	81.926	82.05	82.091	82.649	81.889	81.747	82.004	82.26	82.013	82.471
	DL	10.261	17.537	22.244	22.135	22.237	6.5367	9.1322	8.9983	9.5531	10.918	20.713	10.631
	V	37.726	35.621	33.726	33.8	33.921	39.286	38.023	37.993	37.919	37.589	34.223	37.769
	GS1	678	643	625	619	625	711	690	702	697	677	629	674
	GS2	689	639	619	613	617	704	687	693	692	673	622	670
	GS3	323	23	246	356	10	11	12	12	11	12	12	11
	GS4	410	441	452	436	452	511	544	535	540	536	477	534
	GS5	415	402	406	395	404	466	487	480	487	480	430	479
	GS6	505	452	435	426	439	502	540	546	547	542	477	535
	GS7	408	335	317	308	317	375	428	433	433	426	366	415
	GS8	124	88	85	58	90	102	159	183	185	176	141	164
	#4	0.0065	0.0070	0.0072	0.0089	0.0078	0.0086	0.0090	0.0098	0.0099	0.0117	0.0097	0.0104
	#5	0.0030	0.0042	0.0055	0.0045	0.0054	0.0055	0.0063	0.0066	0.0069	0.0070	0.0071	0.0074
	#6	e	e	e	e	e	e	e	e	e	e	e	e
8IT10	mts			80.118	79.797	79.797	79.999	79.976	79.948			79.77	80.09
	DL			6.8045	7.0405	7.2509	7.2828	7.2637	7.8823			9.1768	9.1641
	V			38.07	37.826	37.764	37.847	37.85	37.621			37.311	37.398
	GS1			474	469	466	464	470	462			457	450
	GS2			318	321	301	303	302	291			285	275
	GS3			13	6	6	9	24	141			160	162
	GS4			343	360	373	460	551	543			572	578
	GS5			33	40	31	28	27	31			29	35
	GS6			582	567	555	554	552	555			548	541
	GS7			567	571	561	550	549	567			558	574
	GS8			502	507	492	480	477	499			487	500
	#4			0.0069	0.0075	0.0072	0.0073	0.0072	0.0082			0.0089	0.0082
	#5			0.0052	0.0057	0.0057	0.0053	0.0058	0.0064			0.0069	0.0079
	#6			0.0077	0.0085	0.0077	0.0077	0.0078	0.0095			0.0085	0.0090
9IT12-1	mts	82.104	81.912	81.885	81.985	81.83	81.821	81.876	81.747	81.624	81.871	80.182	79.472
	DL	6.3135	7.0468	7.0277	7.1234	6.8555	7.0787	6.6706	6.83	6.543	6.7599	6.6068	6.7089
	V	39.367	38.874	38.904	38.841	38.813	38.809	38.967	38.942	39.003	38.892	38.205	37.891
	GS1	367	400	392	406	389	393	413	394	368	431	405	416
	GS2	437	451	444	446	436	438	447	468	460	457	466	452
	GS3	b	b	b	b	b	b	b	b	b	b	b	b
	GS4	56	62	60	78	60	70	62	78	64	60	59	58
	GS5	573	2198	1972	2026	2013	2027	1790	435	195	171	160	179
	GS6	583	568	567	570	565	570	560	590	584	563	553	556
	GS7	858	804	796	800	795	798	773	814	806	778	753	767
	GS8	714	692	689	698	696	702	677	749	734	690	668	692
	GS9	477	493	496	501	501	504	483	573	562	485	481	488
	#4	e	0.0143	0.0145	0.0148	0.0147	0.0149	0.0151	0.0165	0.0166	0.0146	0.0161	0.0160
	#5	e	0.0086	0.0086	0.0091	0.0089	0.0106	0.0091	0.0101	0.0103	0.0090	0.0090	0.0108
9T12-4	mts	79.953	79.752	79.861	79.784	79.912	79.761	80.768		81.184	80.914	80.727	81.377
	DL	17.601	19.342	19.546	19.718	19.629	19.374	17.18		7.3147	6.4857	33.334	5.4525
	V	34.505	33.699	33.692	33.669	33.666	33.722	34.846		38.378	38.566	29.817	39.193
	GS1	538	483	b	b	b	b	b		b	b	b	b
	GS2	202	52	140	36	35	141	37		40	43	51	72
	GS3	241	92	157	21	21	147	20		5	10	5	40
	GS4	289	182	229	189	193	313	208		255	259	248	301
	GS5	221	75	112	25	18	135	28		12	23	20	30
	GS6	721	841	811	804	819	815	887		992	1005	840	1150
	GS7	800	963	926	913	931	922	1024		1111	1114	948	1252
	GS8	551	527	513	504	505	499	527		585	580	464	613
	#4	0.0145	0.0135	0.0131	0.0142	0.0142	0.0133	0.0136		0.0163	0.0158	0.0142	0.0156
	#5	0.0079	0.0109	0.0079	0.0110	0.0082	0.0095	0.0078		0.0102	0.0101	0.0089	0.0111

b = broken gage or maximum exceeded
e = equipment problems

Table 8--Checktest load (kips), strain (me), and crack (in.) means.

Beam	Gage	Checktest											
		0	100k	200k	300k	400k	500k	750k	1M	1.25M	1.5M	1.75M	2M
	mts	43.898						43.957	43.923	43.919	44.026	43.93	
	DL	67.289						66.776	70.279	69.507	68.469	68.523	
	rxtn	43.168						42.602	43.754	43.439	43.271	43.117	
	GS1	58						91	2	55	-13	33	
	GS2	598						647	562	631	556	616	
	GS3	580						626	526	609	514	587	
3IT12	GS4	532						573	486	554	476	533	
	GS5	843						909	826	904	816	892	
	GS6	567						599	508	574	497	555	
	GS7	828						858	816	872	812	871	
	GS8	763						791	743	802	743	802	
	#4	0.0190						0.0196	0.0202	0.0201	0.0202	0.0203	
	#5	0.0263						0.0274	0.0281	0.0280	0.0283	0.0283	
	mts	44.394								41.003	41.19		40.984
	DL	63.703								71.38	71.758		68.303
	rxtn	42.555								43.319	43.495		42.483
	GS1	742								838	820		810
	GS2	260								335	294		305
	GS3	16								765	b		b
3T12	GS4	286								421	412		378
	GS5	91								158	128		134
	GS6	b								b	b		b
	GS7	1023								1116	1105		1103
	GS8	914								1007	983		990
	#4	0.0280								0.0282	0.0285		0.0282
	#6	0.0329								0.0332	0.0334		0.0332
	mts	44.19	44.24	44.236	44.177	44.256	44.232	44.138	44.035	44.077	44.022	44.065	44.065
	DL	94.09	87.748	90.908	89.636	91.731	89.439	95.42	90.171	99.558	94.608	93.935	97.127
	rxtn	54.114	51.641	52.711	52.191	52.891	52.08	53.744	52.013	55.086	53.256	53.038	54.256
	GS1	12	-7	19	29	39	64	7	-7	66	4	23	73
	GS2	42	54	85	105	120	151	104	109	198	147	175	119
	GS3	597	563	13	151	698	339	33	14	985	826	881	b
3IT18	GS4	420	460	502	524	540	574	556	591	690	627	672	845
	GS5	95	108	122	138	143	174	127	137	227	161	185	248
	GS6	733	715	765	784	792	806	827	851	1011	839	866	1139
	GS7	962	946	1026	1058	1065	1083	1153	1217	1451	1299	1191	96
	GS8	407	348	375	428	415	463	448	511	715	553	629	809
	#4	0.0467	0.0479	0.0492	0.0492	0.0497	0.0494	0.0518	0.0528	0.0549	0.0548	0.0558	0.0781
	#5	0.0457	0.0467	0.0473	0.0471	0.0475	0.0470	0.0485	0.0486	0.0492	0.0504	0.0507	0.0611
	mts		44.155		44.226		44.243	44.209	44.211	44.156	44.245	44.175	44.148
	DL		91.157		92.568		91.869	91.87	91.137	91.127	87.642	99.506	92.314
	rxtn		52.548		52.89		52.649	52.614	52.399	52.293	51.215	54.991	52.626
	GS1		31		42		45	32	24	e	e	-5	-15
	GS2		34		47		53	41	36	e	e	-3	-13
5IT12-1	GS3		91		112		125	117	116	e	e	117	109
	GS4		233		256		267	259	259	e	e	256	234
	GS5		446		475		491	486	497	e	e	493	439
	GS6		582		618		647	646	665	e	e	646	570
	GS7		740		800		836	826	868	e	e	852	735
	GS8		1262		1320		1355	1353	1389	e	e	1483	1386
	#5		0.0446		0.0450		0.0452	0.0457	0.0461	0.0467	0.0460	0.0479	0.0471
	mts	44.039	44.077	44.076	44.073	44.12	44.026	44.027	44.103	44.154	44.035	44.088	
	DL	93.18	94.419	89.797	89.807	91.488	92.255	85.125	93.357	87.32	76.797	93.807	
	rxtn	54.066	54.074	52.432	51.865	51.997	52.234	49.857	52.809	50.818	47.21	52.638	
	GS1	1158	1193	1177	1210	1249	1292	1227	1328	1237	1132	1260	
	GS2	877	903	896	937	962	1002	952	1032	957	863	976	
6IT10	GS3	12	14	320	615	644	707	572	18	637	550	17	
	GS4	382	356	349	381	378	423	376	433	363	288	356	
	GS5	560	586	585	609	623	665	612	680	609	534	625	
	GS6	591	614	609	654	667	719	655	730	646	566	674	
	#4	0.0431	0.0440	0.0430	0.0431	0.0441	0.0435	0.0440	0.0444	0.0448	0.0441	0.0449	
	#5	0.0416	0.0420	0.0419	0.0418	0.0424	0.0419	0.0424	0.0424	0.0429	0.0424	0.0428	
	#6	0.0263	0.0266	0.0263	0.0263	0.0270	0.0265	0.0272	0.0272	0.0277	0.0267	0.0271	

Table 8--Checktest load (kips), strain (me), and crack (in.) means (cont.).

Beam	Gage	Checktest 0	100k	200k	300k	400k	500k	750k	1M	1.25M	1.5M	1.75M	2M
6T10	mts	44.167	44.133	44.153	44.149	44.181	44.152	44.146	44.187	44.192	44.182	44.232	44.147
	DL	77.681	80.422	79.362	77.865	79.657	78.159	84.054	80.875	81.042	84.637	81.026	82.415
	V	47.977	48.854	48.531	48.033	48.611	48.129	50.091	49.011	49.088	50.264	49.089	49.524
	GS1	66	41	95	81	86	61	126	101	119	134	104	133
	GS2	47	-2	55	34	39	10	69	35	51	63	28	61
	GS3	124	7	67	88	5	5	5	5	5	5	5	5
	GS4	112	33	74	61	53	33	61	31	45	52	21	53
	GS5	50	-12	31	17	10	-4	31	3	18	24	-4	26
	GS6	84	39	81	66	68	50	108	85	101	116	85	121
	GS7	55	-6	38	25	20	0	60	36	49	58	26	63
	GS8	86	61	101	91	80	60	117	106	118	121	96	126
	#4	0.0617	0.0630	0.0629	0.0626	0.0632	0.0627	0.0637	0.0638	0.0637	0.0639	0.0636	0.0636
	#5	0.0615	0.0618	0.0614	0.0611	0.0616	0.0611	0.0614	0.0615	0.0614	0.0613	0.0613	0.0608
	#6	e	e	e	e	e	e	e	e	e	e	e	e
8IT10	mts			44.139	44.179	44.153	44.163	44.101	44.157			44.141	44.182
	DL			78.33	82.646	83.033	82.438	82.366	82.648			78.78	80.934
	V			48.18	49.619	49.775	49.541	49.548	49.628			48.33	49.069
	GS1			529	559	559	545	555	572			561	579
	GS2			56	102	110	86	100	136			167	188
	GS3			-3	-3	-3	-10	-50	-333			-375	-356
	GS4			88	121	129	129	166	205			258	308
	GS5			154	164	163	151	156	163			174	182
	GS6			461	492	470	441	464	494			477	494
	GS7			479	505	494	477	491	514			496	507
	GS8			414	438	419	388	406	433			417	430
	#4			0.0228	0.0230	0.0229	0.0229	0.0228	0.0231			0.0228	0.0229
	#5			0.0152	0.0152	0.0152	0.0152	0.0151	0.0151			0.0149	0.0150
	#6			0.0282	0.0284	0.0283	0.0282	0.0280	0.0283			0.0279	0.0280
9IT12-1	mts	44.063	44.092	43.96	44.09	44.055	44.087	44.094	44.103	44.148	44.174	44.07	44.125
	DL	80.139	82.835	82.685	83.016	82.117	82.553	83.725	78.974	74.022	82.31	78.942	81.873
	V	48.745	49.636	49.602	49.718	49.421	49.581	49.976	48.395	46.748	49.462	48.37	49.333
	GS1	356	379	374	378	375	370	391	345	324	386	356	360
	GS2	490	567	570	578	581	578	600	563	543	604	578	586
	GS3	b	b	b	b	b	b	b	b	b	b	b	b
	GS4	82	123	130	134	140	134	152	145	140	154	138	131
	GS5	693	-68	2311	2440	2509	2558	2323	725	621	600	534	503
	GS6	697	741	743	750	758	741	761	755	725	771	738	741
	GS7	923	932	926	932	940	918	940	935	897	944	899	907
	GS8	691	692	691	700	711	693	706	728	696	720	682	693
	GS9	457	472	473	476	487	464	482	527	490	489	447	451
	#4	e	0.0373	0.0372	0.0375	0.0373	0.0377	0.0374	0.0376	0.0374	0.0379	0.0379	0.0387
	#5	e	0.0289	0.0288	0.0291	0.0289	0.0293	0.0288	0.0296	0.0296	0.0293	0.0292	0.0299
9T12-4	mts	44.123	44.106	44.066	44.133	44.094	44.13	44.102		44.107	44.084	44.071	44.079
	DL	76.207	90.068	88.592	88.878	89.467	88.213	84.789		78.423	75.904	65.152	77.172
	V	47.464	52.113	51.582	51.712	51.888	51.488	50.314		48.216	47.343	43.769	47.762
	GS1	318	449	b	b	b	b	b		b	b	b	b
	GS2	0	23	36	30	34	32	-3		21	30	45	52
	GS3	-1	17	34	31	36	36	-10		3	2	3	2
	GS4	179	291	315	317	328	330	297		328	325	331	346
	GS5	10	29	41	36	40	39	-44		-22	-32	-21	-28
	GS6	482	651	642	641	657	650	677		682	735	762	927
	GS7	661	1095	1092	1105	1131	1131	112		1218	1312	1414	1624
	GS8	273	419	420	422	436	432	428		447	447	405	480
	#4	0.0732	0.0768	0.0763	0.0767	0.0771	0.0758	0.0771		0.0773	0.0782	0.0797	0.0812
	#5	0.0177	0.0192	0.0188	0.0190	0.0191	0.0191	0.0198		0.0192	0.0198	0.0190	0.0201

b = broken gage or maximum exceeded
e = equipment problems

Table 9—Equivalent constant amplitude strain range pairs on a common crack.

Specimen	Gage	Distance from the south support (in.)	Distance from the stem end (in.)	Distance to the nearest crack (in.)	Strain range ($\mu\varepsilon$)
3IT12	GS3	72	22	1.4	259
	GS7	59	26.75	0	388
5IT12-1	GS7	106.875	20.875	0	616
	GS8	95.375	29.375	0	724
8IT10	GS2	82	22	1.2	348
	GS6	74.5	29.25	0	545
	GS3	92	22	1	143
	GS7	83.875	29.5	0	558
9T12-4	GS6	59.625	14	0	926
	GS7	72.375	31	0	1045

Table 10—Equivalent constant amplitude strain range pairs on a common stirrup.

Specimen	Gage	Distance from the south support (in.)	Distance from the stem end (in.)	Distance to the nearest crack (in.)	Strain range ($\mu\varepsilon$)
3IT12	GS2	60	22	3.3	157
	GS7	59	26.75	0	388
	GS5	96	22	0.5	444
	GS8	95	20	0	444
3T12	GS4	84	22	1.8	229
	GS8	85	23	0	510
3IT18	GS2	63	22	7	36
	GS6	62.75	33	0	697
	GS3	81	22	2	800
	GS7	80.875	25.5	0	1002
	GS4	99	22	5.7	268
	GS8	99	13.125	0	980
5IT12-1	GS6	96	22	0.8	596
	GS8	95.375	29.375	0	724
6IT10	GS4	91.75	12.75	0	305
	GS5	91.875	24.25	0	408
6T10	GS2	50.25	23.75	0	649
	GS3	50.625	16.5	0	341
8IT10	GS1	72	22	7.8	449
	GS6	74.5	29.25	0	545
	GS2	82	22	1.2	348
	GS7	83.875	29.5	0	558
	GS4	102	22	1.1	530
	GS8	104.125	21.125	0	493
9IT12-1	GS1	72	22	0.5	396
	GS6	71.5	36.125	0	558
	GS2	84	22	5.3	431
	GS7	83.125	27.625	0	778
	GS4	108	22	7.3	56
	GS9	107.375	14.5	0	504
9T12-4	GS4	96	22	2	216
	GS8	95.875	13.75	0	541
	GS2	72	22	12	36
	GS7	72.375	31	0	1045

PREDICTION OF STIRRUP STRESS RANGE UNDER SERVICE LOADS

A method was developed to predict the average stirrup stress range under service loads and a sectional analysis program was examined to determine whether stirrup stress ranges could be estimated directly. Since the specimens were cycled at service-range load magnitudes after formation of the diagonal cracks, elastic behavior was assumed in the diagonally cracked section and the stresses and strains were considered to have a linear relationship. Shear forces in a beam are widely considered to be carried by tension in the stirrups, shear across the compression block, aggregate interlock along the cracked surface, and dowel forces in the longitudinal reinforcement. In the case of service level loads on diagonally precracked girders, the shear was assumed to be carried by the stirrups and compression zone only. Aggregate interlock was not considered; diagonal crack motions perpendicular to the crack were observed to be about three times greater than those parallel to the crack (Higgins, 2004a), indicating that bearing along the diagonal crack surface was unlikely to be significant. Dowel forces were disregarded since no offset or motion was observed at the level of the flexural reinforcement.

Referring to Figure 20, which shows the dimensions and forces considered here, the applied shear force, V_{APP}, is resisted by the force in the stirrups, V_s, and the shear in the compression block, V_{cz}; aggregate interlock, V_a, and dowel force, V_d, are shown but not used. Therefore, the stirrup shear force is determined by:

$$V_s = V_{APP} - V_{cz}\,. \tag{4}$$

When the applied shear force and the contribution of the compression zone are known, stirrup stress is calculated from the force in the stirrups.

Experimental Data Validation and Average Stress Range Prediction

The experimental stirrup stresses were verified by approximating the distribution of the applied shear force and then used to develop a simple equation to estimate average stirrup stresses under a given cracked condition and service level shear load. Several specimens of varying stirrup spacing and flexural reinforcement anchorages had diagonal cracks that were instrumented by bonded strain gages on the engaged stirrup legs over the majority of the cracks' lengths. The following stirrup strain gages along diagonal cracks were chosen over other diagonal cracks that were less fully monitored:

- 3IT18—GS6, GS7, GS8
- 6IT10—GS1, GS2, GS3, GS4
- 6T10—GS3, GS4, GS5

- 9IT12-1—GS6, GS7, GS8, GS9
- 9T12-4—GS6, GS7

Where stirrups were not instrumented, stirrup stress ranges were extrapolated from the position of the strain gages and the observation that the compression zone and flexural steel confine the crack, causing lower stirrup stress ranges away from mid-height.

The stirrup contribution, V_s, was estimated by summing the measured and extrapolated stirrup strains and multiplying by the elastic modulus and area of steel. The compression zone shear was estimated by the formula:

$$V_{cz} = \frac{2}{3} * \frac{c}{d_v} * V_{APP} \tag{5}$$

where c is the height of the compression block, d_v is the distance between the resultant compression force and the centroid of the tensile reinforcement, and V_{APP} is the shear at the south support (MacGregor, 1997, p. 185). Again referring to Fig. 20, this formula calculated the average shear stress, v, in the concrete between cracks; assumed a parabolic shear stress distribution in the compression zone, shown as a shaded area; and integrated the shear stress over the area of the compression zone to find the resultant shear force carried by the uncracked concrete in the section of interest.

The calculated shears and experimental values, measured towards the end of fatigue cycling and before fracture in specimen 3IT18, are summarized and compared in Table 11. Approximating stress ranges for non-instrumented stirrups proved to be subject to interpretation but tended to fall within the bounds dictated by the height at which they crossed the diagonal crack. The calculated compression zone shears were approximately 10% of the applied shear. Using this approach, equation (5) reasonably estimated V_{cz} and the forces in the stirrups and compression zone were generally found to account for nearly all the experimentally applied shear.

Referring to Fig. 20, the stirrup force, V_s, in terms of the geometry of the cracked section is:

$$V_s = A_v * f_v * \frac{d_v * \cot\theta}{s} \tag{6}$$

where Av is the cross-sectional area of a double-legged stirrup, fv is the stress in the stirrups, d_v is the distance between the resultant compression force and the centroid of the tensile reinforcement, θ is the diagonal crack angle, and s is the stirrup spacing. The last term is essentially the number of stirrups crossed by the diagonal crack. Combining equations (4), (5), and (6) and changing V_{APP} to V_u, the commonly used notation for required strength although in this case the shear is a service level load, the following equation for average stirrup stress across a diagonal crack is derived:

$$f_v = \frac{V_u * \left(1 - \frac{2c}{3d_v}\right)}{A_v} * \frac{s}{d_v * \cot\theta} \tag{7}$$

where the last term may be simplified further in the field by merely counting the number of stirrups crossing the diagonal crack. It is important to note that equation (7) calculates the *average* stirrup stress range at service level loads whereas actual stress magnitudes are unequally distributed among the stirrups. The maximum stress range at service load was previously estimated by applying an amplification factor (Robelo, 2004).

Response 2000™

The above distribution of applied shear force into two components was used to evaluate the ability of Response 2000™ (Bentz, 2000), a sectional analysis program based on MCFT freely available on the internet, to directly predict stirrup stress range from a service level fatigue load. It is typically used to predict the strength of a beam having no prior load, but to simulate a precracked condition the concrete tensile strength was reduced to a negligible amount. The section properties along the crack of interest and the actual material properties were entered as input and the M/V ratio was specified as being at the crack tip, Fig. 21.

The "Sectional Response" option was used to evaluate the specimens. Concrete stresses and strains at a particular load, taken to be the magnitude of the applied shear range since elastic behavior was assumed, are shown in Fig. 22. When the compression zone shear stresses calculated by the program, circled in Fig. 22, were integrated over the compression block, V_{cz} was found to be 5 to 10% of the applied shear. Figure 23 shows stress and strain in the stirrup reinforcement at the specified load, with the stirrup stress at the crack circled.

Figure 24 displays experimental and calculated stirrup stresses relative to vertical position by beam orientation, the starred points and solid lines, respectively. For completeness, the stresses associated with added strain gages at other cracks, marked by Xs; embedded strain gages not at a crack, marked by upward-pointing triangles; and extrapolated strain amplitudes, marked by downward-pointing triangles, were also plotted. Given the variability of the experimental specimens, the calculated stirrup stress distributions approximated the actual measurements well at the cracked section of interest for most of the specimens examined.

Response 2000™ was conservatively higher than the average measured stirrup stresses, shown as a dotted line; note that the average measured stirrup stresses reflect only the measured values and do not include all the stirrup stresses along the entire diagonal crack.

The exception was specimen 9T12-4, where the experimental stirrup stresses at the crack were much higher than the calculated values. Examining the results of the Response 2000™ analysis more closely, Fig. 25 shows that the crack angle was calculated to be approximately 40° from the horizontal. The actual crack angle was 54°, which meant fewer stirrups were crossed by the diagonal crack and thus these stirrups had higher stresses in order to carry the same amount of load. The other analyses by Response 2000™ approximated the actual crack angle more closely, illustrated in Fig. 26. This indicates that the program does not produce accurate stress values if the calculated diagonal crack angle differs greatly from the actual angle. Further testing is required to determine whether an adjustment factor for crack angle may be employed.

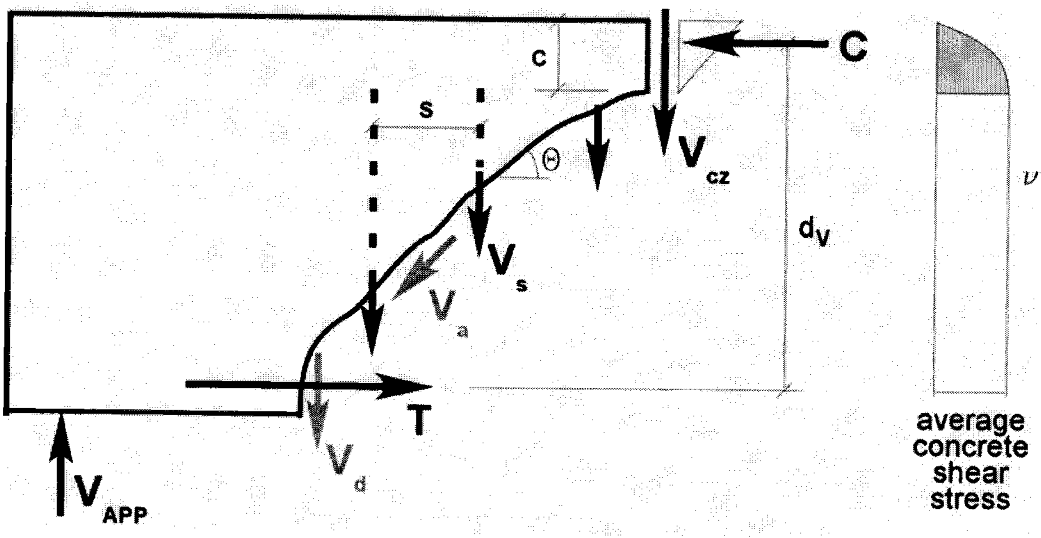

Figure 20—Illustration of dimensions and force components acting on a cracked section.

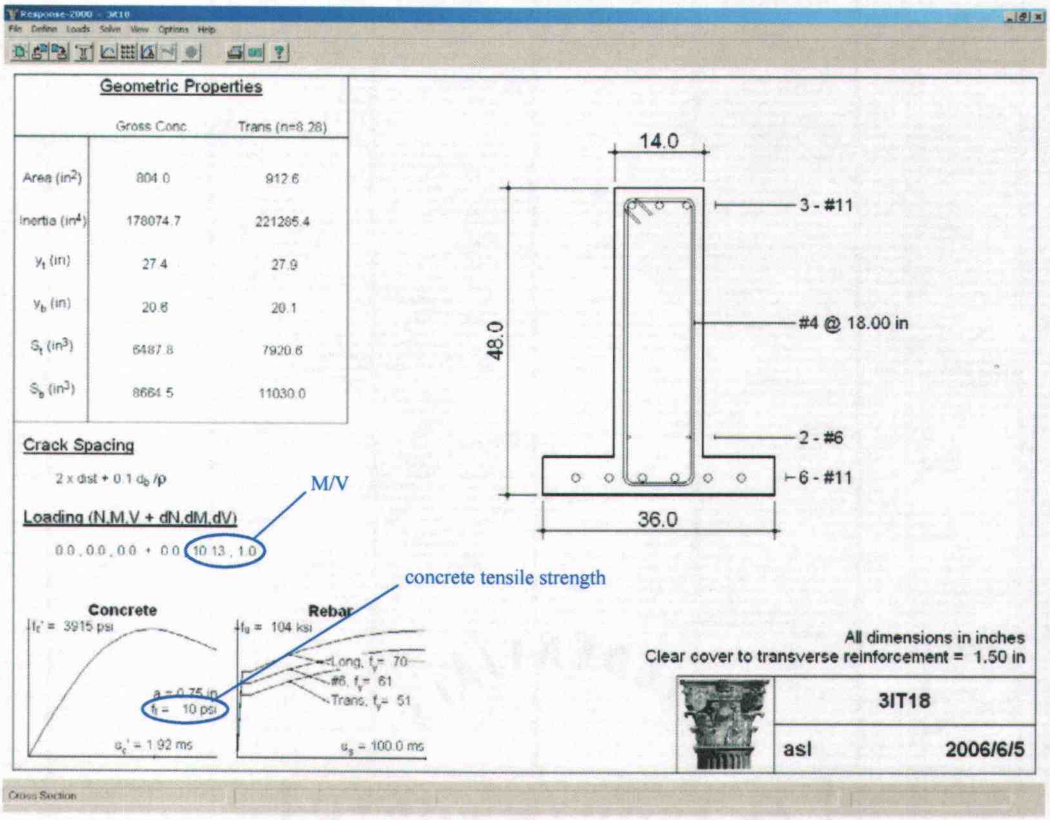

Figure 21—Example cross section in Response 2000^{TM}, specimen 3IT18.

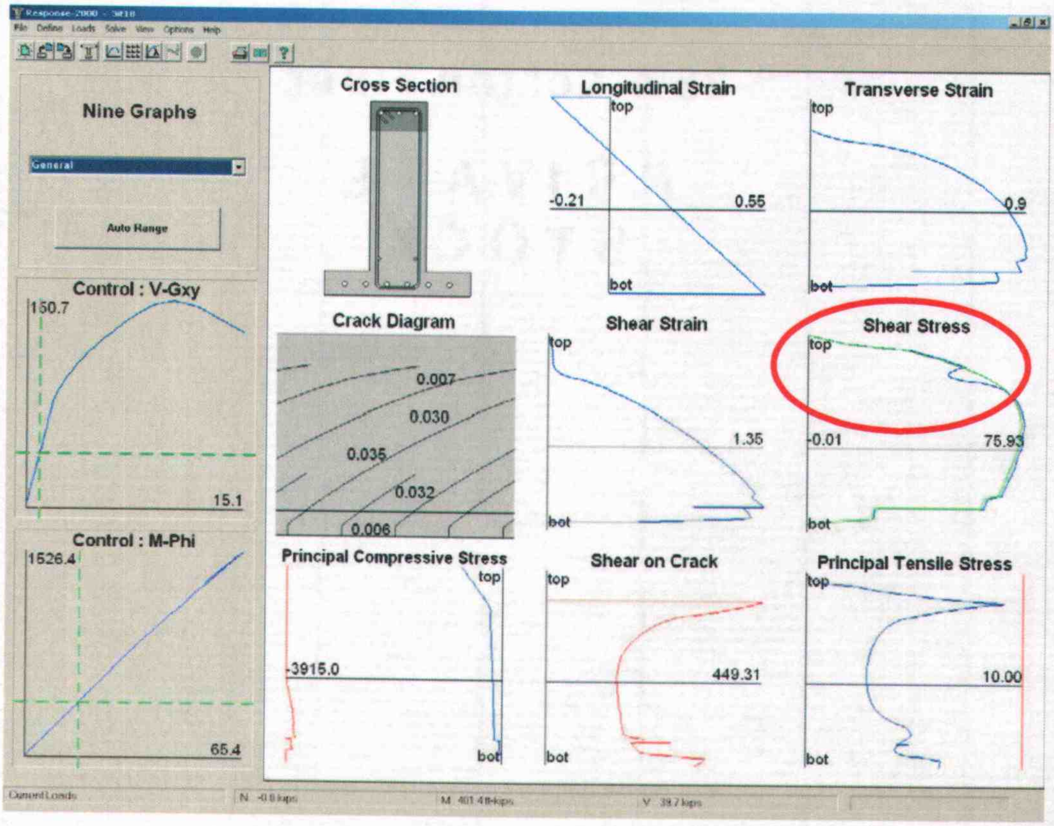

Figure 22—Example concrete stress and strain output in Response 2000™, specimen 3IT18. "Shear Stress" is used to calculate V_{cz}.

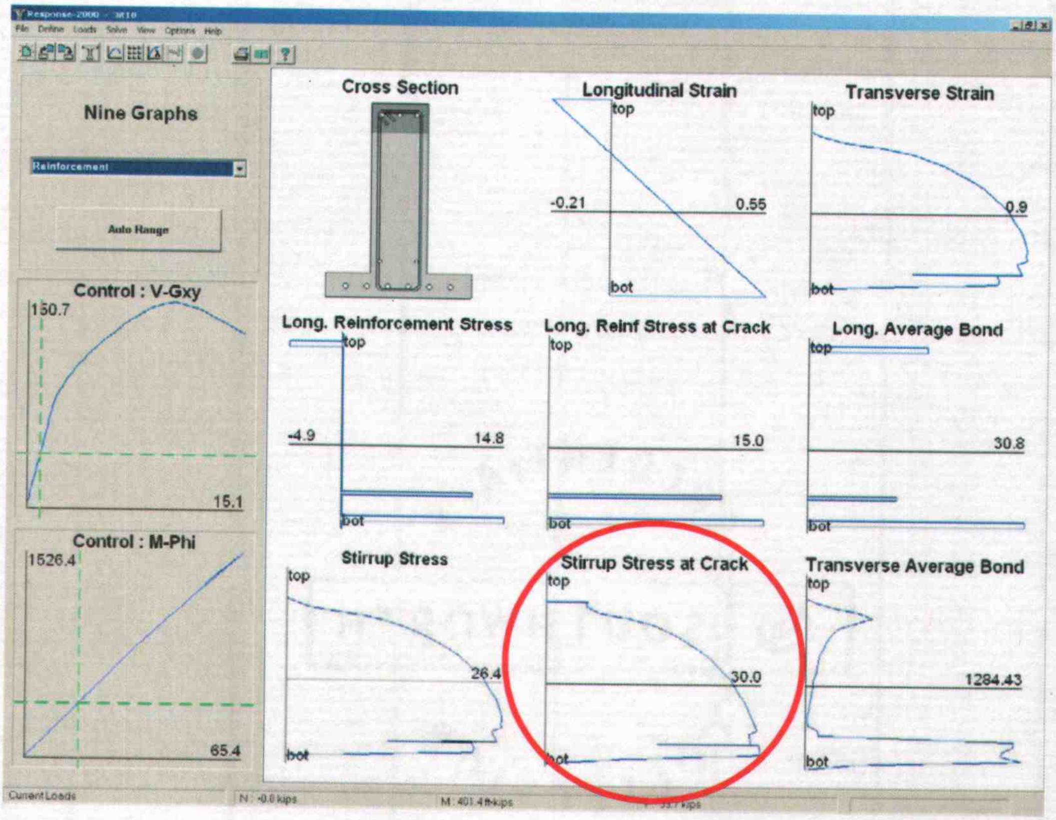

Figure 23—Example reinforcement stress and strain output in Response 2000™, specimen 3IT18. "Stirrup Stress at Crack" is compared to the experimental data.

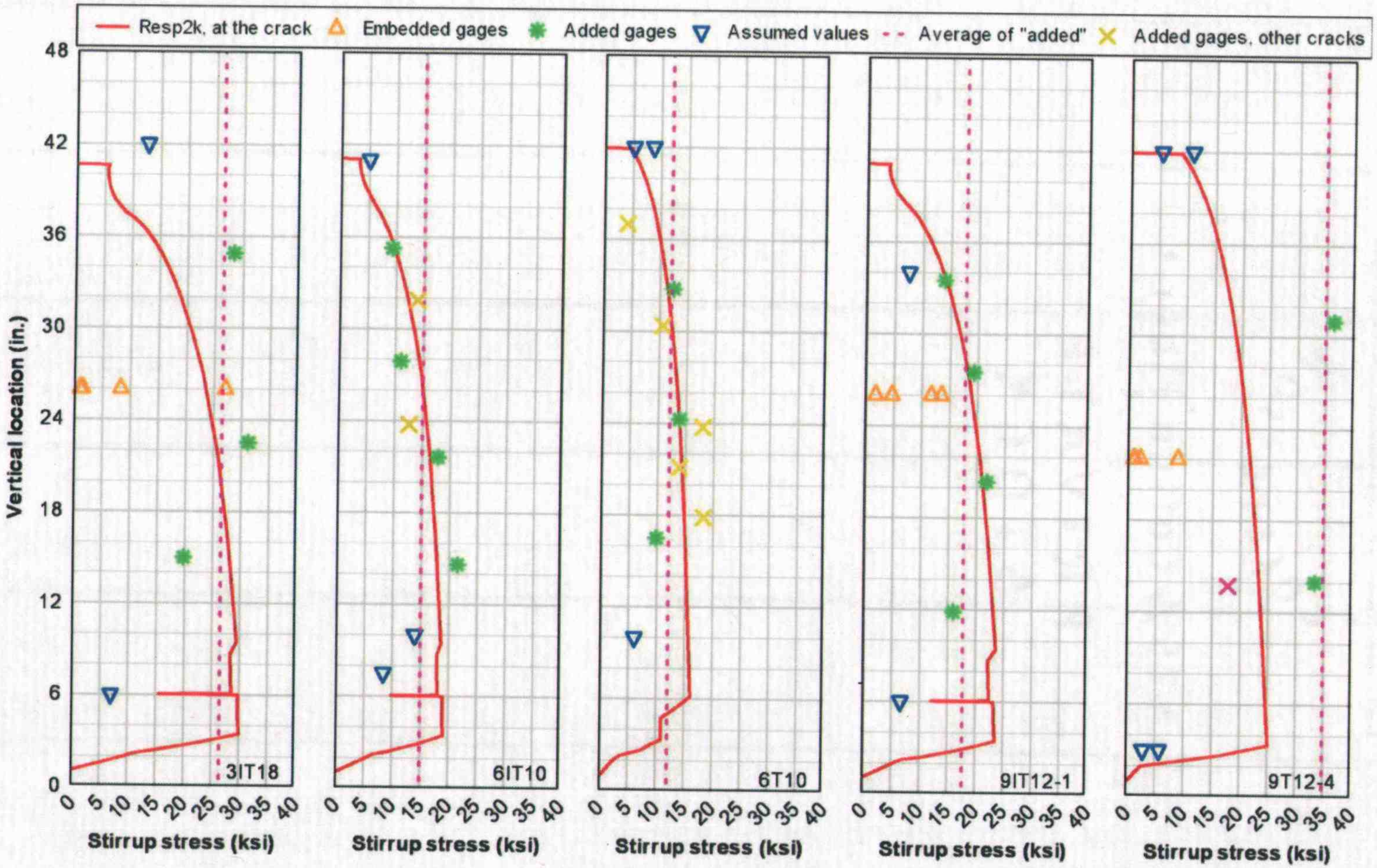

Figure 24—Stirrup stress from laboratory measurements and Response 2000™.

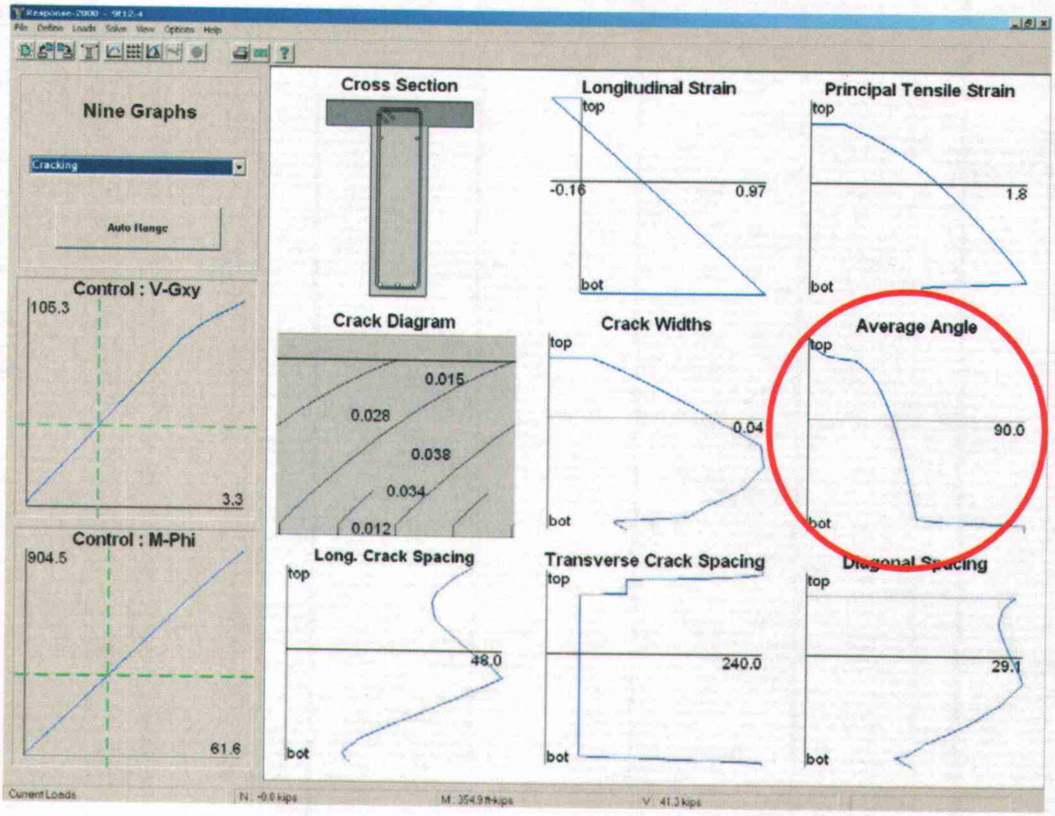

Figure 25—Crack angle for specimen 9T12-4 from Response 2000™.

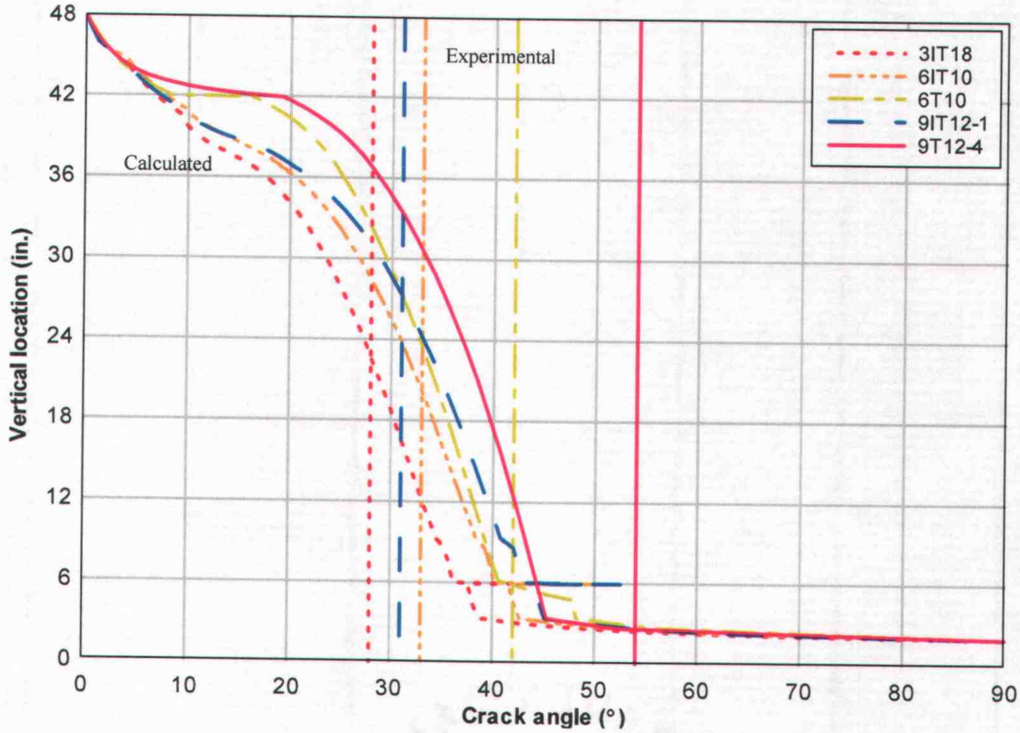

Figure 26—Comparison of crack angle as observed experimentally and calculated by Response 2000™.

Table 11—Experimental shear in stirrups and compression zone.

Specimen	Approximated stirrup values: Distance from the south support (in.)	Distance from the stem end (in.)	Stress range (ksi)	Measured stirrup values: Gage	Stress range (ksi)	Vcz (kips)	Vapp (kips)
3IT18	45	42	7.0	GS6	19.8		
	117	6	12.8	GS7	31.2		
				GS8	28.3		
		Force (kips)	7.9		31.7	3.7	
				Sum (kips)		**43.4**	**40.1**
6IT10	42	40.5	8.4	GS1	21.4		
	52	38	13.9	GS2	17.8		
	102	7	5.1	GS3	11.0		
				GS4	9.3		
		Force (kips)	11.0		23.8	4.7	
				Sum (kips)		**39.5**	**39.7**
6T10	32	10	6.1	GS3	9.9		
	42	10	6.1	GS4	13.8		
	80	42	8.7	GS5	12.5		
	90	42	5.2				
		Force (kips)	10.4		14.5	3.3	
				Sum (kips)		**28.3**	**34.2**
9IT12-1	59	42	6.7	GS6	16.0		
	119	14	7.5	GS7	21.8		
				GS8	19.4		
				GS9	13.9		
		Force (kips)	5.7		28.5	5.1	
				Sum (kips)		**39.3**	**38.2**
9T12-4	36	3	2.9	GS6	33.3		
	48	3	5.8	GS7	36.3		
	84	42	10.9				
	96	42	5.4				
		Force (kips)	10.0		27.9	3.8	
				Sum (kips)		**41.6**	**39.2**

CONCLUSIONS

Nine full-size girders were loaded to create diagonal cracks and then subjected to fatigue loading to impose the equivalent damage caused by 50 years of use. By means of various gages and measurements, trends in behavior were noted and the shear was attributed to the stirrups and compression zone. The observed values were compared to those predicted by a sectional analysis program that employs MCFT and found to correlate well. The following conclusions are presented:

- The beams were loaded with an average 19% to 40% range of the AASHTO LRFD MCFT nominal shear capacity which induced a stress range of 13.8 ksi, the range required to produce the estimated equivalent service life damage in 2,000,000 cycles, in at least one monitored location.
- Strains typically had no net change in range and a very small increase in mean, while cracks typically showed a subtle but definite increase in both range and mean.
- Crack widths and extensions were not reliable indicators of changes in strain, although there appears to be a linear relationship between strain range during cycling and change in crack width.
- Brittle fracture occurred only in the specimen with the widest stirrup spacing, towards the end of the prescribed cycling protocol and at stresses significantly larger than the observed in situ service range. The opposite

stirrup leg acquired most of the force formerly carried by the fractured bar but adjacent stirrups also showed increases.

- A shallower crack angle results in higher stirrup strain ranges due to increased vertical movement for the transverse reinforcement and less flexure from offset crack faces, based on observations that diagonal crack motion is largely perpendicular to the crack. This appears to be valid until the crack becomes even steeper and crack movement takes on more parallel motion. Measured strain ranges are also affected by proximity to a crack.
- Cracks are constrained by the compression zone and flexural reinforcement, causing larger motions and correspondingly higher strain ranges in the middle of the crack.
- Shear in the compression zone can easily be calculated by assuming a parabolic stress distribution. Average stirrup stresses in a diagonal crack under service load can also be calculated using a simple equation, although estimating the maximum stress in the diagonal crack requires an amplification factor.
- Response 2000™ may be manipulated to simulate a precracked state by setting the tensile strength of concrete very low.
- The stirrup stresses calculated by Response 2000™ conservatively approximate the average ranges measured experimentally and nearly match

the maximum observed ranges where the calculated and actual crack angles are similar.

REFERENCES

AASHTO, (2002). *Standard Specification for Highway Bridges.* 17th Edition, AASHTO, Washington, D. C.

ACI 318-02, (2002). *Building Code Requirements for Structural Concrete.* American Concrete Institute, Farmington Hills, Michigan.

ACI Committee 215R-92 (1992). *Considerations for Design of Concrete Structures Subjected to Fatigue Loading.* American Concrete Institute, Detroit, Michigan.

ACI SP-41 (1974). *Abeles Symposium - Fatigue of Concrete.* American Concrete Institute, Detroit, Michigan.

ACI SP-75 (1982). *Fatigue of Concrete Structures.* S.P. Shah (editor), American Concrete Institute, Detroit, Michigan.

Balazs, G.L., (1998). Bond under repeated loading. SP 180-6: Bond under Repeated Loading, A Tribute to Dr. Peter Gergely, Leon, R. (Editor), American Concrete Institute, Farmington Hills, Michigan, pp. 125-143.

Bentz, E. (2000). Sectional analysis of reinforced concrete members. Ph.D. thesis, Department of Civil Engineering, University of Toronto, Toronto, Canada.

Bresler, B., and Bertero, V. (September 15-7, 1966). Reinforced concrete prism under repeated loads. *RILEM International Symposium on The Effects of Repeated Loading of Materials and Structural Elements*, Mexico City.

Chang, T.S. and C.E. Kesler, (1958). Static and fatigue strength in shear of beams with tensile reinforcement. *Journal of the American Concrete Institute*, Vol. 29, No. 12, pp. 1033-1053.

Constantinescu, A., Dang Van, K., & Maitournam, M. H. (2003). A unified approach for high and low cycle fatigue based on shakedown concepts. *Fatigue & fracture of engineering materials & structures*, 26, pp. 561-568.

Corley, W.G., Hanson, J.M., and T. Helgason, (1978). Design of reinforced concrete for fatigue. *Journal of the Structural Division,* ASCE, Vol. 104, No. ST6, pp. 921-932.

Hanson, J.M., Burton, K.T., and E. Hognestad, (1968). Fatigue tests of reinforcing bars – effect of deformation pattern. *Journal of the PCA Research and Development Laboratories*, Vol. 10, No. 3, pp.2-13.

Hanson, J.M. and Hulsbos, C.L. and D.A. VanHorn, (1970). Fatigue tests of prestressed concrete I-beams. *Journal of the Structural Division,* ASCE, Vol. 96, No. ST11, pp. 2443-2464.

Hanson, J.M., Somes, M.F. and T. Helgason, (1974). Investigation of design factors affecting fatigue strength of reinforcing steel – test program. *SP-41: Abeles Symposium - Fatigue of Concrete*, American Concrete Institute, Detroit, Michigan, pp. 71-106.

Hawkins, N.M. (1974). Fatigue characteristics in bond and shear of reinforced concrete beams. *SP-41: Abeles Symposium - Fatigue of Concrete*, American Concrete Institute, Detroit, Michigan, pp. 203-236.

Helgason, T. and J.M. Hanson, (1974). Investigation of design factors affecting fatigue strength of reinforcing steel – statistical analysis. *SP-41: Abeles Symposium - Fatigue of Concrete*, American Concrete Institute, Detroit, Michigan, pp. 107-138.

Higgins, C., et al. (2004a). *Assessment methodology for diagonally cracked reinforced concrete deck girders* (Report No. FHWA-OR-RD-05-04). Available WWW: From the National Technical Information Service (NTIS) or through the Oregon Department of Transportation (ODOT) at http://www.odot.state.or.us/tddresearch.

Higgins, C., Yim, S. C., Miller, T. H., Robelo, M. J., & Potisuk, T. (2004b). *Remaining life of reinforced concrete beams with diagonal-tension cracks* (Report No. FHWA-OR-RD-04-12). Available WWW: From the National Technical Information Service (NTIS) or through the Oregon Department of Transportation (ODOT) at http://www.odot.state.or.us/tddresearch.

Higgins, C., Farrow III, W. C., Nicholas, B. S., & Potisuk, T. (in publication queue). *High-cycle fatigue of diagonally-cracked RC bridges—field tests.* Oregon State University.

Jhamb I.C. and J.G. MacGregor, (1974). Effects of surface characteristics on fatigue strength of reinforcing steel. *SP-41: Abeles Symposium - Fatigue of Concrete*, American Concrete Institute, Detroit, Michigan, pp. 139-168.

Kaar, P. H., and Mattock, A. H. (January 1963). High strength bars as concrete reinforcement, part 4—control of cracking. *Journal of the PCA Research and Development Laboratories*, Vol. 5, No. 1, pp. 15-38).

Kreger, M.E., Bachman, P.M., and J.E. Breen, (1989). An exploratory study of shear fatigue behavior of prestressed concrete girders. *PCI Journal,* July/August pp. 104-125.

Kwak, K-H. and J-G. Park, (2001). Shear-fatigue behavior of high-strength concrete under repeated loading. *Structural Engineering and Mechanics,* Vol. 11, No. 3, pp. 301-314.

Kwak, K-H., Suh, J., and C-Z., T. Hsu, (1991). Shear-fatigue behavior of steel fiber reinforced concrete beams. *ACI Structural Journal,* Vol. 88, No. 2, pp. 155-160.

MacGregor, J. G. (1997). *Reinforced Concrete: Mechanics and Design* (3rd ed.). Upper Saddle River, NJ: Prentice-Hall, Inc.

Okamura, H., Farghaly, S. A., and Ueda, T. (April 1981). Behaviors of reinforced concrete beams with stirrups failing in shear under fatigue loading. *Proceedings of the Japan Society of Civil Engineers*, Issue 308, pp. 109-122.

OTIA III Bridge Oversight Committee (March 2005). *Appendix A: History and condition of Oregon's bridges* [Online Web site]. Available WWW: http://www.oregon.gov/ODOT/COMM/docs/bridge_options/bor_A.pdf.

Price, K.M. and A.D. Edwards, (1971). Fatigue strength in shear of prestressed concrete I-beams. *ACI Journal,* ACI, Vol. 68, April, pp. 282-292.

Rehm, G. and R. Eligehausen, (1979). Bond of ribbed bars under high-cycle repeated loads. *ACI Journal,* Vol. 76, Feb., pp. 297-309.

RILEM Committee 36-RDL (1984). Long term random dynamic loading of concrete structures, *Materials and structures*, Vol. 17, No. 97, pp. 1-28.

Robelo, M. J. (2004). Analysis of diagonally cracked conventionally reinforced concrete girders in the service load range. M.S. thesis, Oregon State University, Corvallis, Oregon.

Teng, S., Ma, W., Tan, K.H., and F.K. Kong, (1998). Fatigue tests of reinforced concrete deep beams. *The Structural Engineer*, Vol. 76, No. 18, pp. 347-352.

Ueda, T. and H. Okamura, (1983). Behavior in shear of reinforced concrete beams under fatigue loading. *Journal of the Faculty of Engineering,* The University of Tokyo, Vol. 37, No. 1, pp. 17-48.

Ueda, T. and H. Okamura, (1981). Behavior of stirrup under fatigue loading. *Transactions of the Japan Concrete Institute,* JCI, Vol. 3, pp. 305-318.

APPENDICIES

APPENDIX A

SPECIMENS

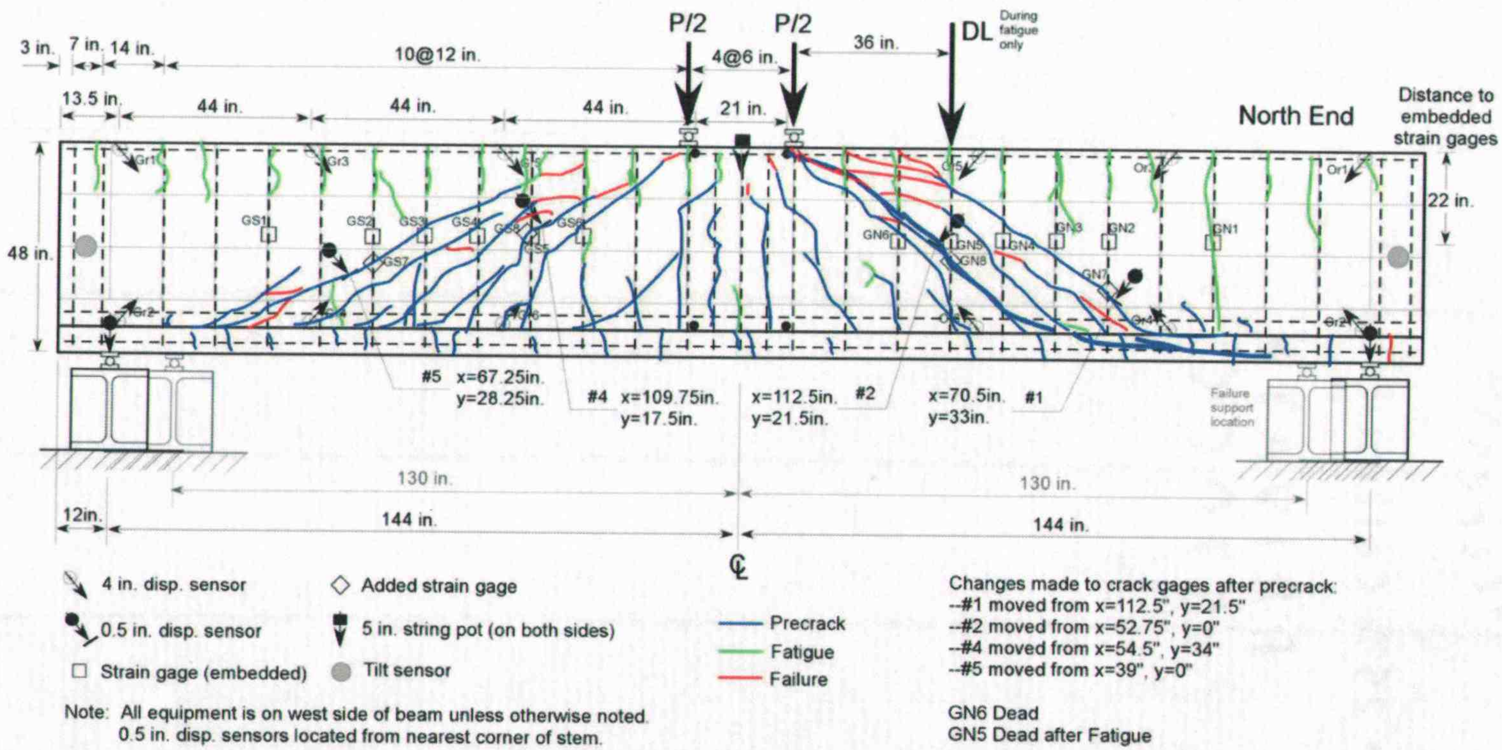

Figure A1a–Specimen 3IT12 instrumentation and crack pattern.

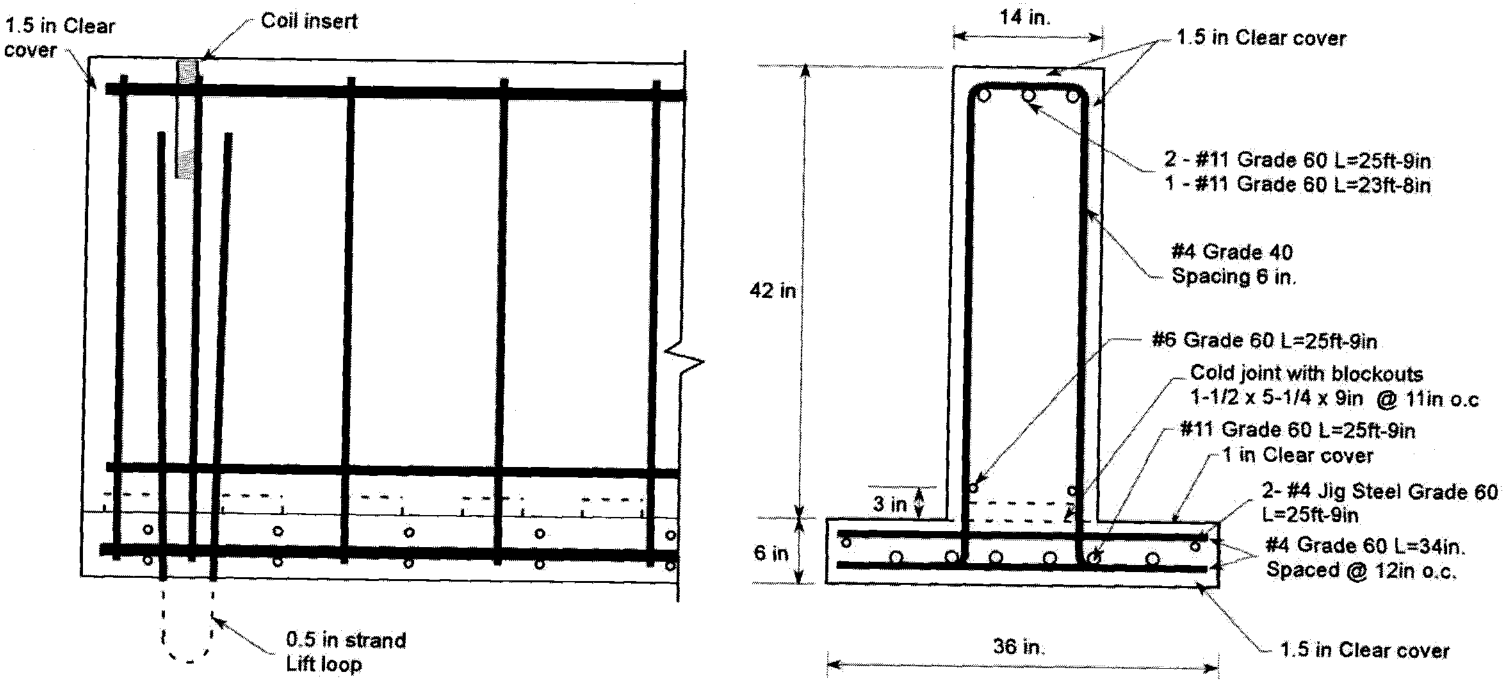

Figure A1b–Specimen 3IT12 cross-section and detailing.

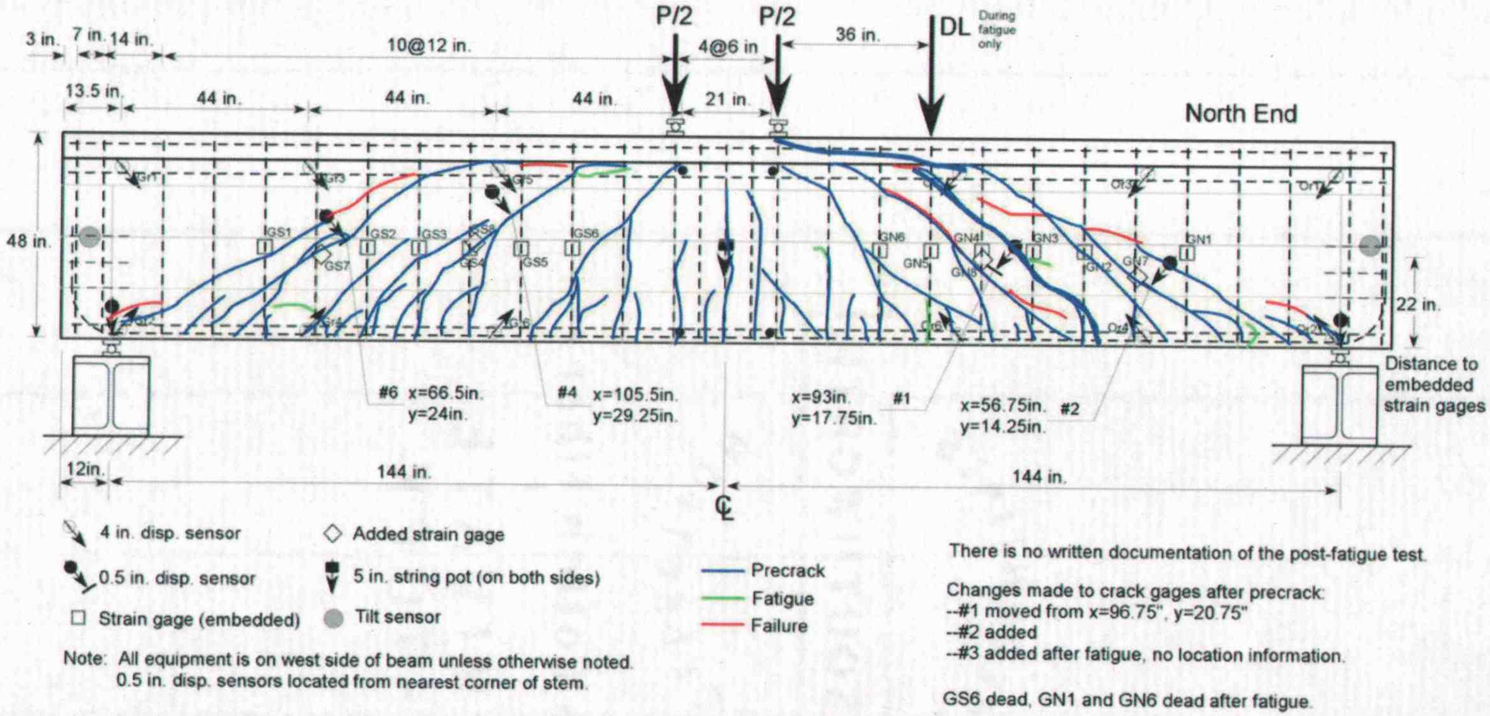

Figure A2a–Specimen 3T12 instrumentation and crack pattern.

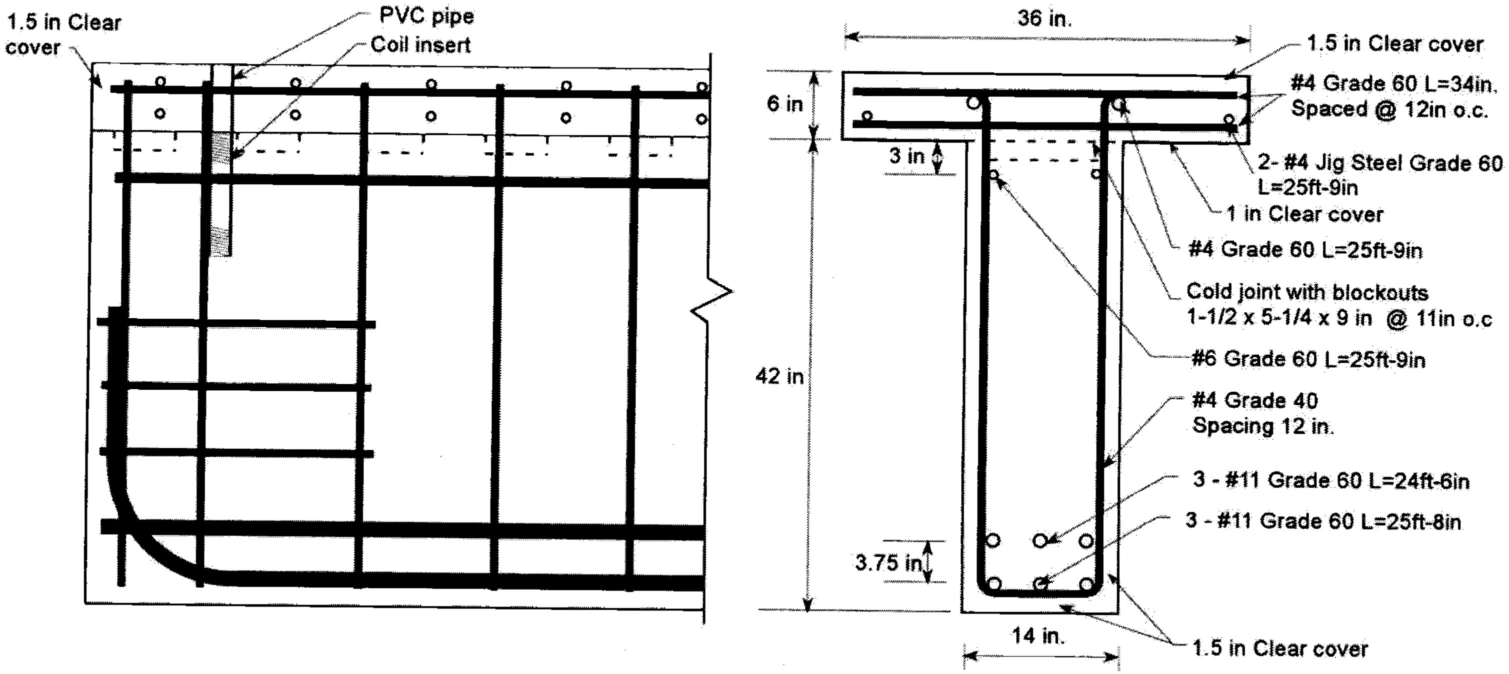

Figure A2b–Specimen 3T12 cross-section and detailing.

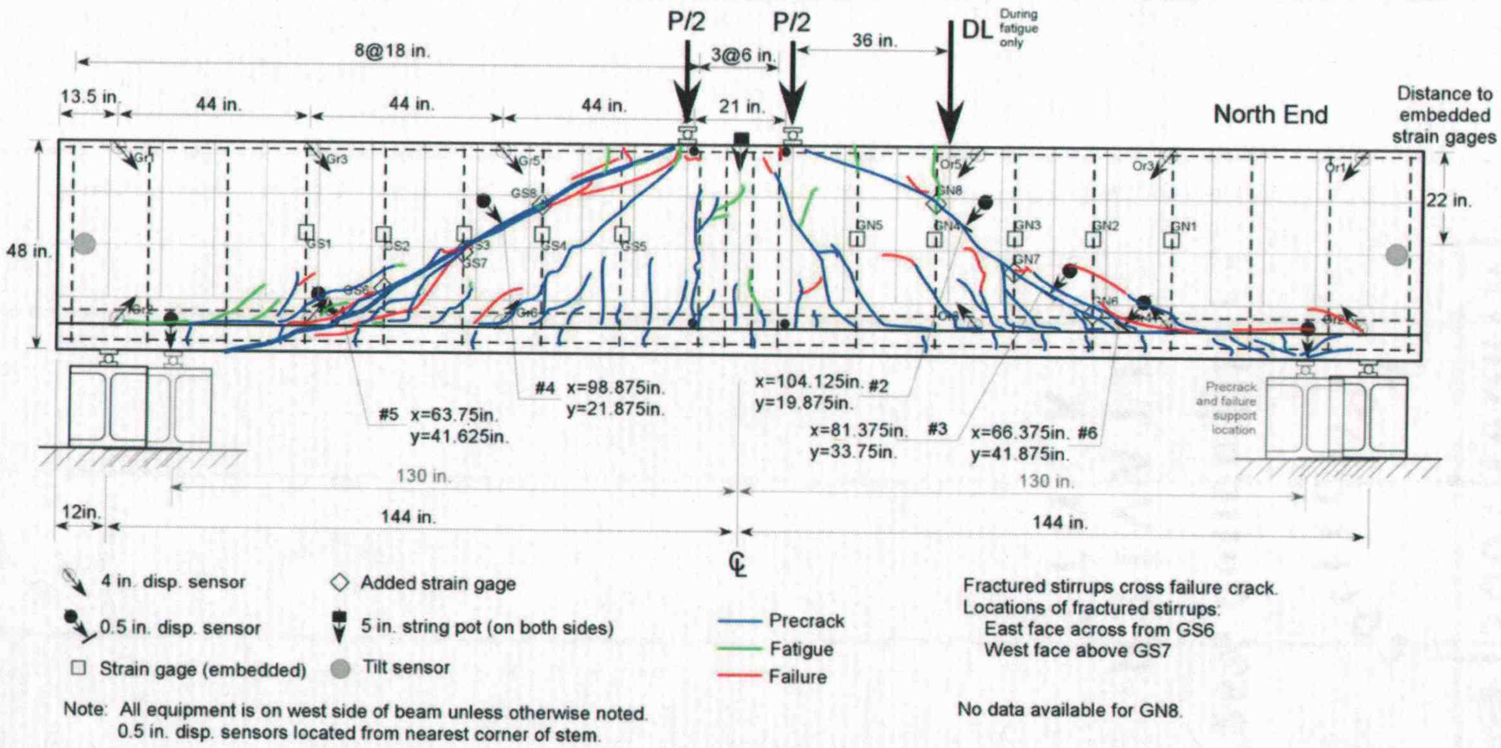

Figure A3a–Specimen 3IT18 instrumentation and crack pattern.

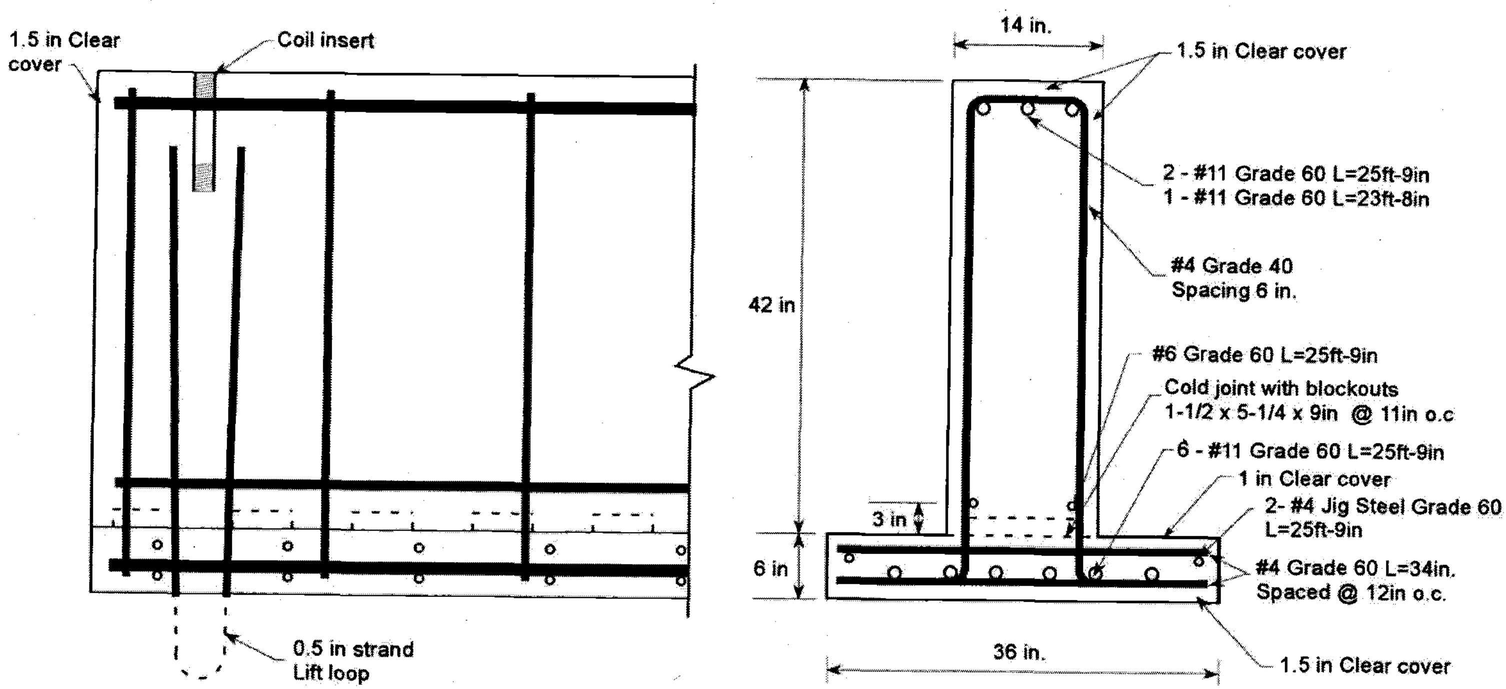

Figure A3b–Specimen 3IT18 cross-section and detailing.

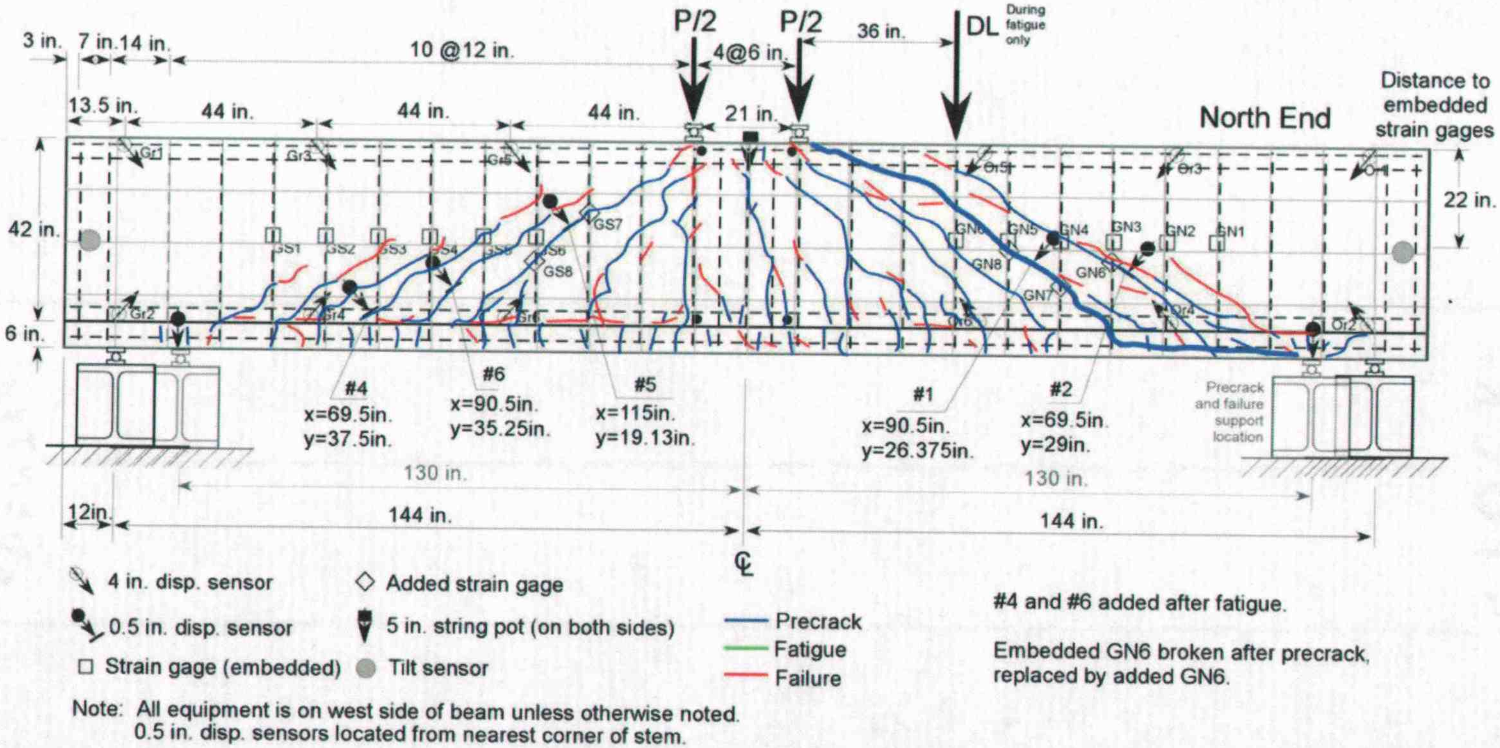

Figure A4a–Specimen 5IT12-1 instrumentation and crack pattern.

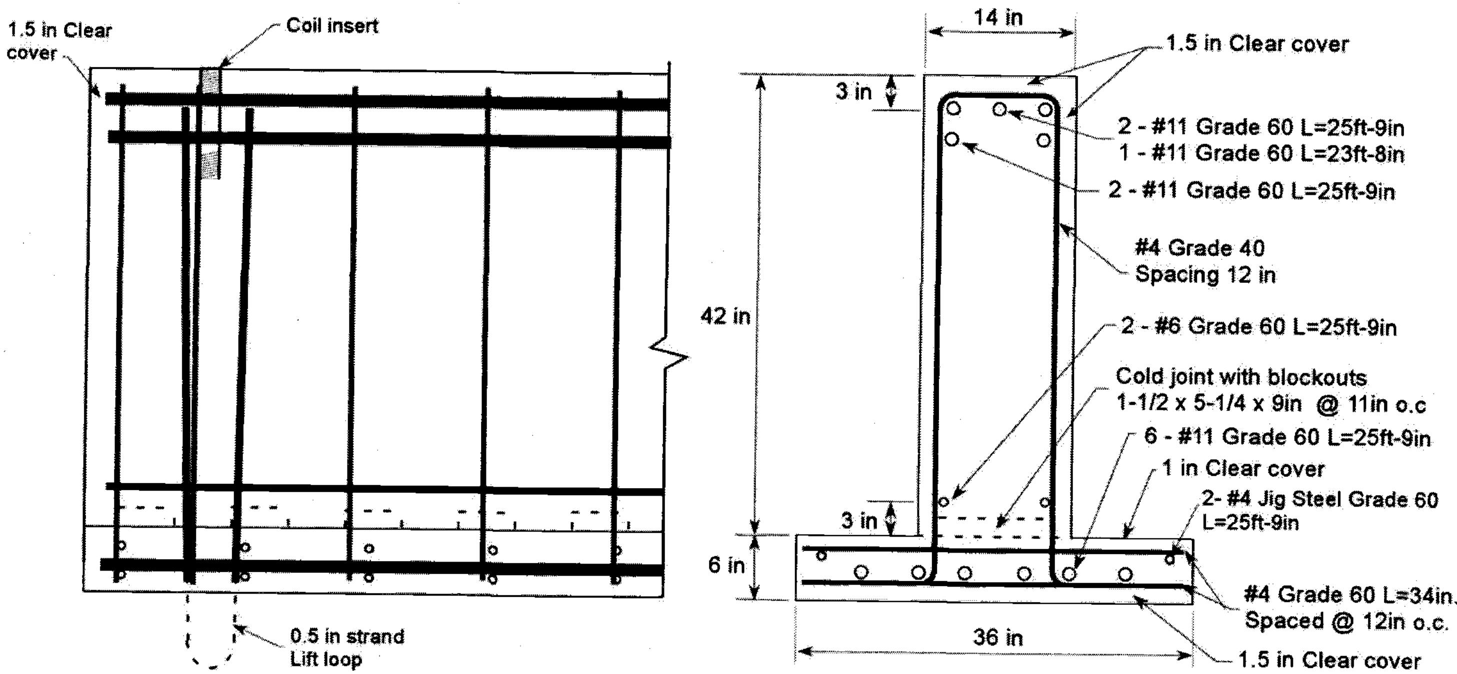

Figure A4b–Specimen 5IT12-1 cross-section and detailing.

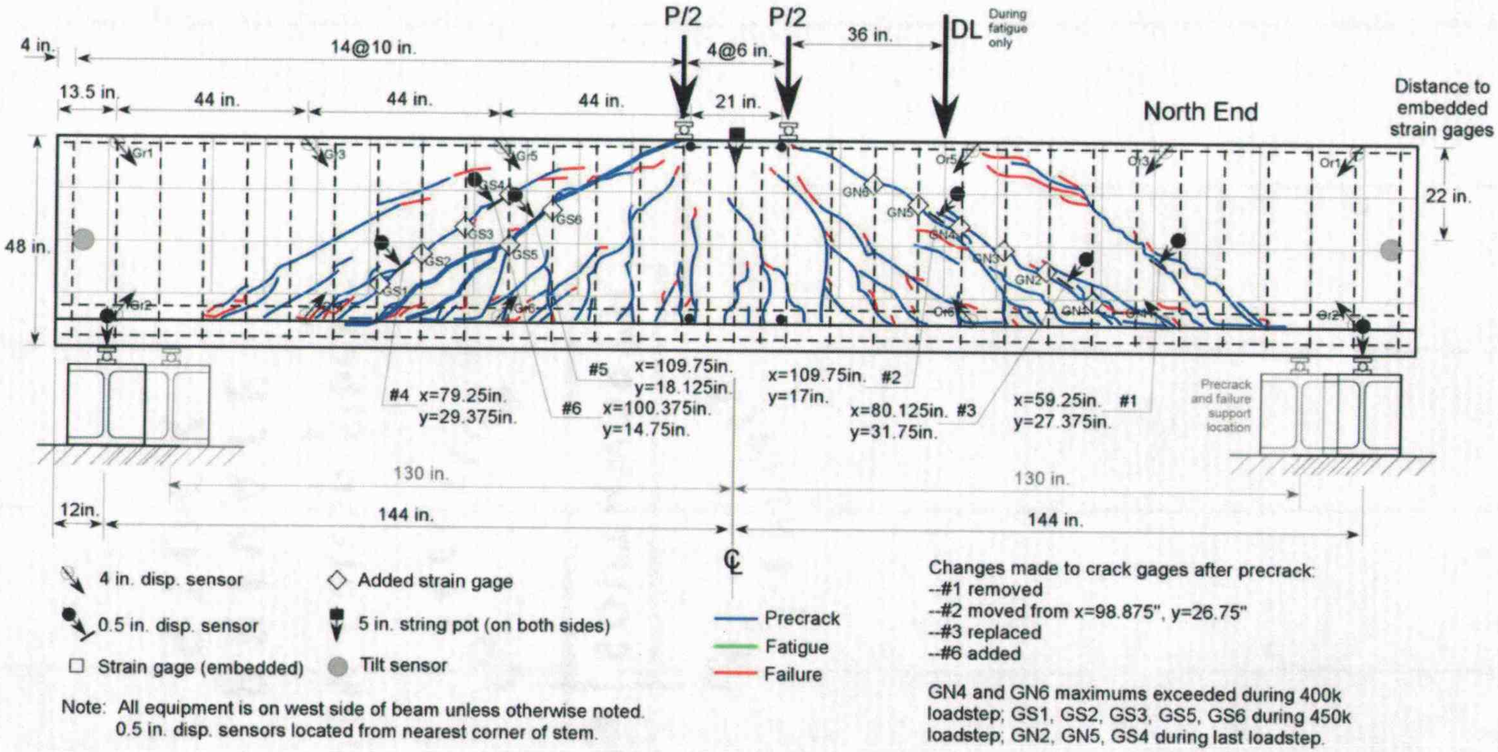

Figure A5a–Specimen 6IT10 instrumentation and crack pattern.

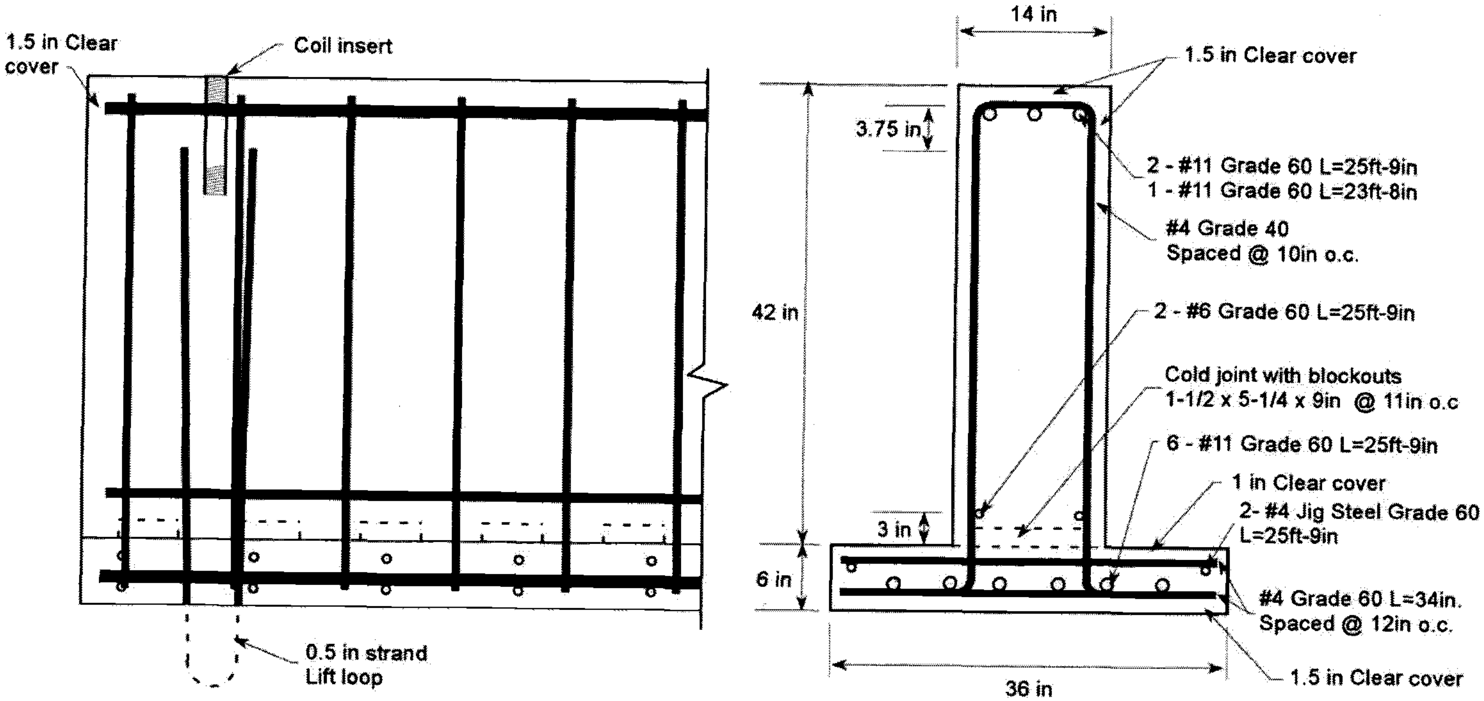

Figure A5b–Specimen 6IT10 cross-section and detailing.

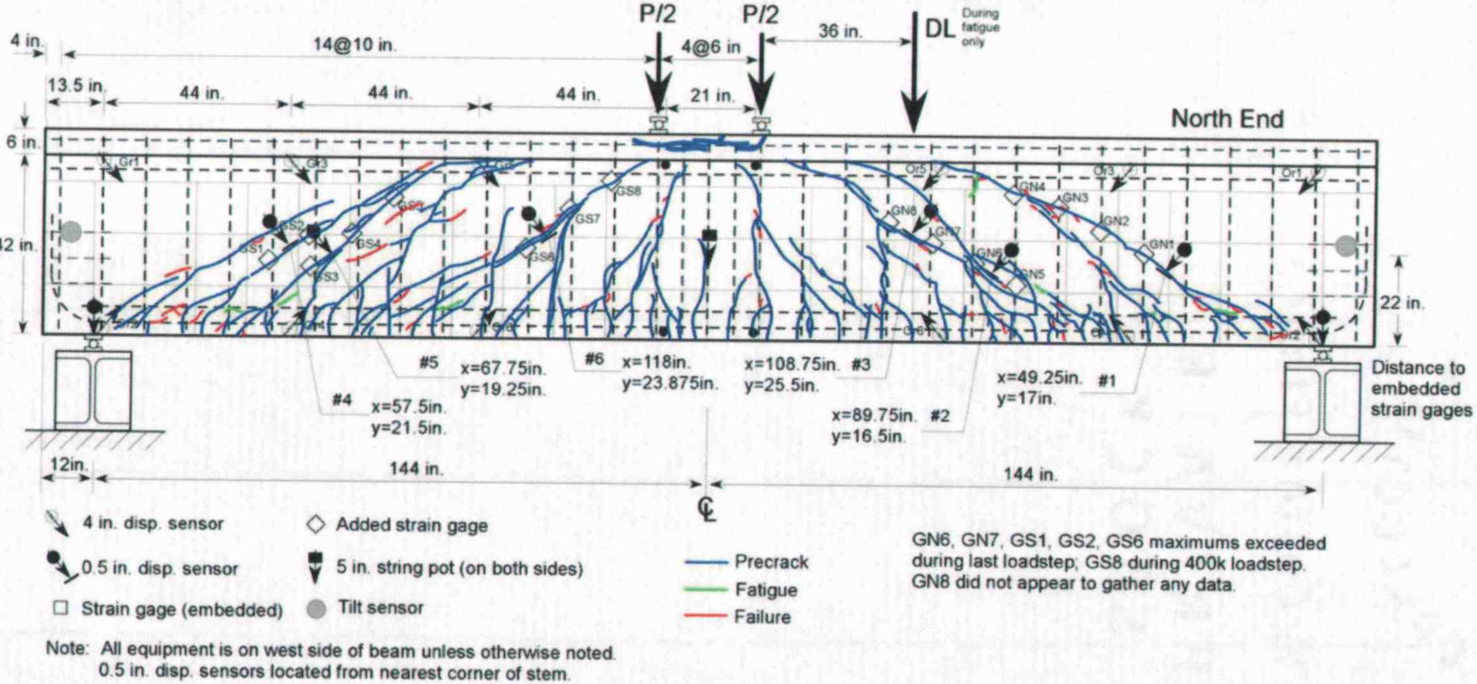

Figure A6a–Specimen 6T10 instrumentation and crack pattern.

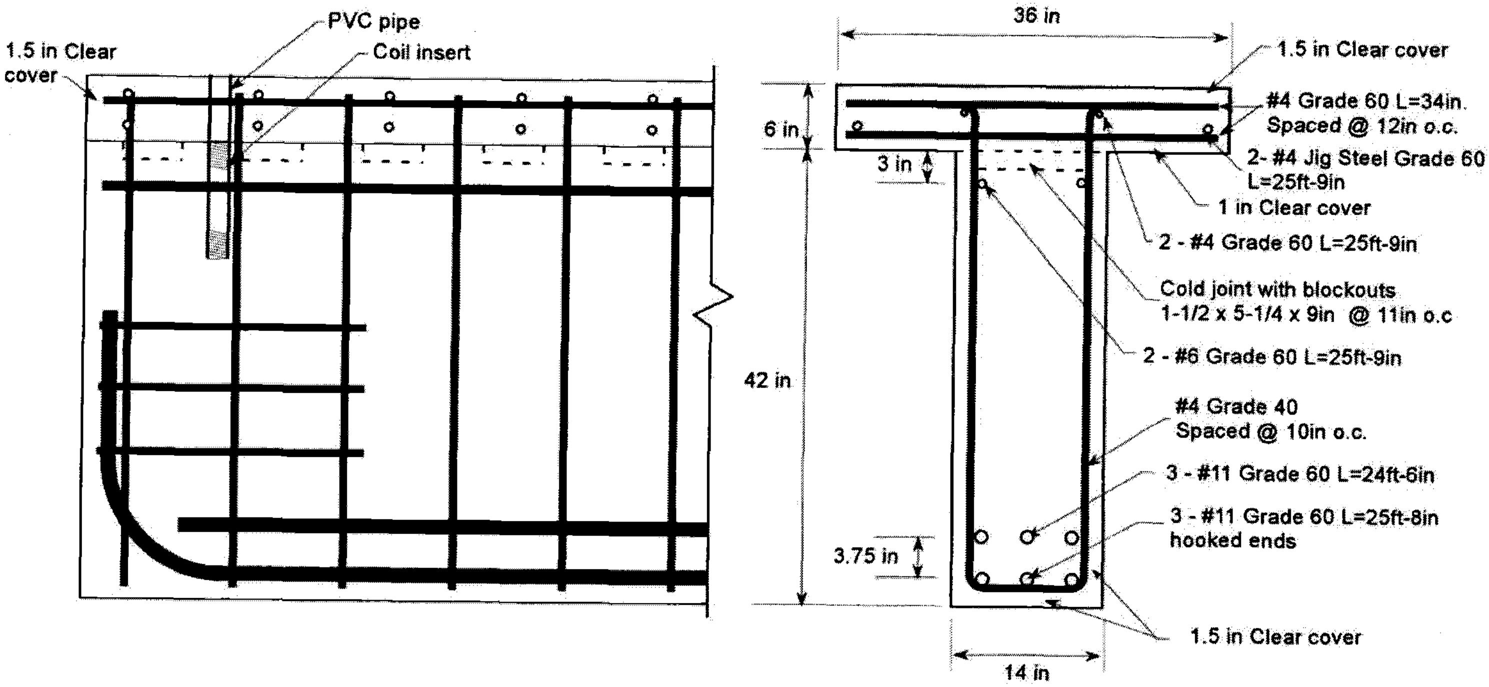

Figure A6b–Specimen 6T10 cross-section and detailing.

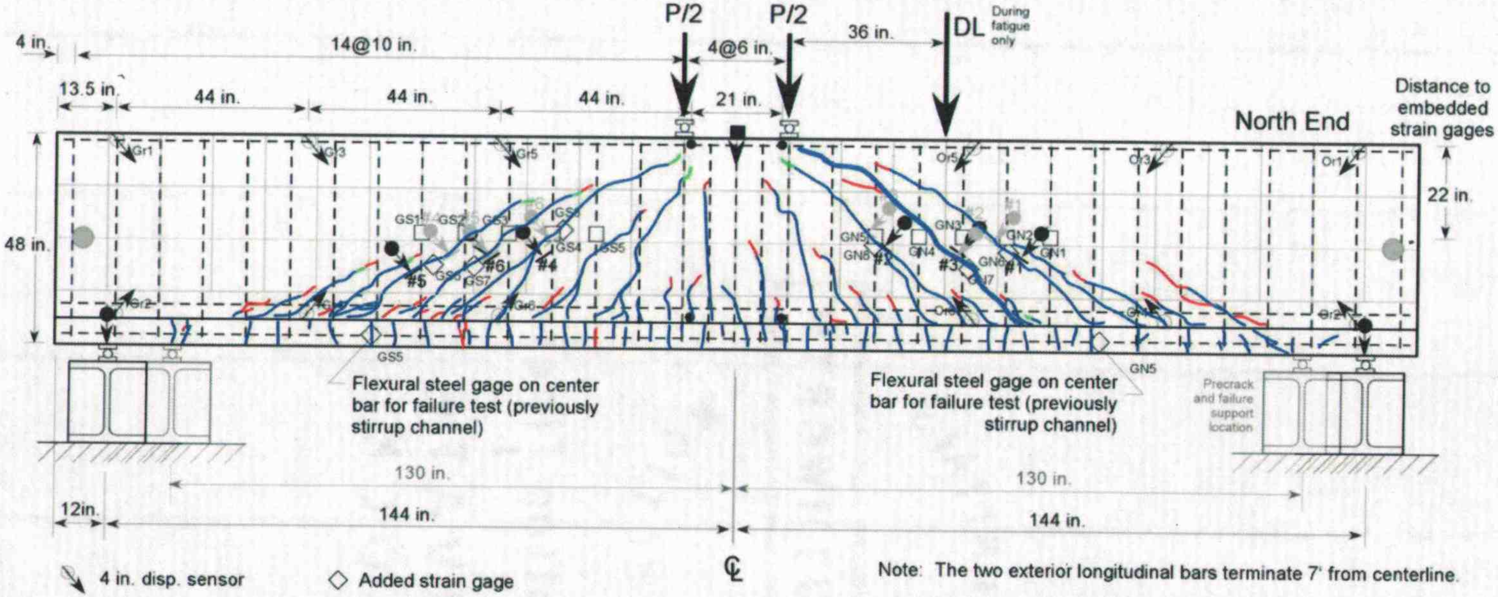

4 in. disp. sensor

0.5 in. disp. sensor

□ Strain gage (embedded)

◇ Added strain gage

5 in. string pot (on both sides)

Tilt sensor

Precrack

Fatigue

Failure

Note: All equipment is on west side of beam unless otherwise noted.
0.5 in. disp. sensors located from nearest corner of stem.

Note: The two exterior longitudinal bars terminate 7' from centerline.

External strain gages on east face, crack motion sensors used during fatigue on east face.

Precrack: GN5 broke on the 300k loadstep. GS3 maximum exceeded on the 300k loadstep, GS2 on the 350k loadstep
Post-fatigue: GN2 broke on the 400k loadstep and GN8 did not appear to gather any data. GN6 maximum exceeded on the 350k loadstep, GN7 and GS6 on the 400k loadstep, GS7 and GS8 on the last loadstep.

Figure A7a–Specimen 8IT10 instrumentation and crack pattern.

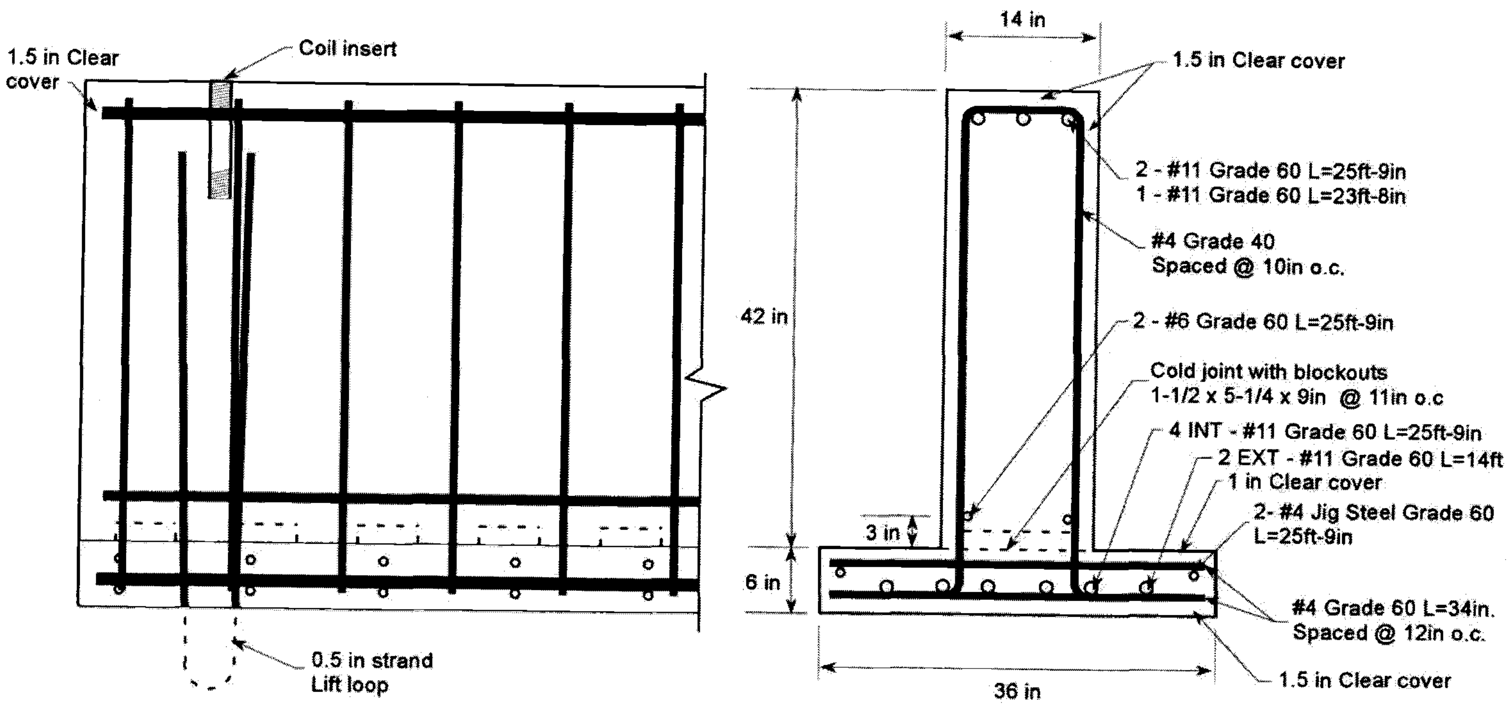

Figure A7b–Specimen 8IT10 cross-section and detailing.

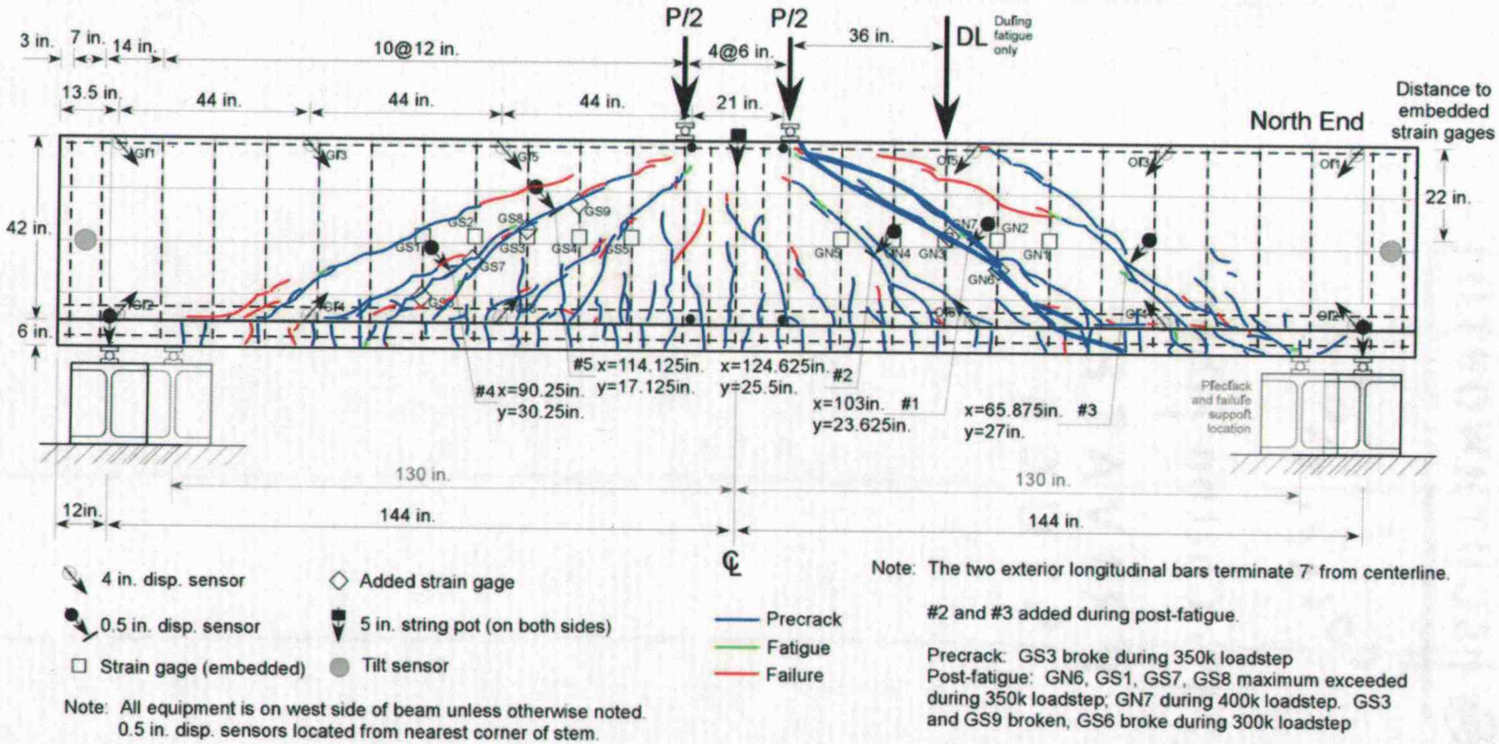

Figure A8a–Specimen 9IT12-1 instrumentation and crack pattern.

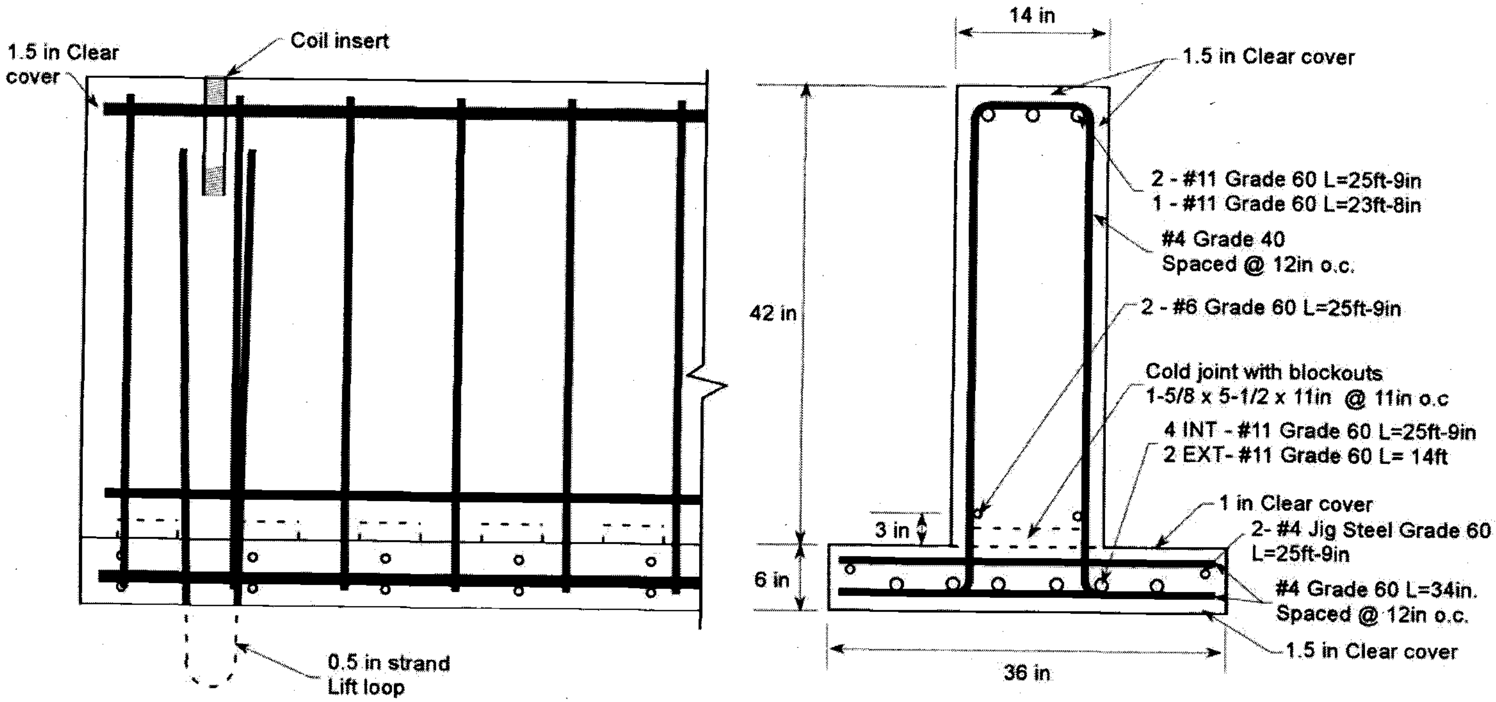

Figure A8b–Specimen 9IT12-1 cross-section and detailing.

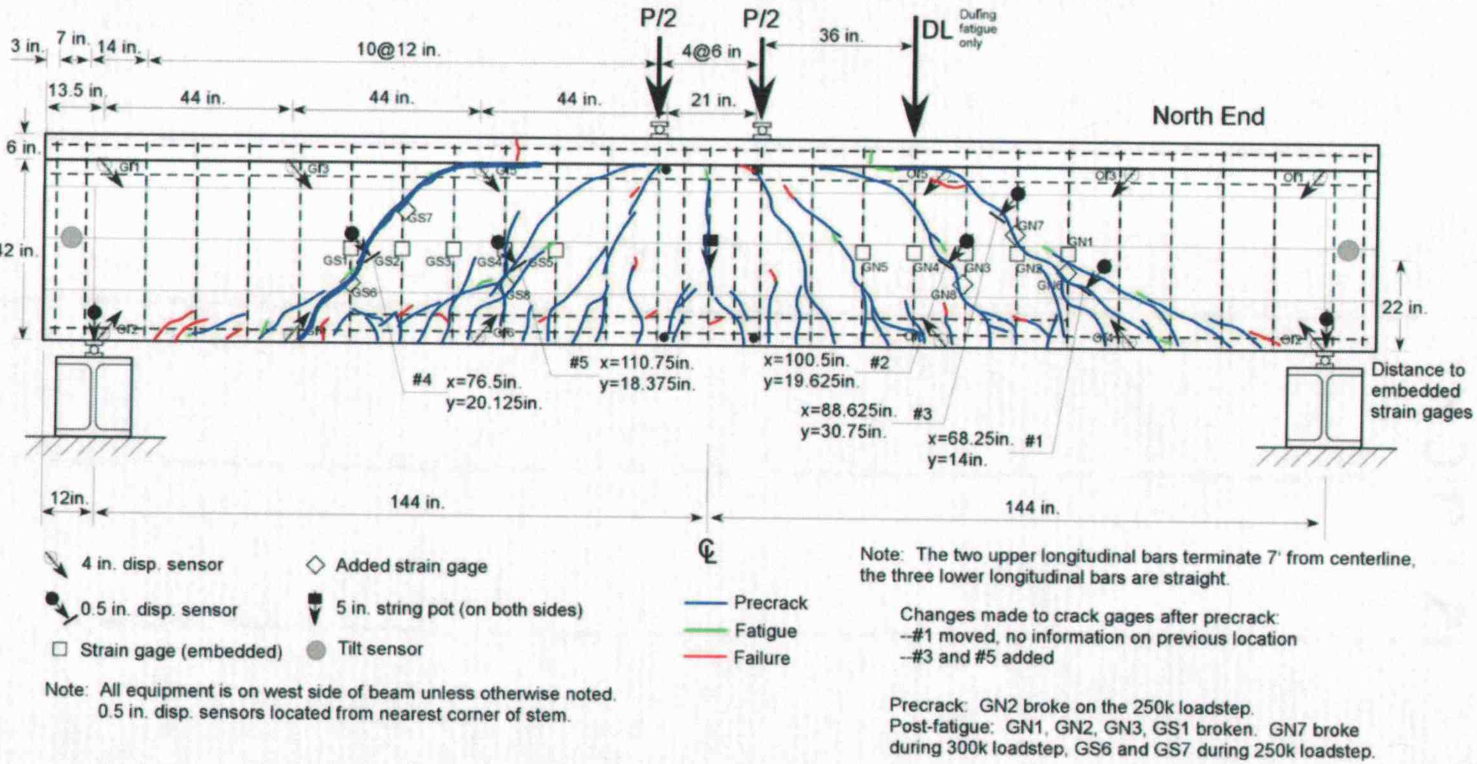

Figure A9a–Specimen 9T12-4 instrumentation and crack pattern.

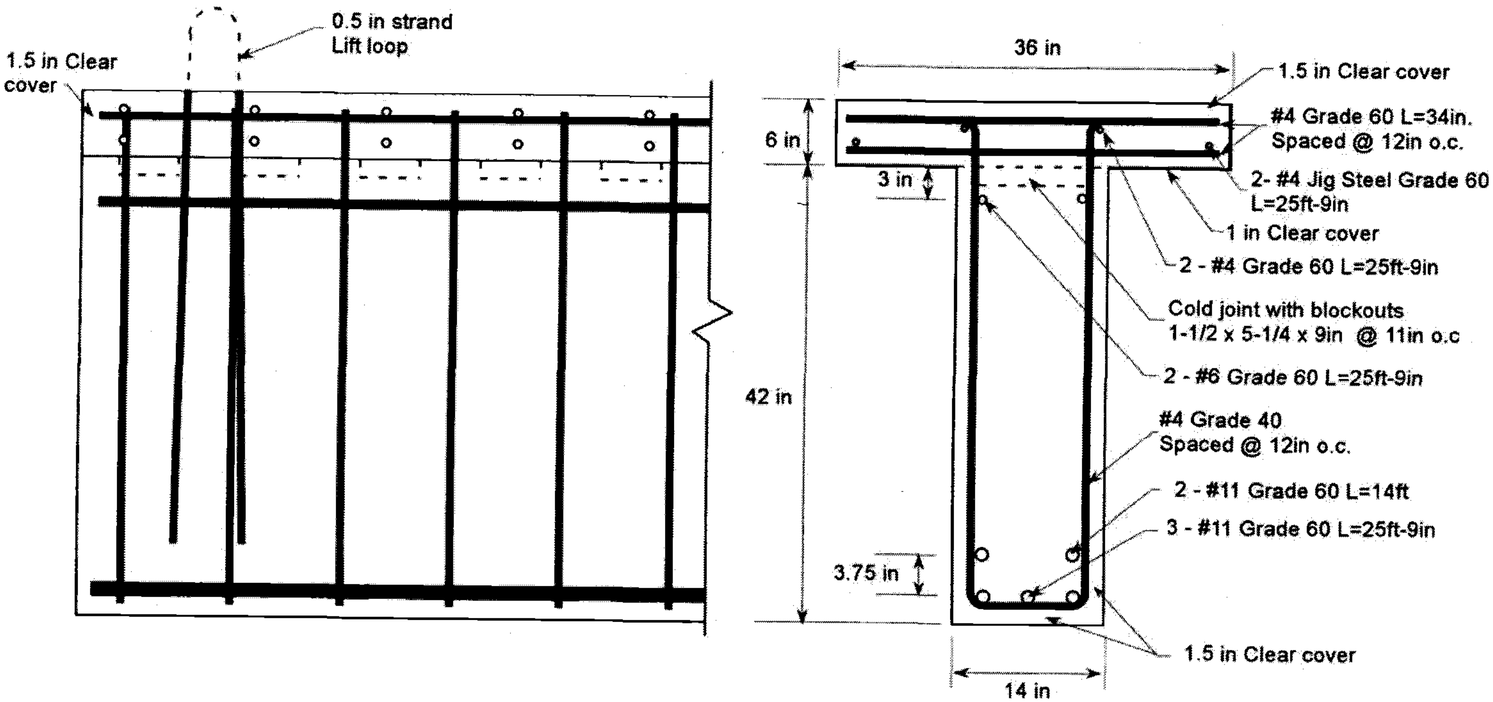

Figure A9b–Specimen 9T12-4 cross-section and detailing.

APPENDIX B

CYCLING PLOTS

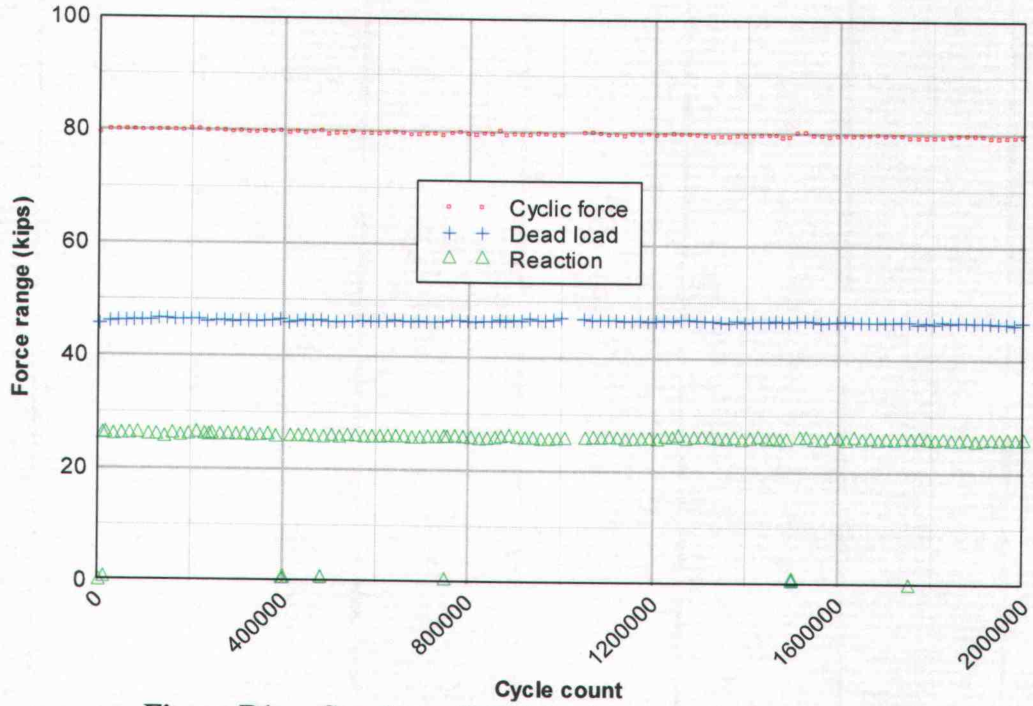

Figure B1a—Specimen 3IT12 load ranges during fatigue.

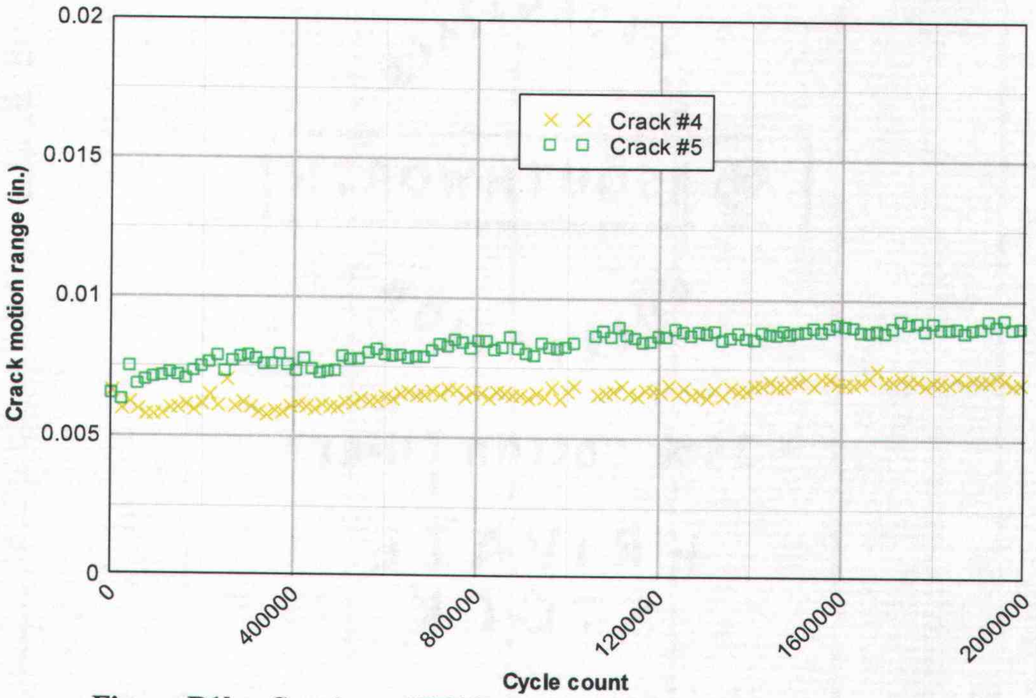

Figure B1b—Specimen 3IT12 south crack ranges during fatigue.

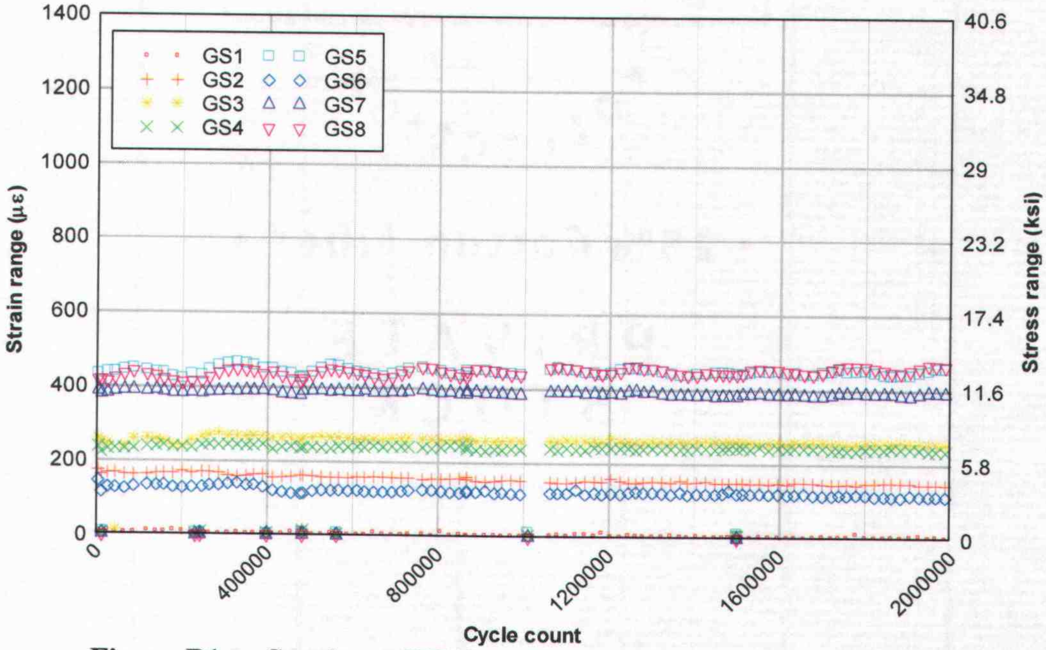

Figure B1c—Specimen 3IT12 south strain ranges during fatigue.

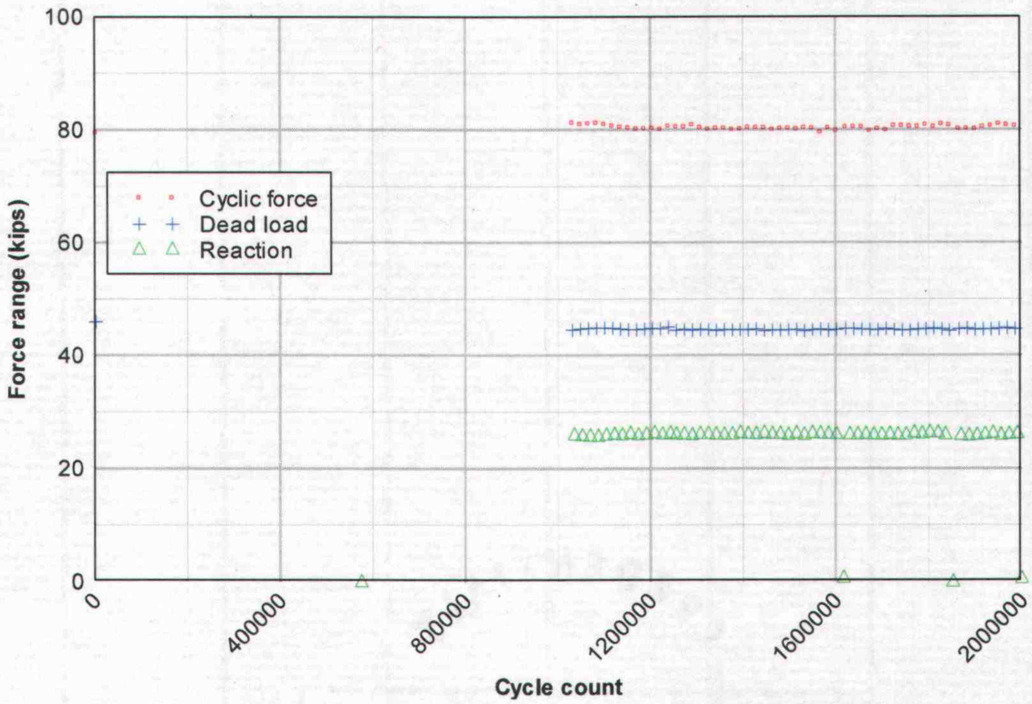

Figure B2a—Specimen 3T12 load ranges during fatigue.

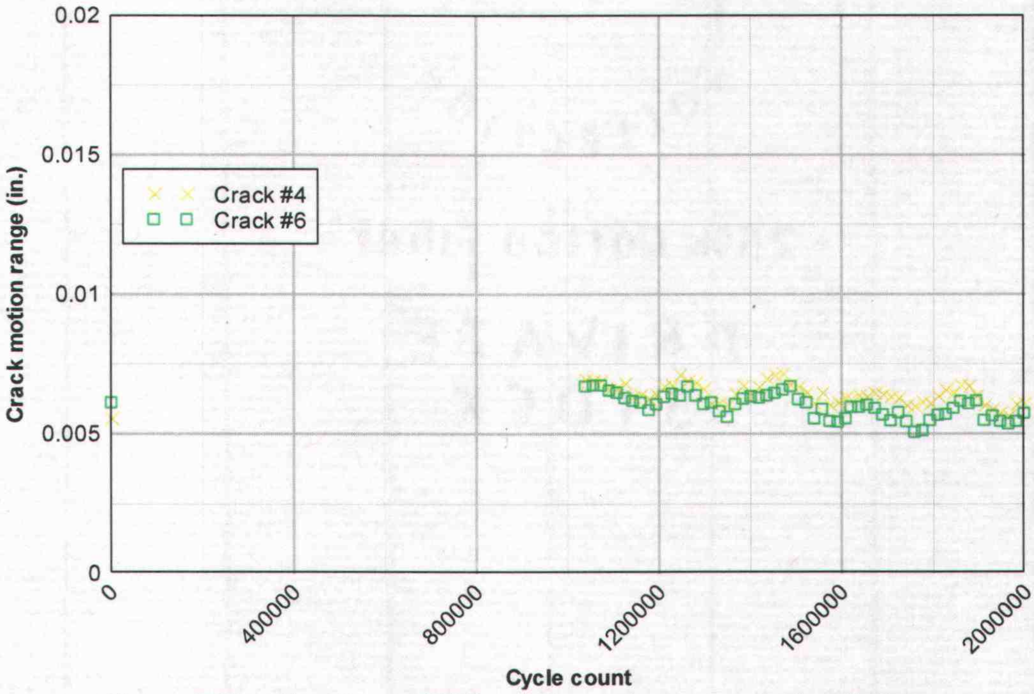

Figure B2b—Specimen 3T12 south crack ranges during fatigue.

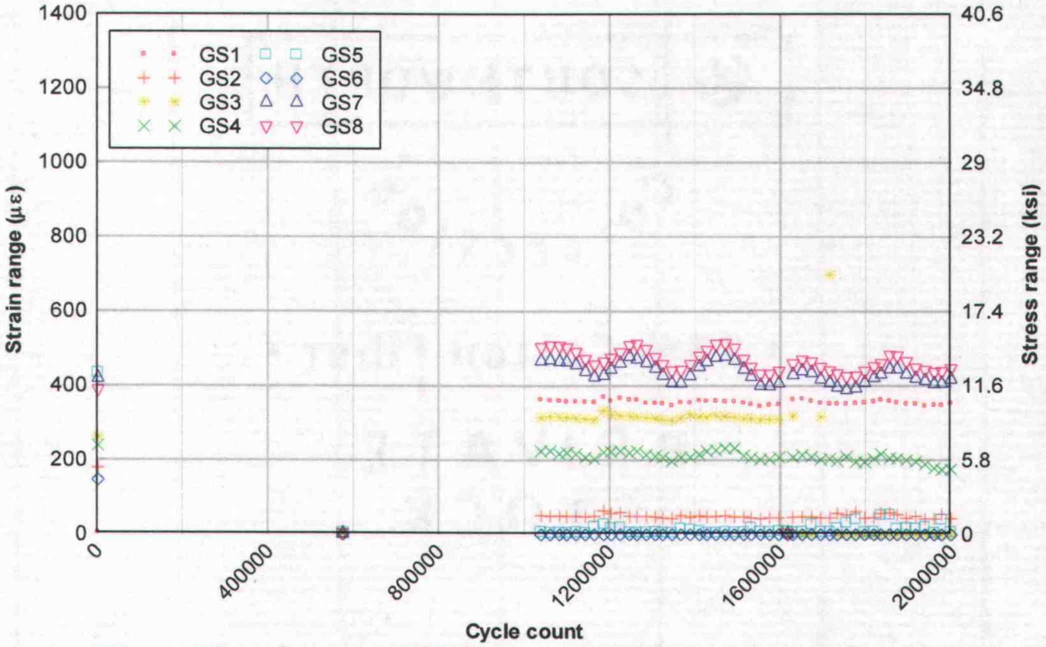

Figure B2c—Specimen 3T12 south strain ranges during fatigue.

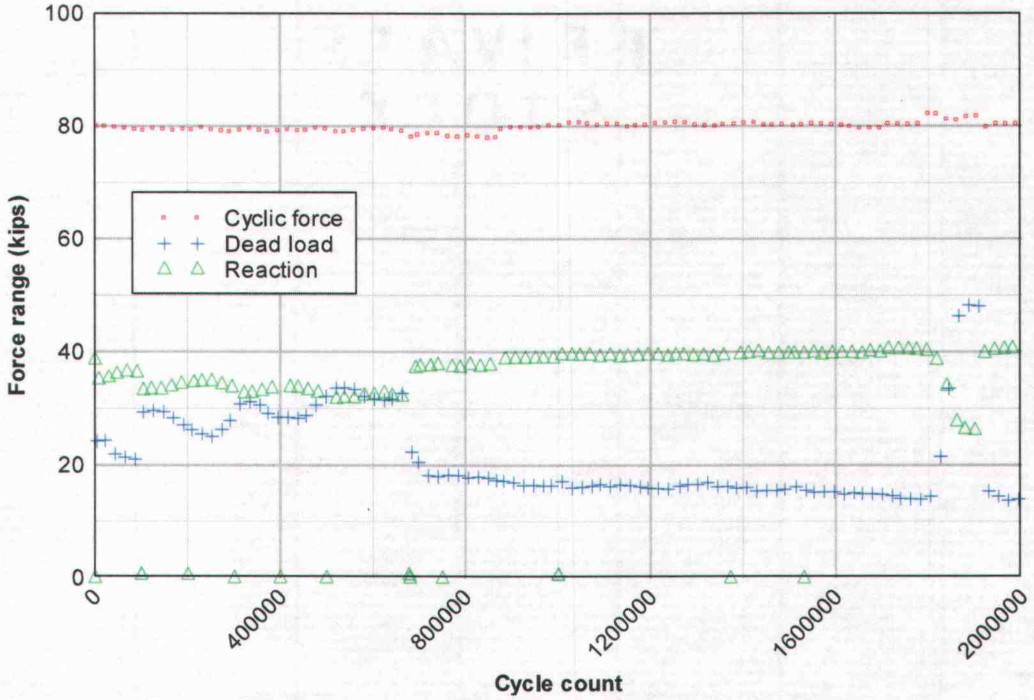

Figure B3a—Specimen 3IT18 load ranges during fatigue.

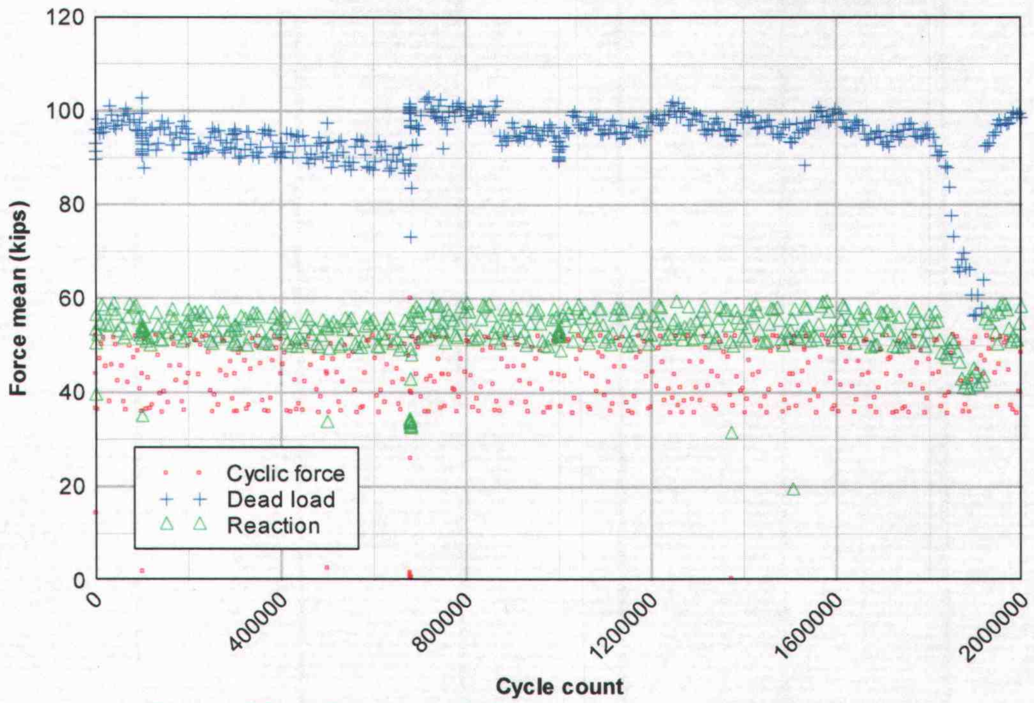

Figure B3b—Specimen 3IT18 load means during fatigue.

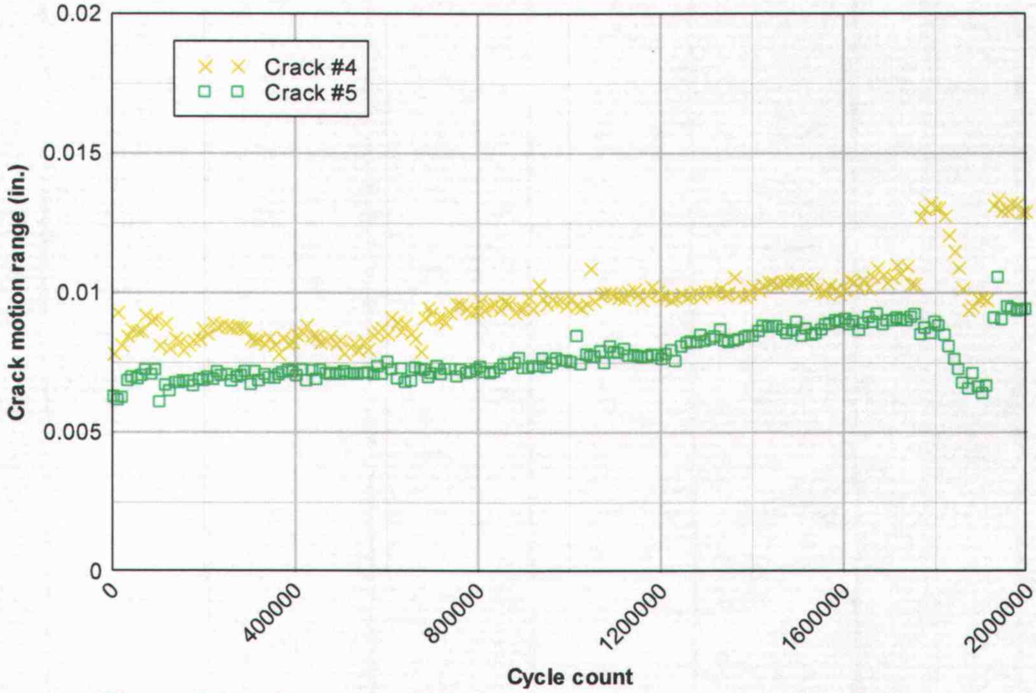

Figure B3c—Specimen 3IT18 south crack ranges during fatigue.

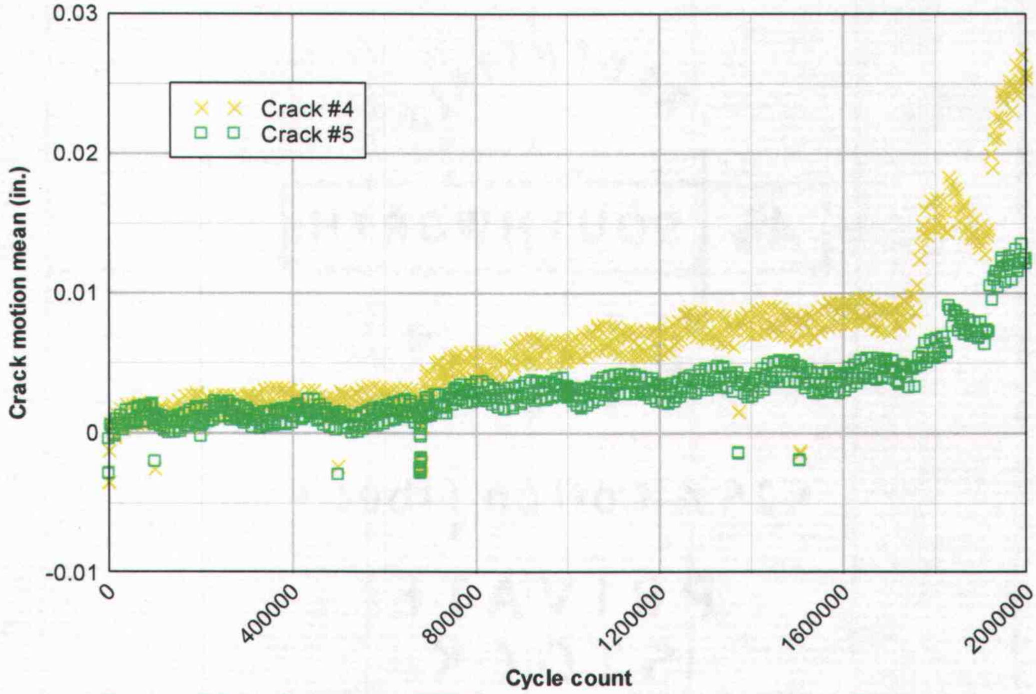

Figure B3d—Specimen 3IT18 south crack means during fatigue.

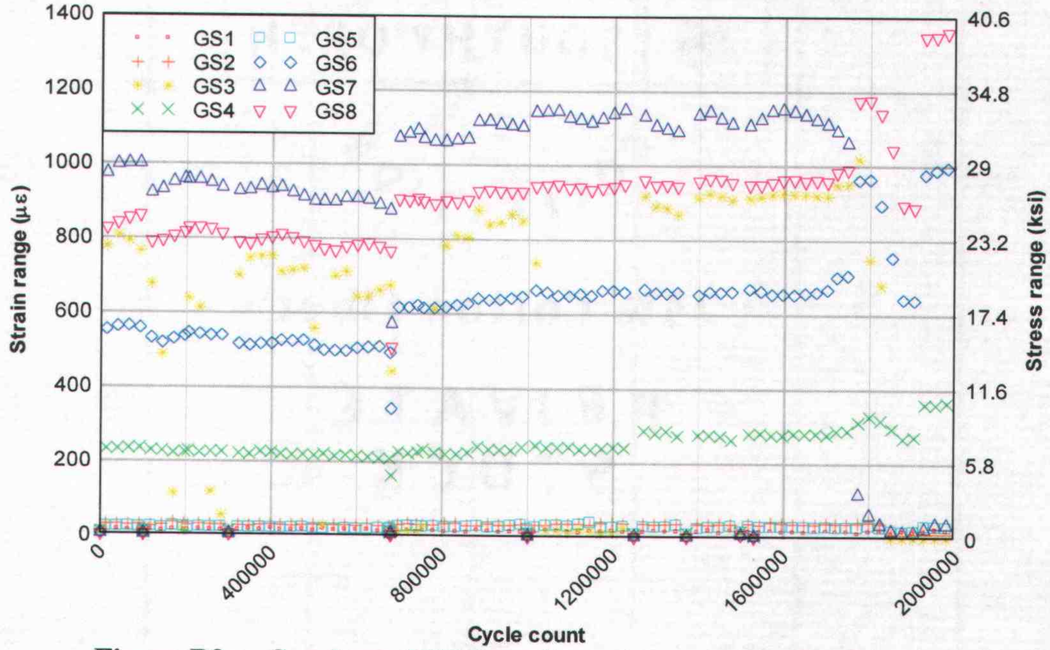

Figure B3e—Specimen 3IT18 south strain ranges during fatigue.

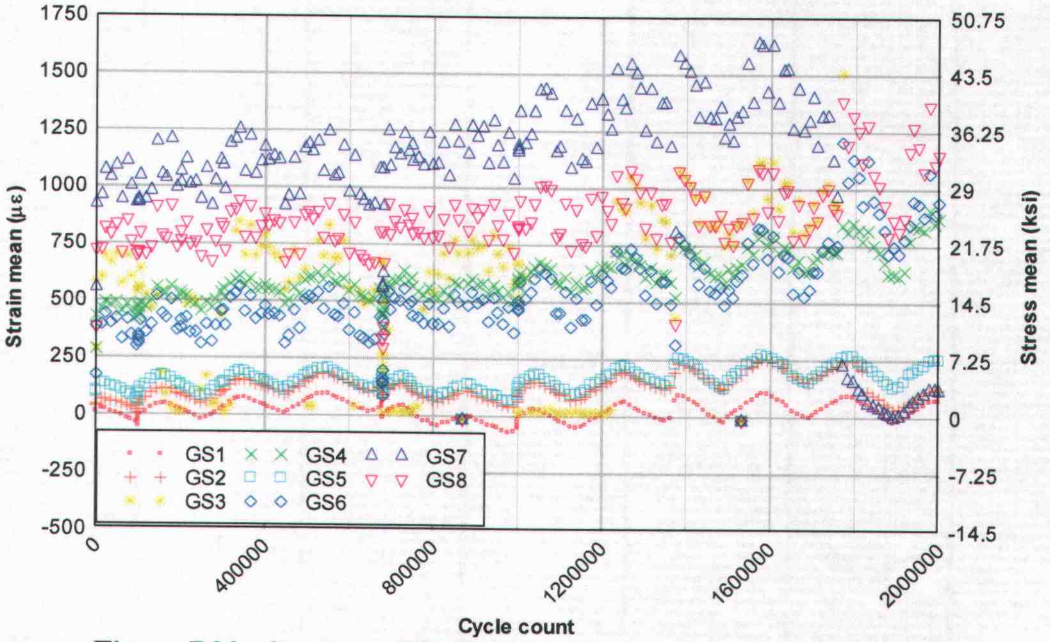

Figure B3f—Specimen 3IT18 south strain means during fatigue.

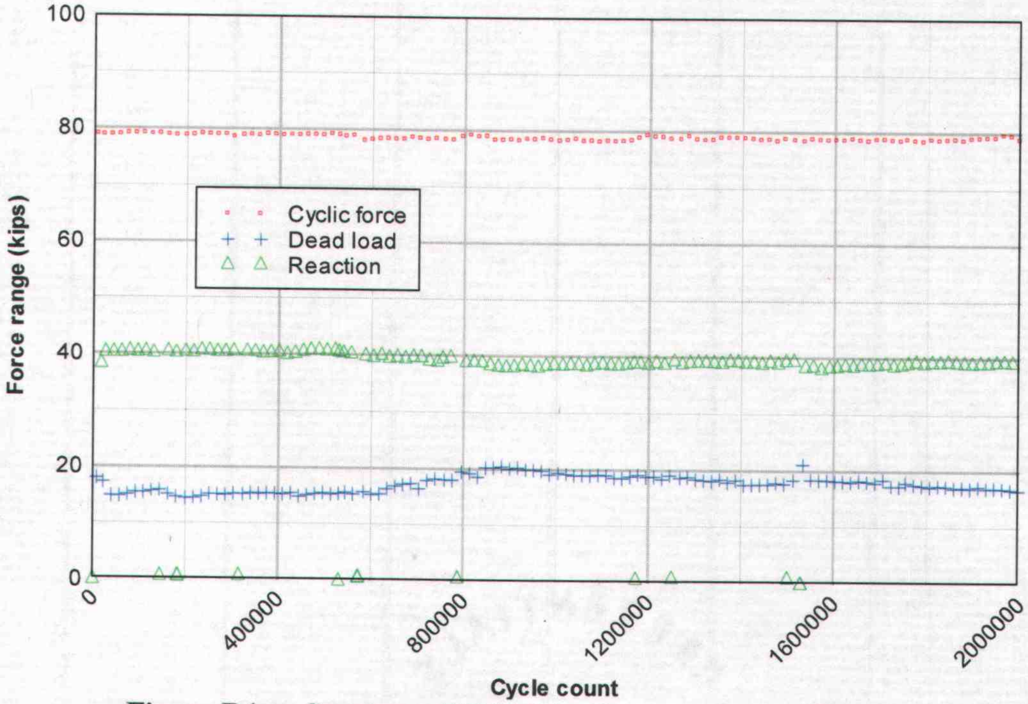

Figure B4a—Specimen 5IT12-1 load ranges during fatigue.

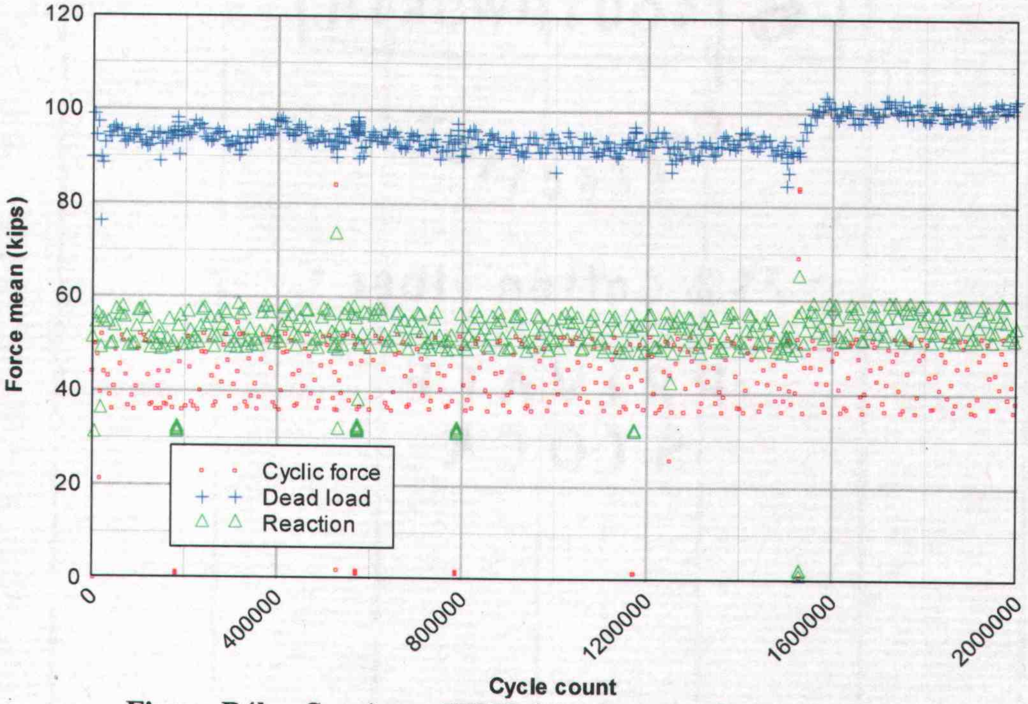

Figure B4b—Specimen 5IT12-1 load means during fatigue.

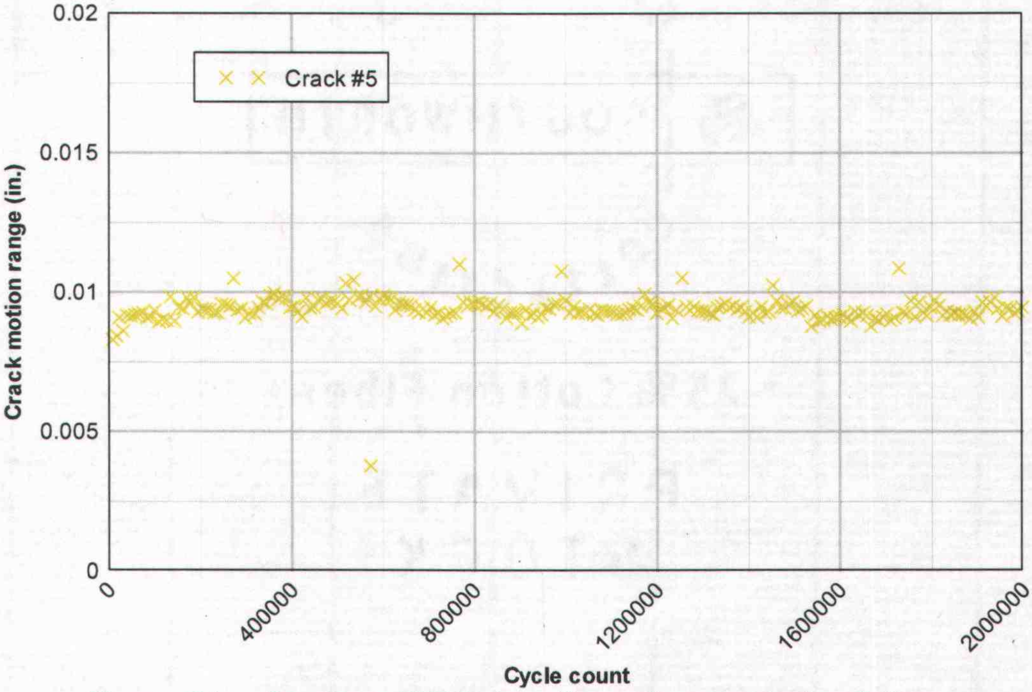

Figure B4c—Specimen 5IT12-1 south crack range during fatigue.

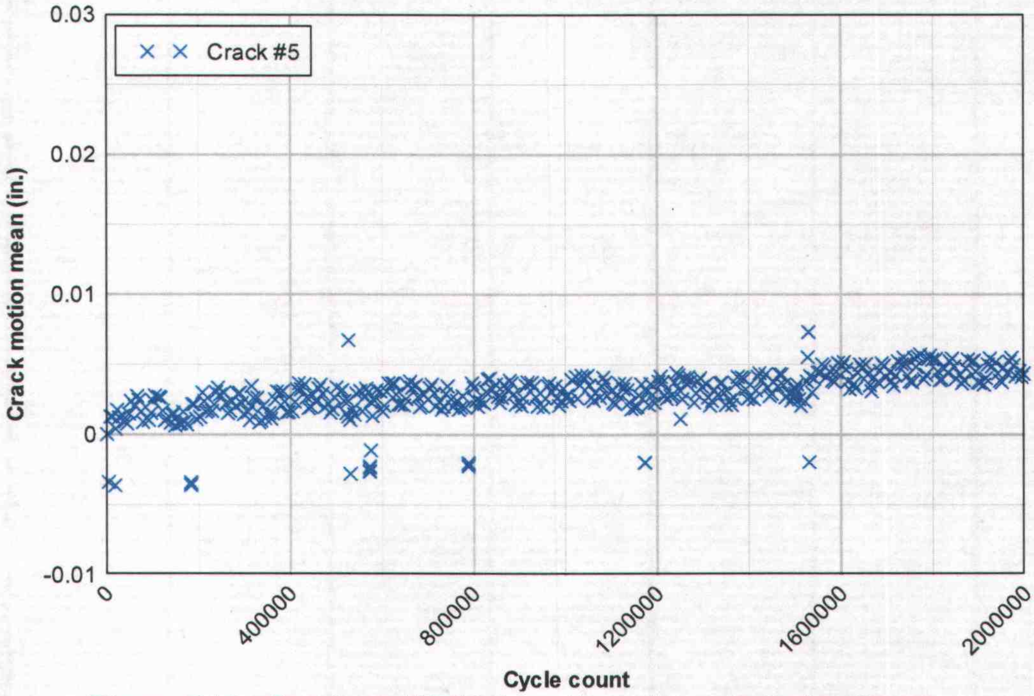

Figure B4d—Specimen 5IT12-1 south crack mean during fatigue.

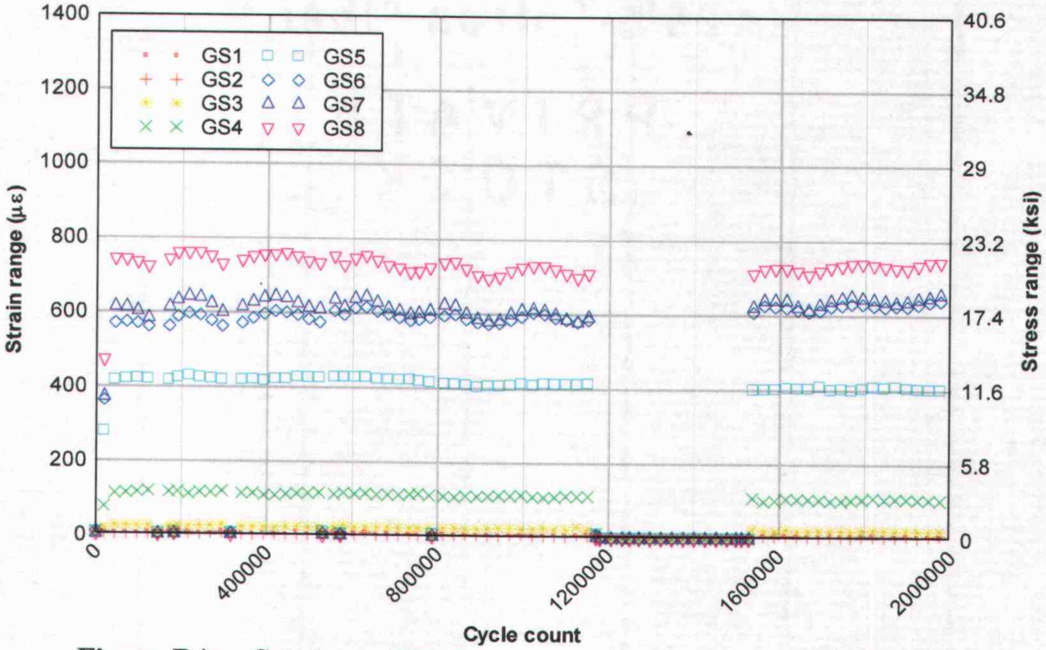

Figure B4e—Specimen 5IT12-1 south strain ranges during fatigue.

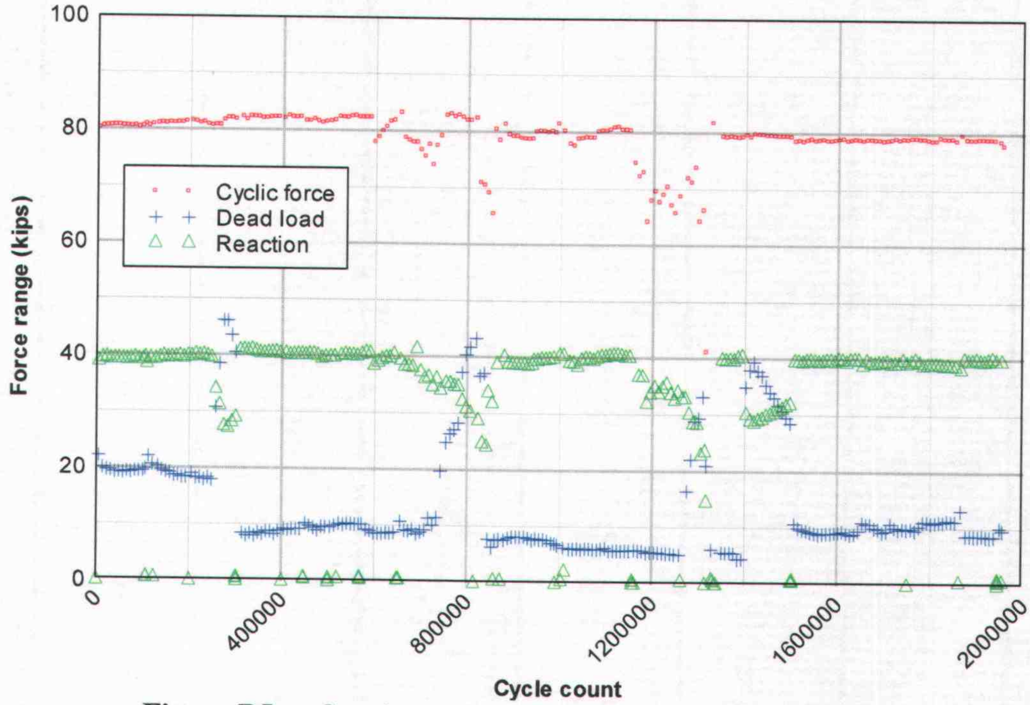

Figure B5a—Specimen 6IT10 load ranges during fatigue.

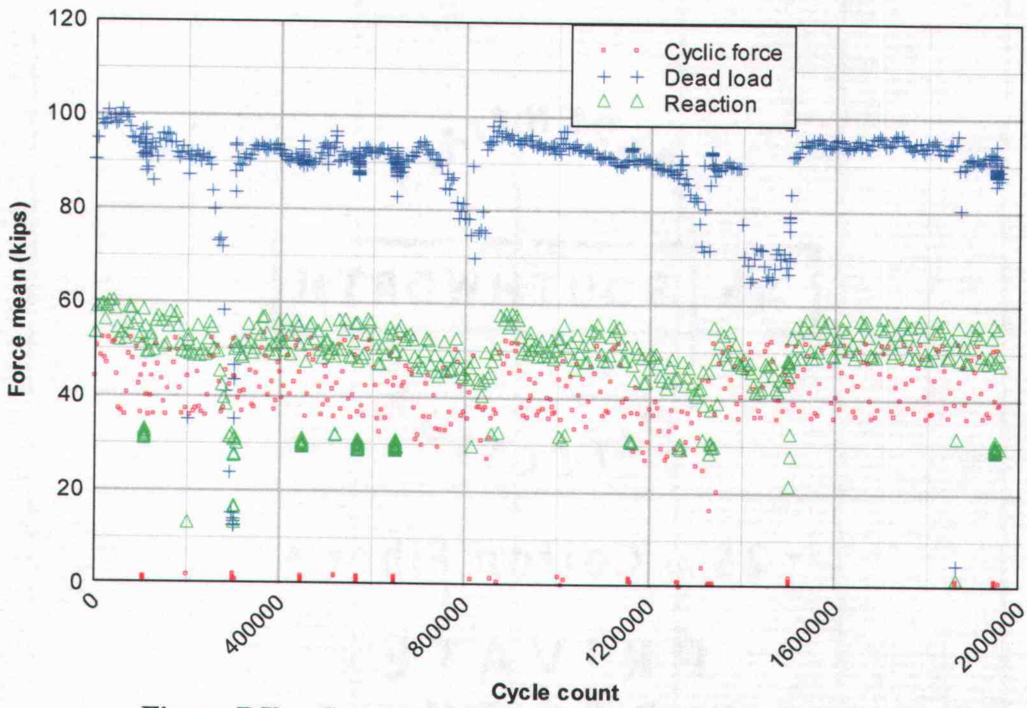

Figure B5b—Specimen 6IT10 load means during fatigue.

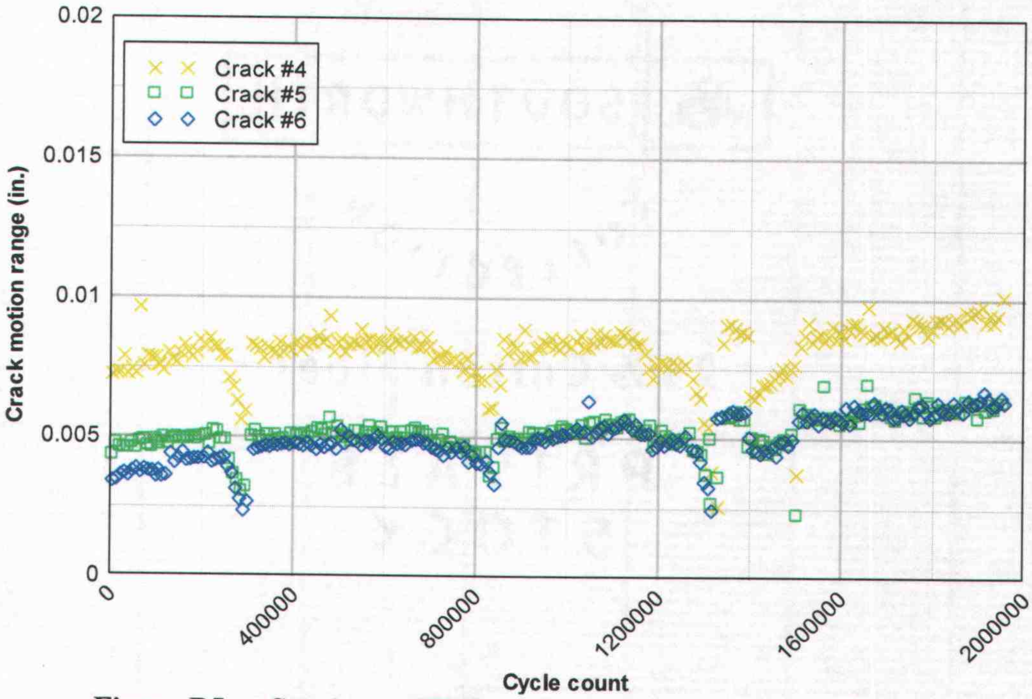

Figure B5c—Specimen 6IT10 south crack ranges during fatigue.

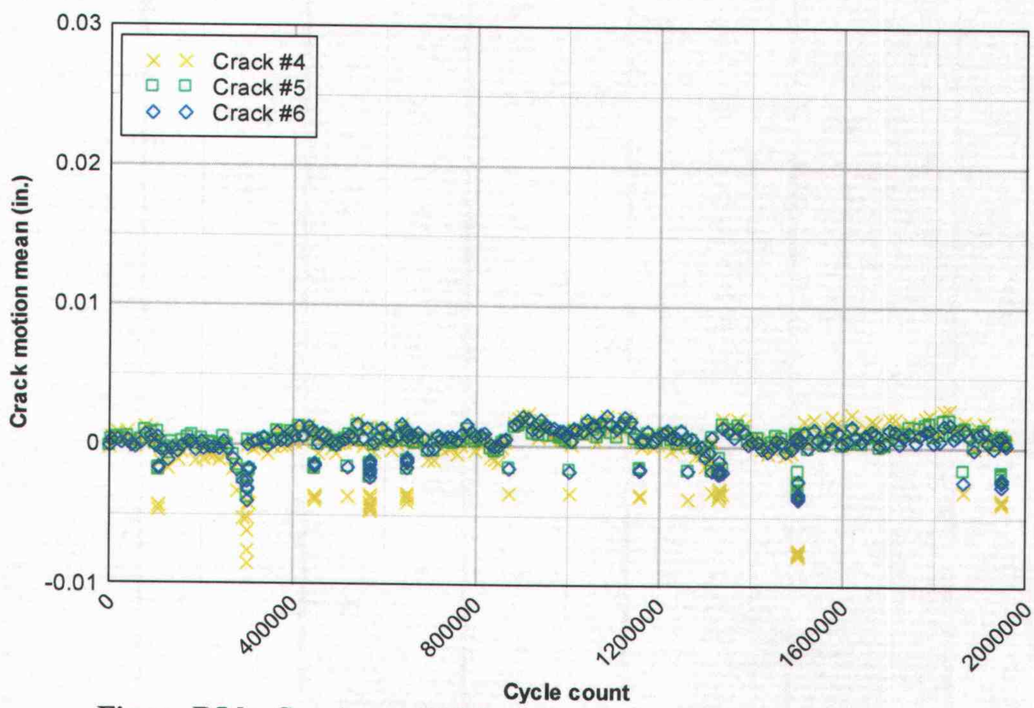

Figure B5d—Specimen 6IT10 south crack means during fatigue.

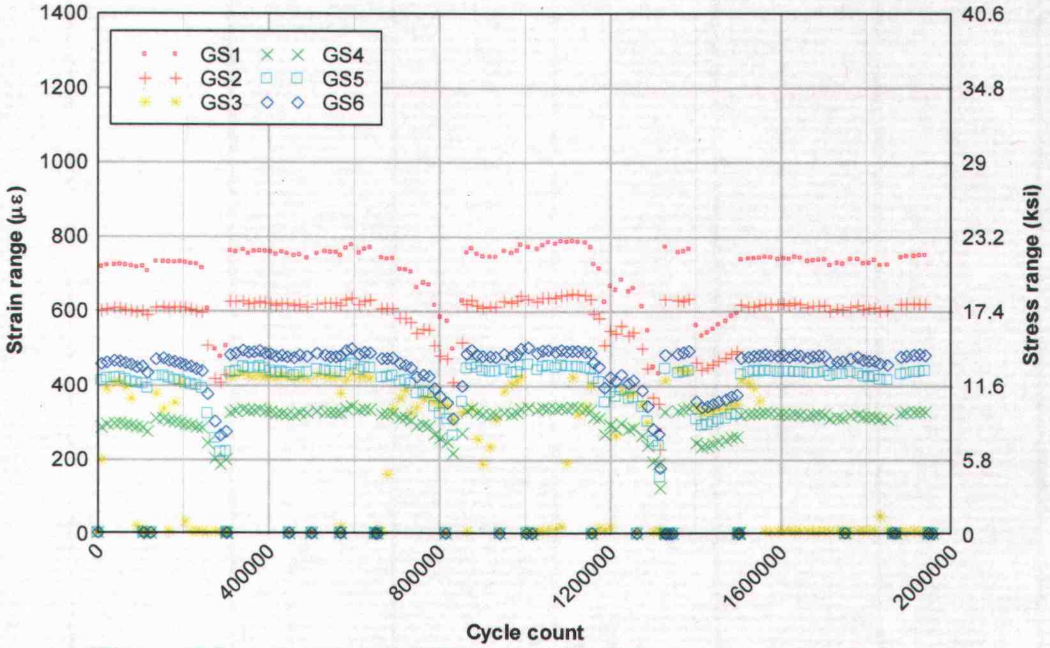

Figure B5e—Specimen 6IT10 south strain ranges during fatigue.

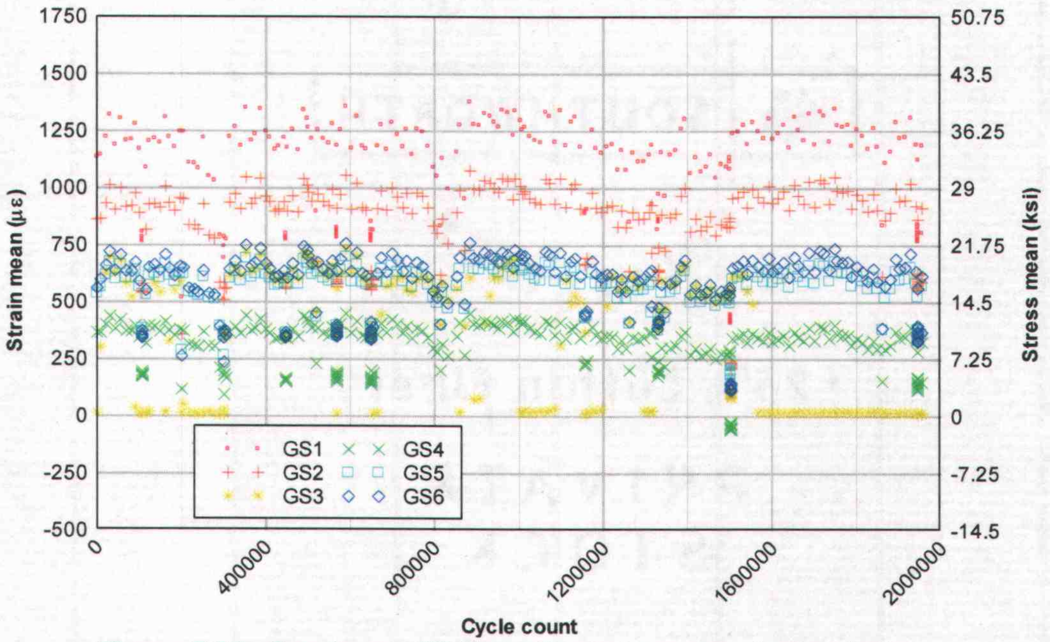

Figure B5f—Specimen 6IT10 south strain means during fatigue.

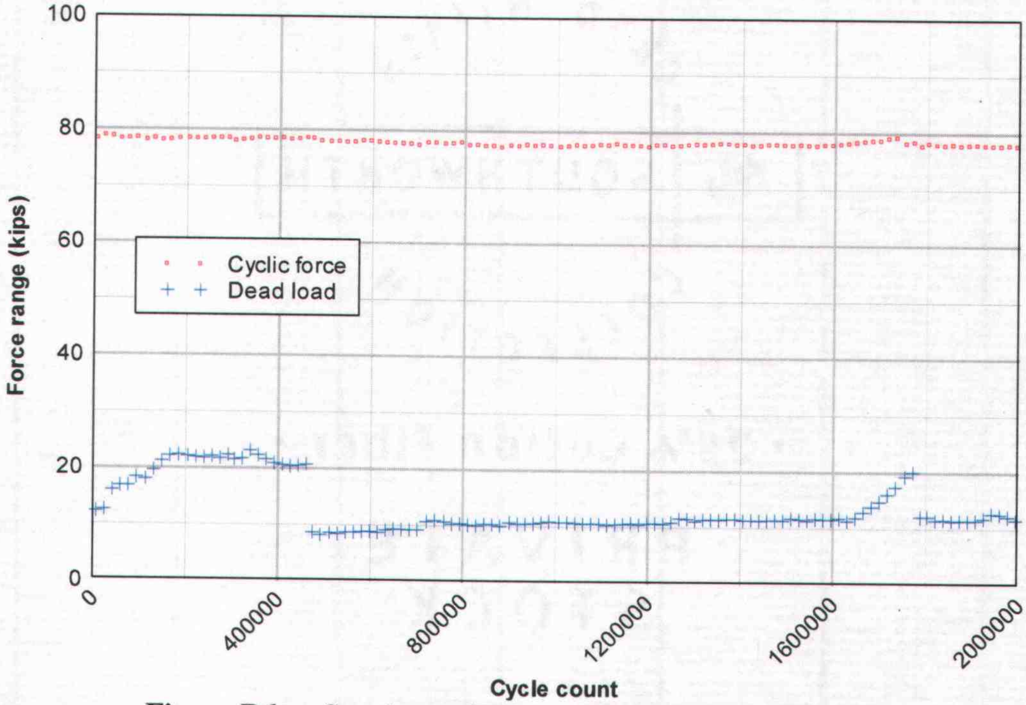

Figure B6a—Specimen 6T10 load ranges during fatigue.

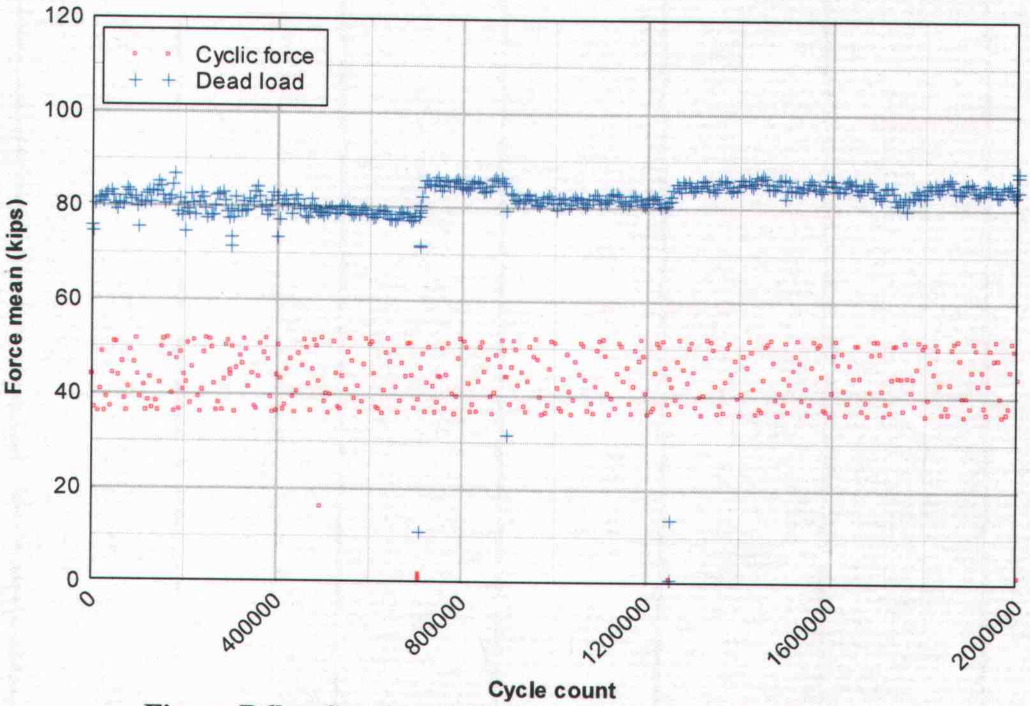

Figure B6b—Specimen 6T10 load means during fatigue.

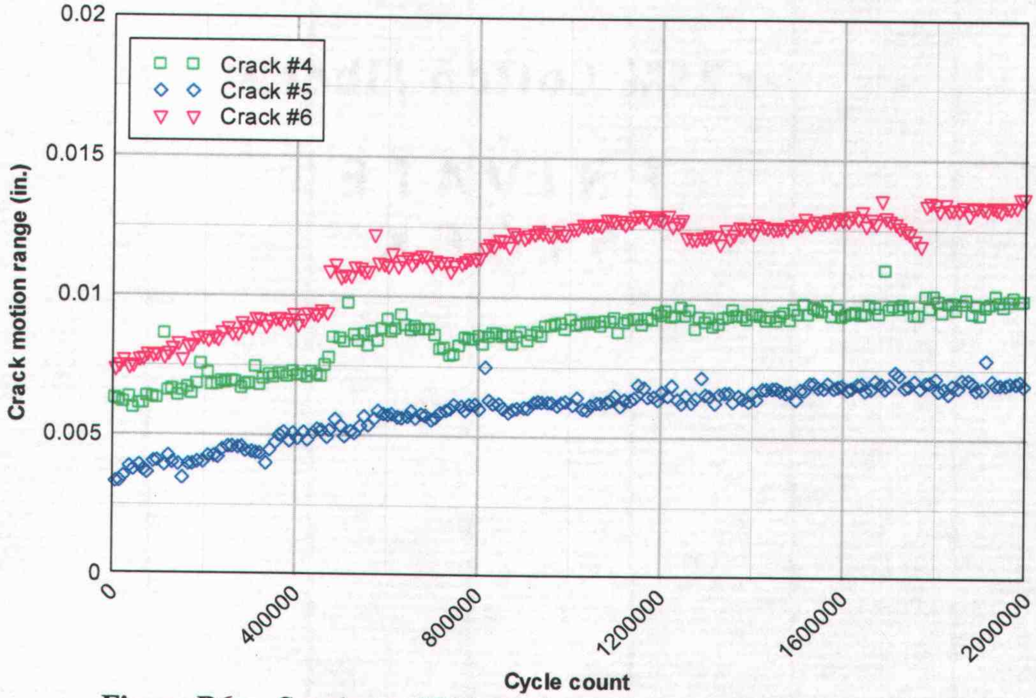

Figure B6c—Specimen 6T10 south crack ranges during fatigue.

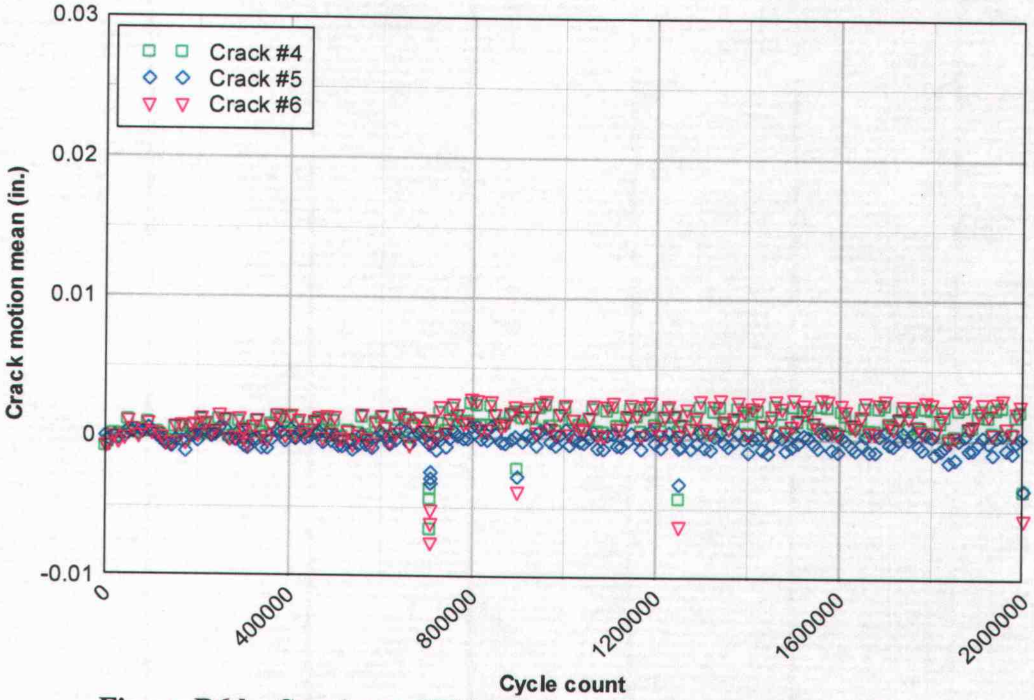

Figure B6d—Specimen 6T10 south crack means during fatigue.

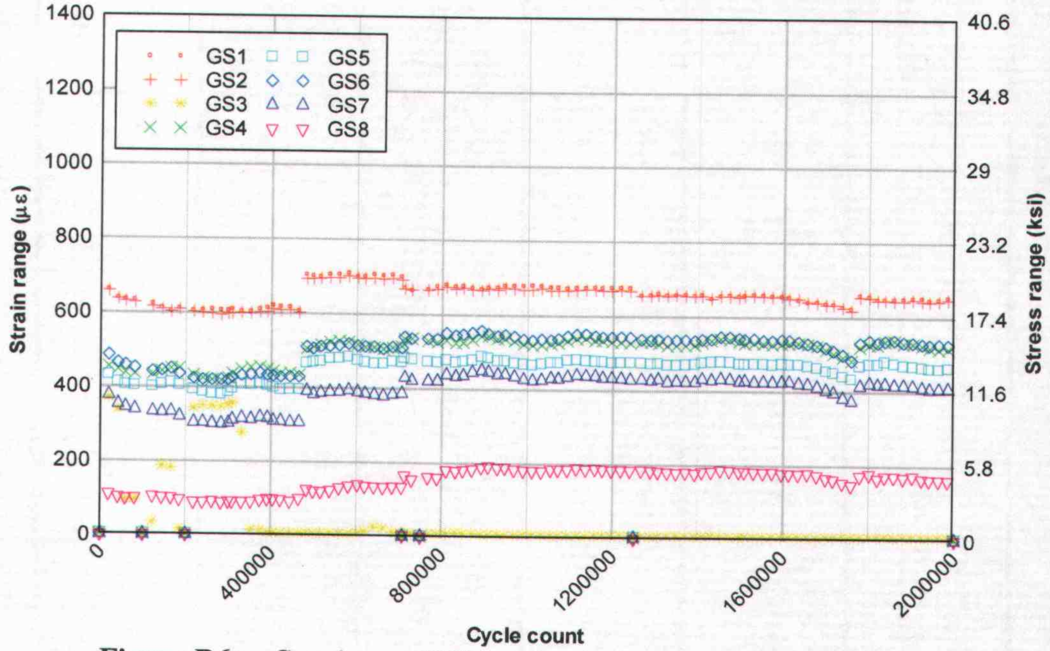

Figure B6e—Specimen 6T10 south strain ranges during fatigue.

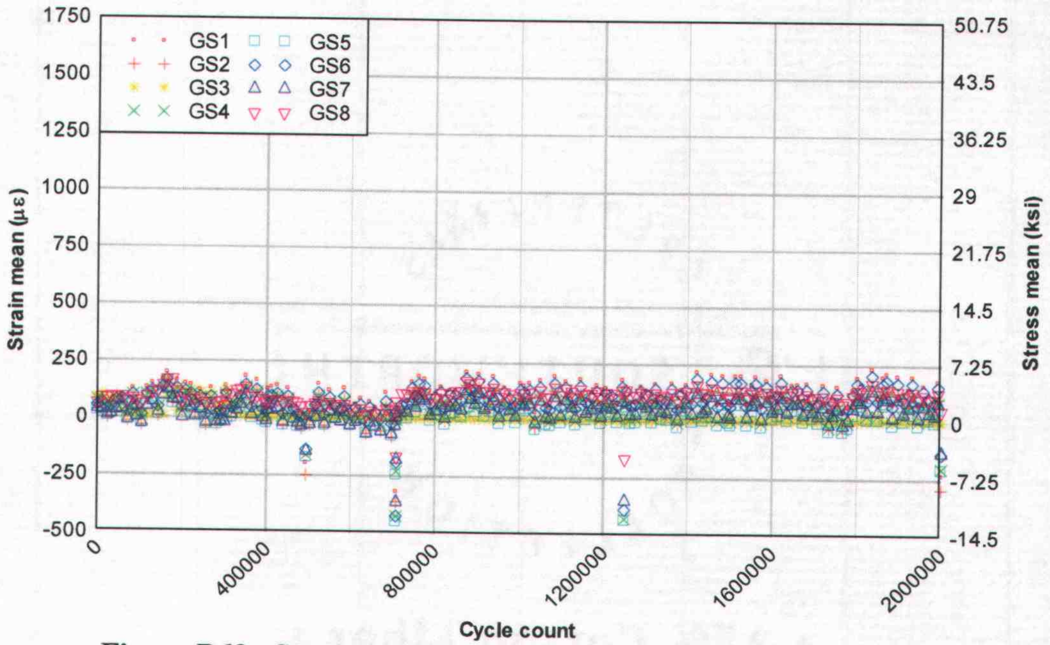

Figure B6f—Specimen 6T10 south strain means during fatigue.

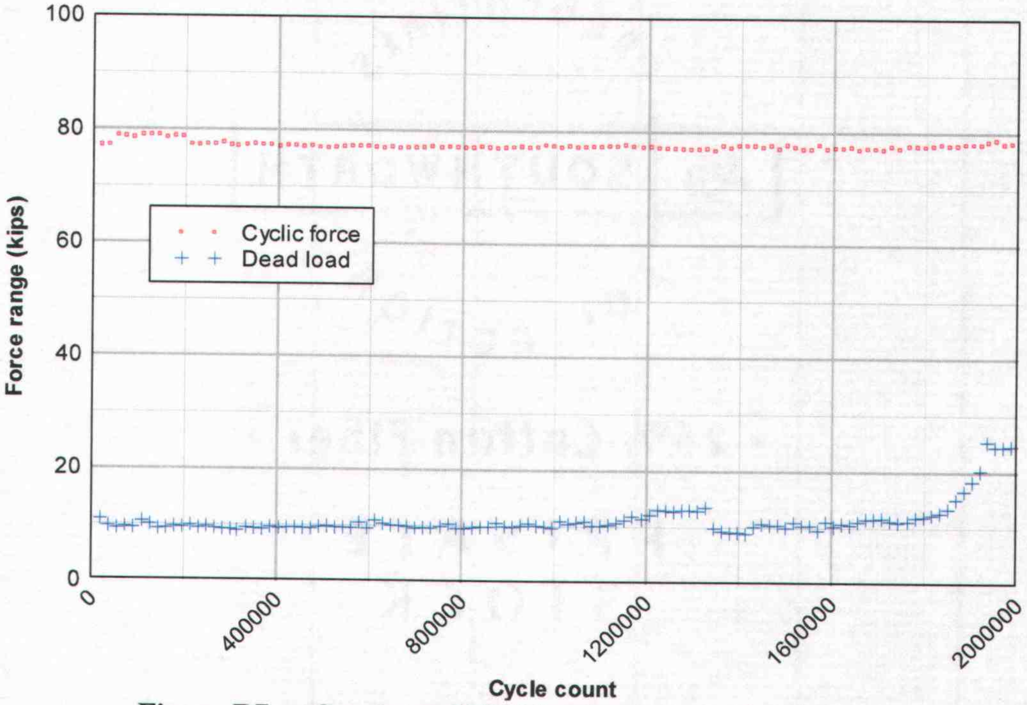

Figure B7a—Specimen 8IT10 load ranges during fatigue.

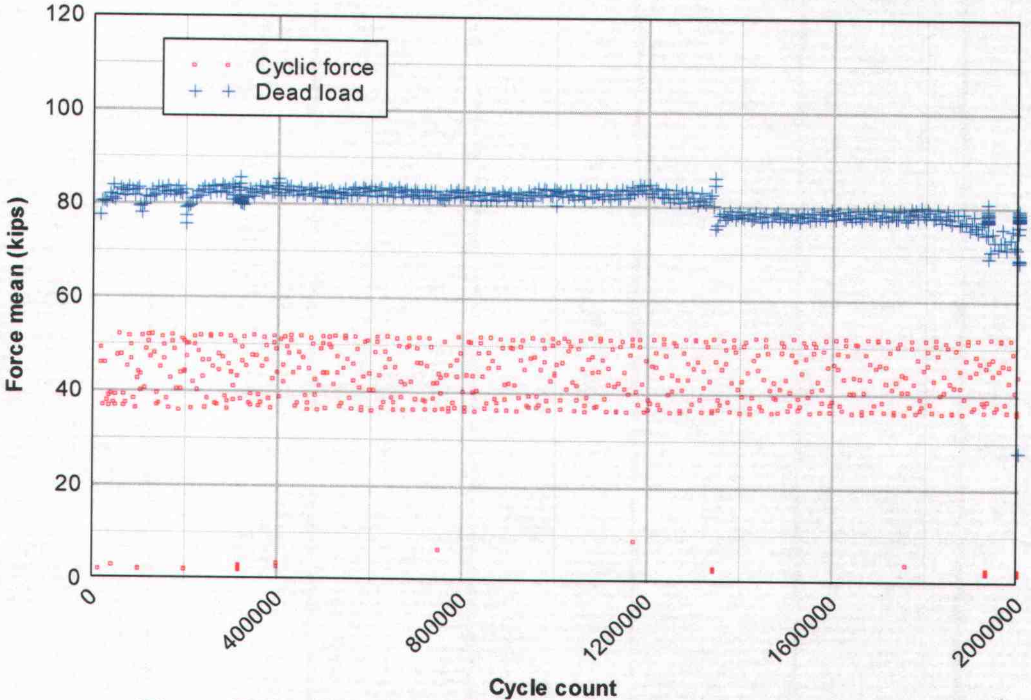

Figure B7b—Specimen 8IT10 load means during fatigue.

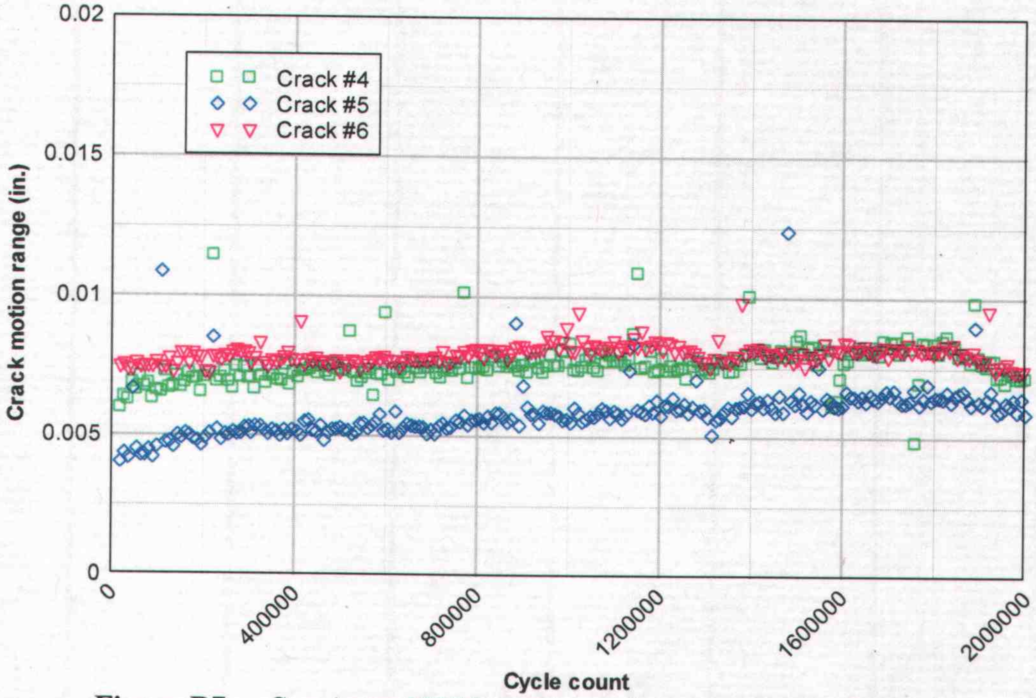

Figure B7c—Specimen 8IT10 south crack ranges during fatigue.

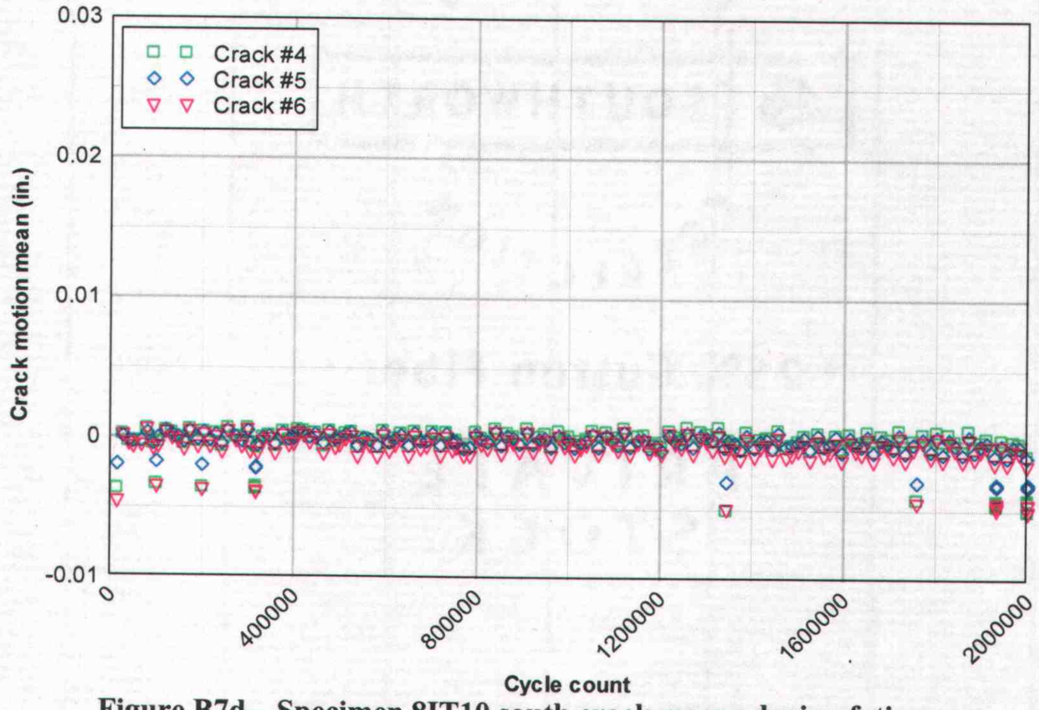

Figure B7d—Specimen 8IT10 south crack means during fatigue.

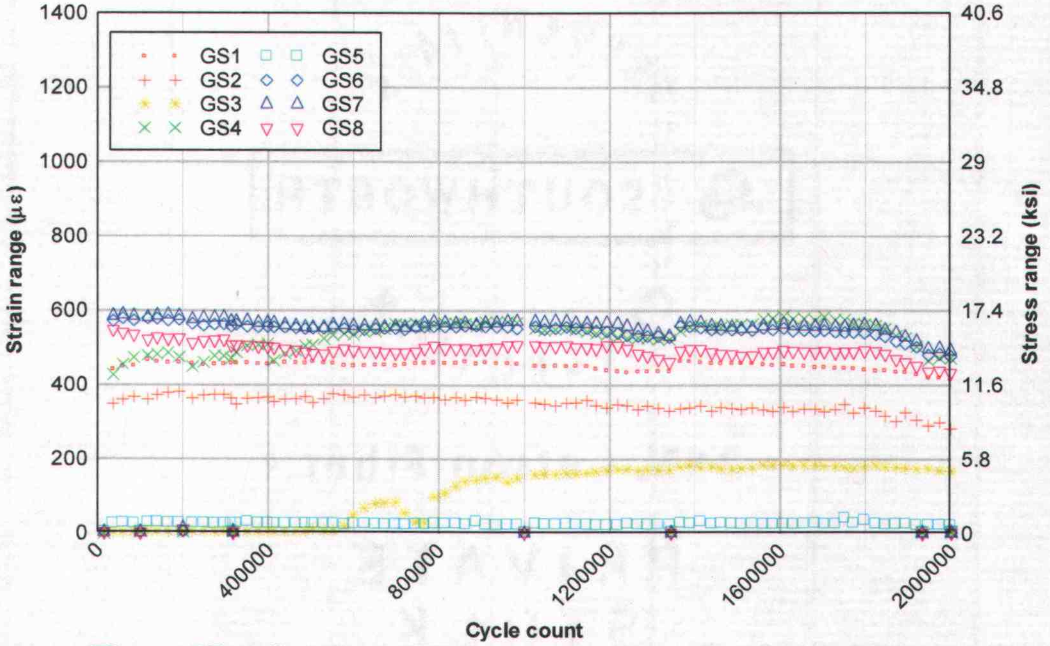

Figure B7e—Specimen 8IT10 south strain ranges during fatigue.

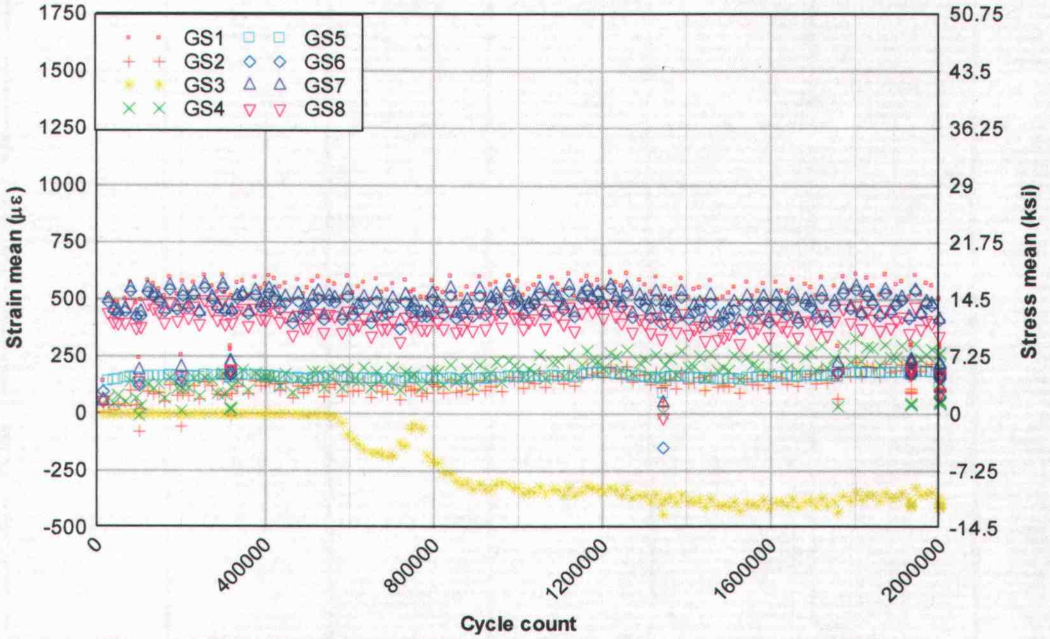

Figure B7f—Specimen 8IT10 south strain means during fatigue.

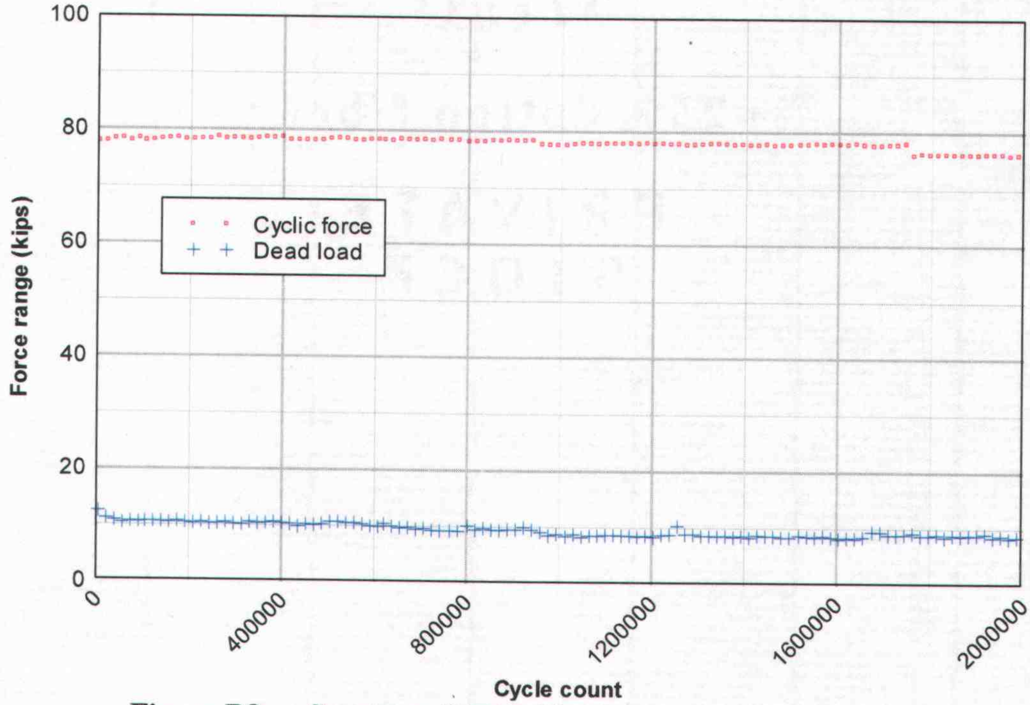

Figure B8a—Specimen 9IT12-1 load ranges during fatigue.

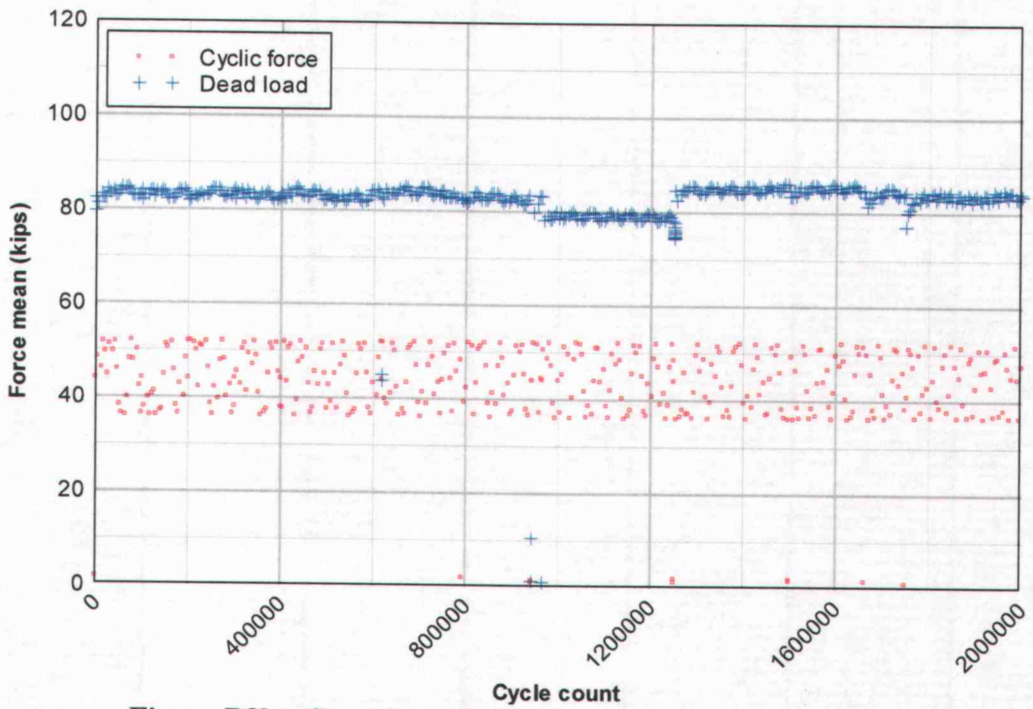

Figure B8b—Specimen 9IT12-1 load means during fatigue.

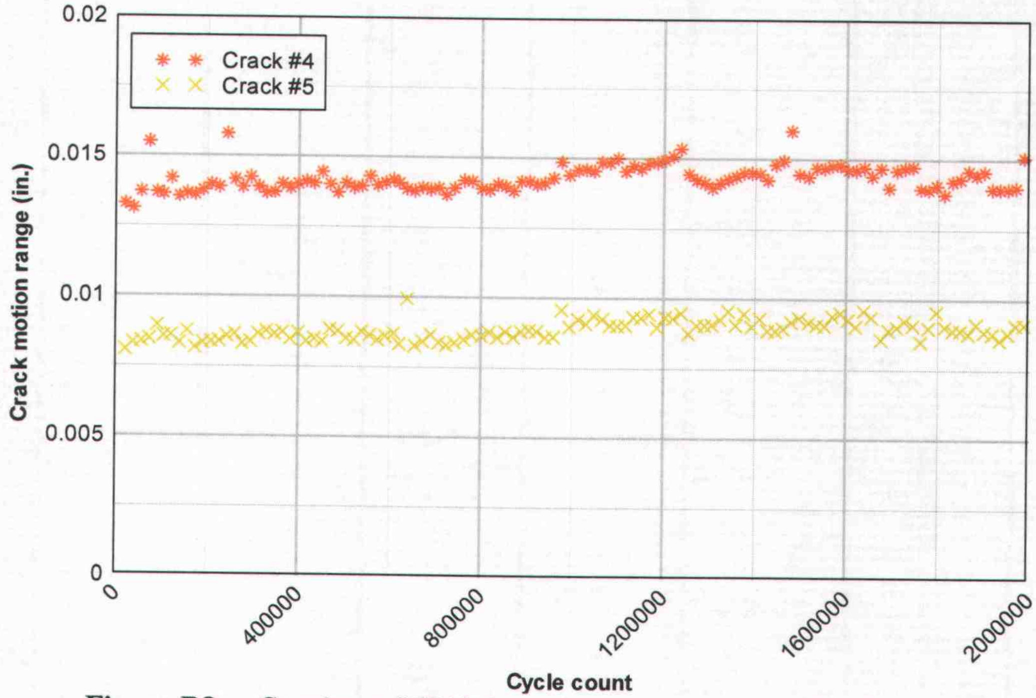

Figure B8c—Specimen 9IT12-1 south crack ranges during fatigue.

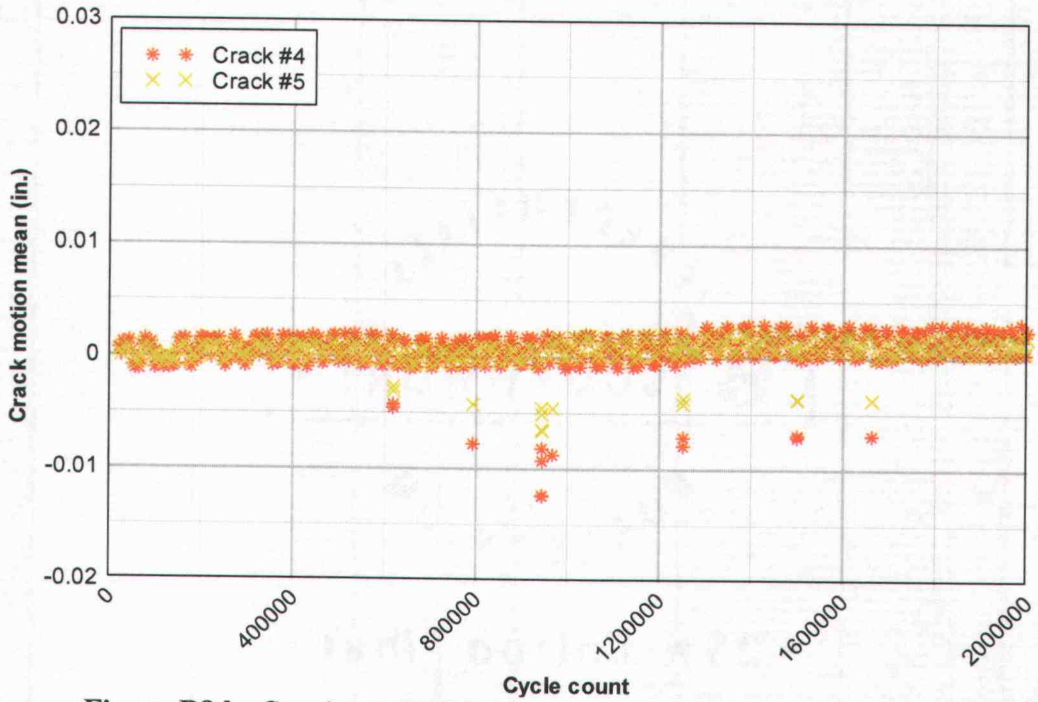

Figure B8d—Specimen 9IT12-1 south crack means during fatigue.

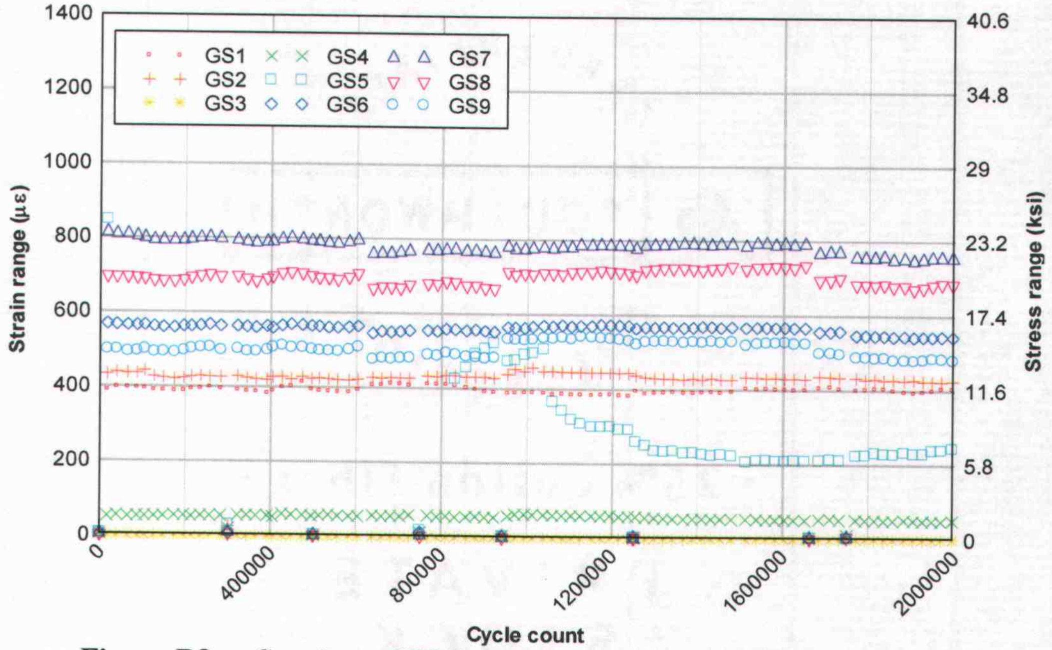

Figure B8e—Specimen 9IT12-1 south strain ranges during fatigue.

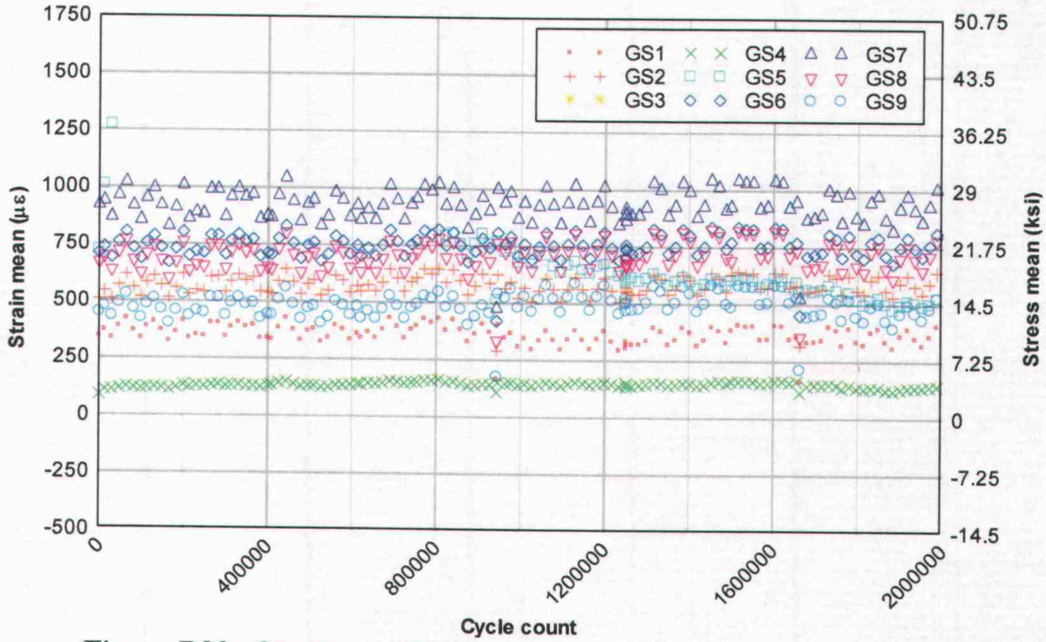

Figure B8f—Specimen 9IT12-1 south strain means during fatigue.

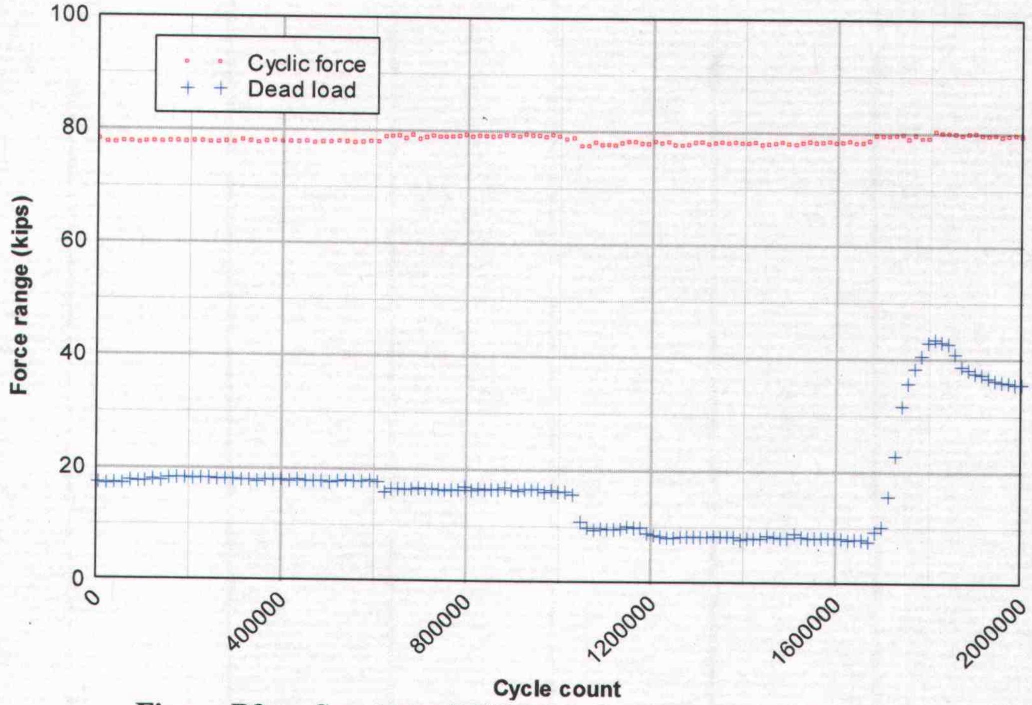

Figure B9a—Specimen 9T12-4 load ranges during fatigue.

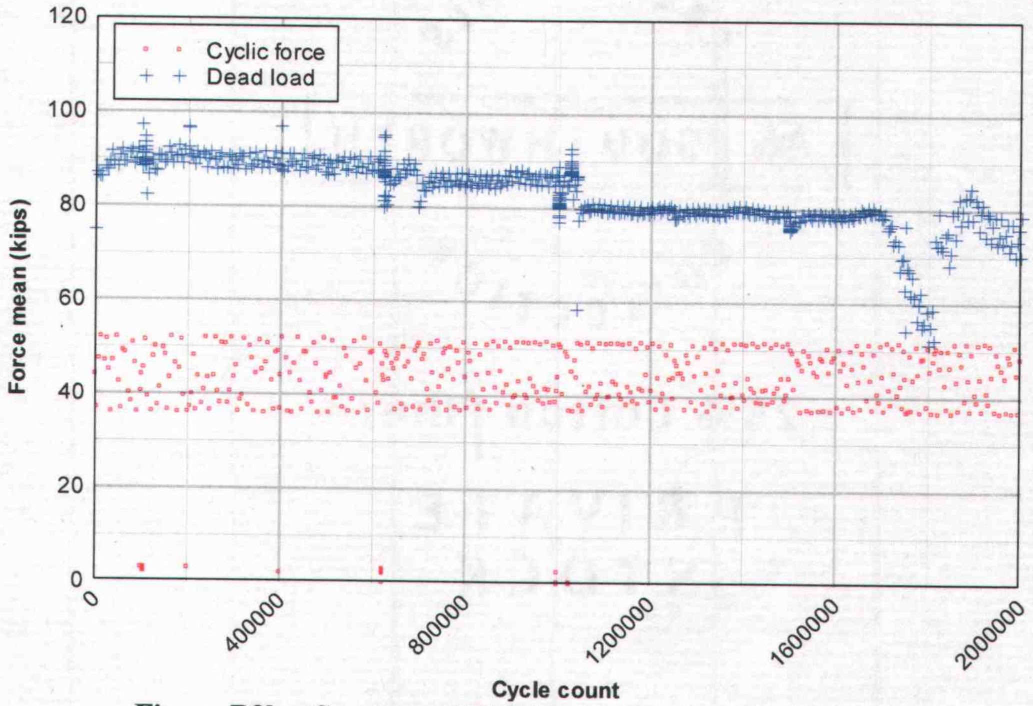

Figure B9b—Specimen 9T12-4 load means during fatigue.

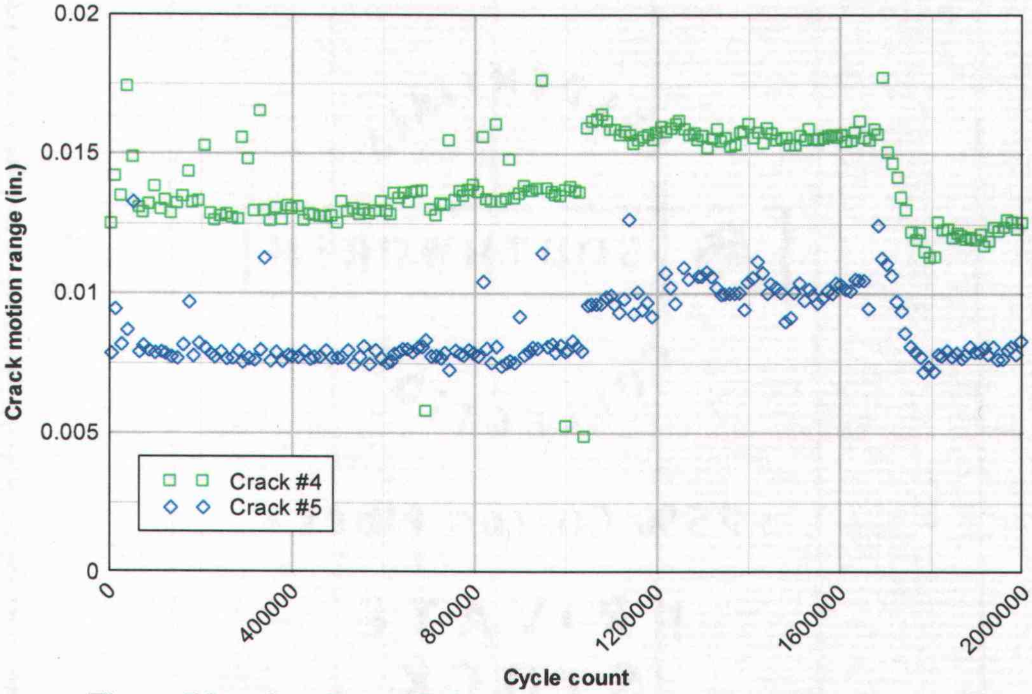

Figure B9c—Specimen 9T12-4 south crack ranges during fatigue.

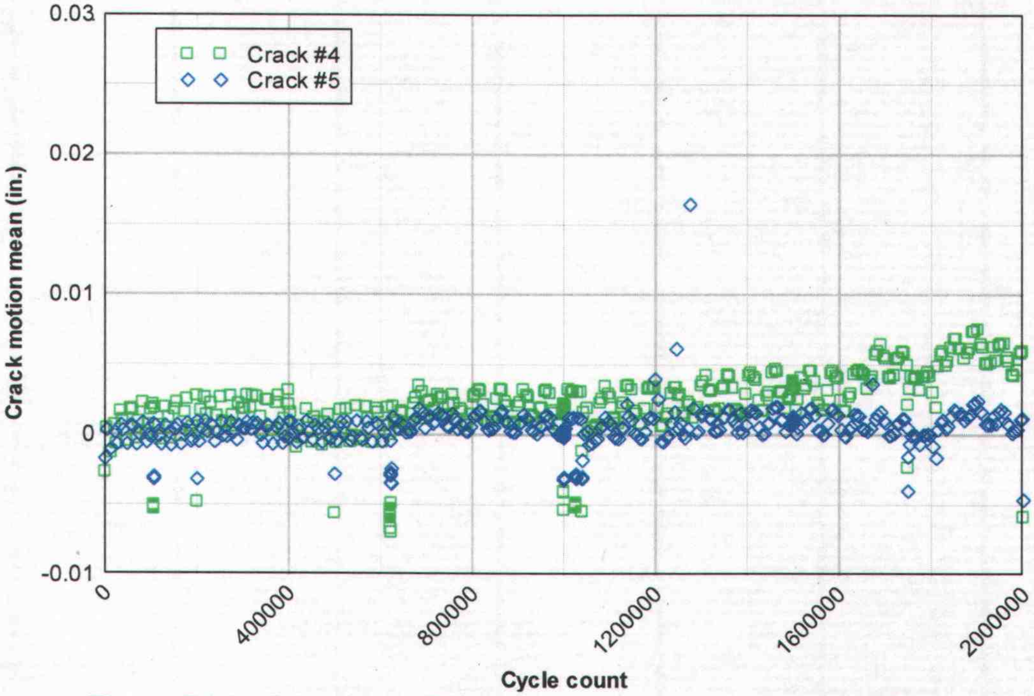

Figure B9d—Specimen 9T12-4 south crack means during fatigue.

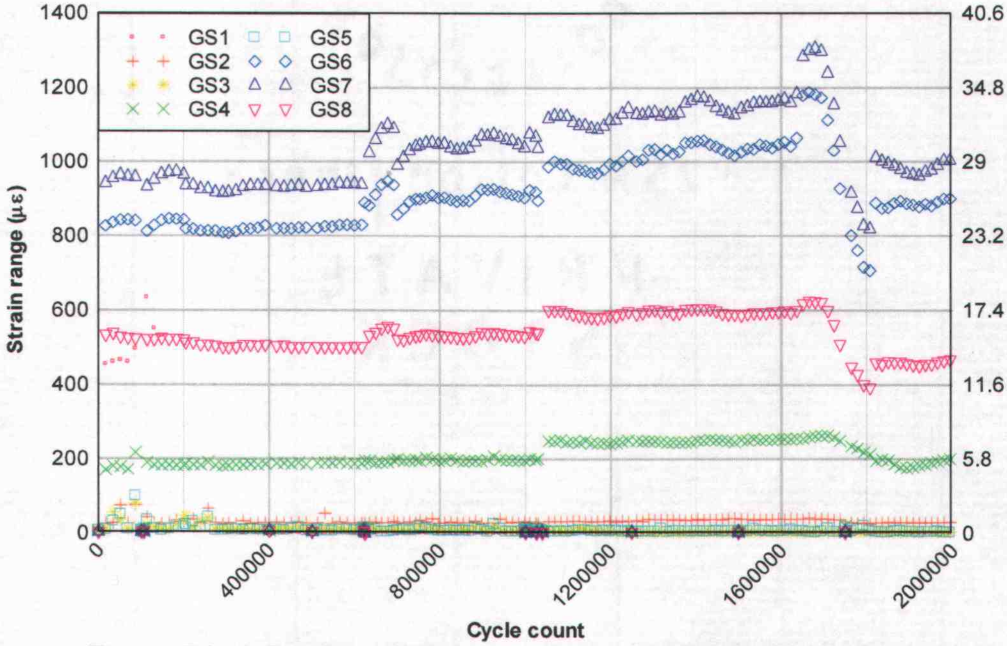

Figure B9e—Specimen 9T12-4 south strain ranges during fatigue.

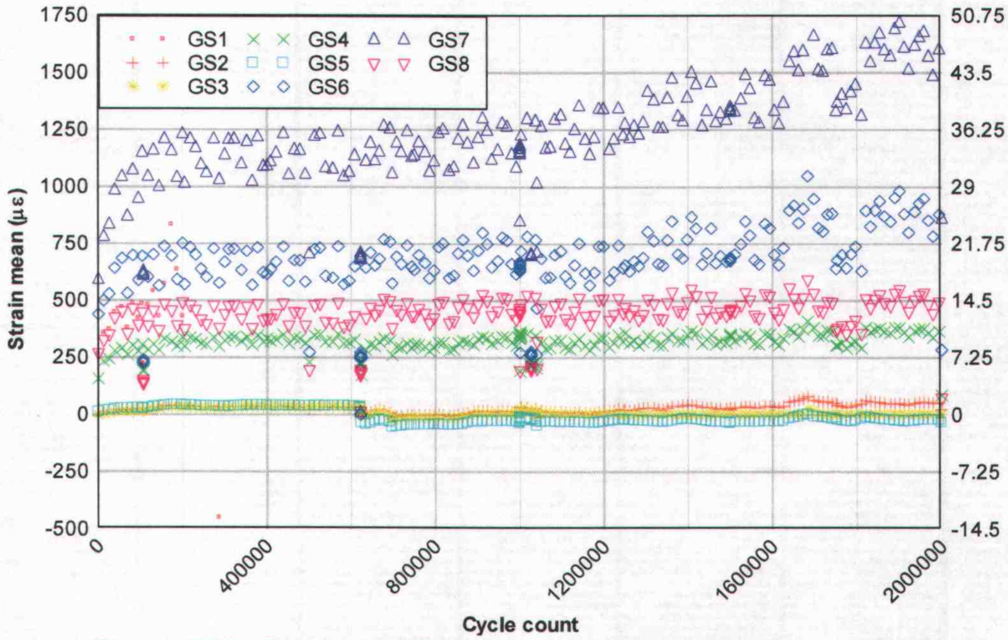

Figure B9f—Specimen 9T12-4 south strain means during fatigue.